Astronomy & Astrophysics manuscript no. famed1
March 11, 2020

Fast and Automated Peak Bagging with DIAMONDS (FAMED)

E. Corsaro[1], J. M. McKeever[2], and J. Kuszlewicz[3]

[1] INAF – Osservatorio Astrofisico di Catania, via S. Sofia 78, 95123 Catania, Italy
[2] Astronomy Department, Yale University, New Haven, CT 06511, USA
[3] Max-Planck-Institut für Sonnensystemforschung, Justus-von-Liebig-Weg 3, D-37077 Göttingen, Germany

Preprint online version: March 11, 2020

ABSTRACT

Stars of low and intermediate mass that exhibit oscillations may show tens of detectable oscillation modes each. Oscillation modes are a powerful tool to constrain the internal structure and rotational dynamics of the star, hence for obtaining an accurate stellar age. The tens of thousands of solar-like oscillators discovered thus far are representative of the large diversity of fundamental stellar properties and evolutionary stages available. Because of the wide range of oscillation features that can be recognized in such stars, it is particularly challenging to properly characterize the oscillation modes in detail, especially in the light of large stellar samples. Overcoming this issue requires an automated approach, which has to be fast, reliable, and flexible at the same time. In addition, this approach should be not only capable of extracting the oscillation mode properties of frequency, linewidth, and amplitude from stars in different evolutionary stages, but also able to assign a correct mode identification for each of the modes extracted. Here we present the new freely available pipeline FAMED, which is capable of performing an automated and detailed asteroseismic analysis in stars ranging from main sequence up to the core-Helium-burning phase of stellar evolution, therefore including sub-giant stars and stars evolving along the red giant branch (RGB), but also stars likely evolving towards the early asymptotic giant branch. In this paper we additionally show how FAMED can detect rotation from dipolar oscillation modes in main sequence, sub-giant, low-luminosity RGB, and core-Helium-burning stars. FAMED can be downloaded from its public GitHub repository (https://github.com/EnricoCorsaro/FAMED).

Key words. stars: oscillations – stars: late-type – stars: solar-type – methods: statistical – methods: numerical – methods: data analysis

1. Introduction

Thanks to the photometric space missions CoRoT (Baglin et al. 2006), NASA *Kepler* and K2 (Borucki et al. 2010; Koch et al. 2010; Howell et al. 2014), and more recently NASA TESS (Ricker et al. 2014), the number of low- and intermediate-mass stars with detected oscillations now accounts for several tens of thousands of targets. The best characterized stars in terms of oscillations still remain those observed by the nominal *Kepler* mission (e.g. Corsaro et al. 2015a; Lund et al. 2017). This is because of its long observing time – exceeding four years with high duty cycle – and photometric precision. New high-quality observations are however being added thanks to TESS, especially in its continuous viewing zones (CVZs), where the observing length can be up to one full year (Stassun et al. 2019). In this scenario, we have tens of thousands of stars, mostly red giants, for which a detailed analysis of their oscillation properties, known as peak bagging, can be performed. The peak bagging analysis is an essential step to accomplish if one wants to extract the most from the asteroseismic observations. This is because it is with the individual oscillation mode properties that one is able to reconstruct the internal structure and rotational stratification of the star, and consequently to obtain more accurate stellar ages (e.g. Pérez Hernández et al. 2016; Silva Aguirre et al. 2017). However the peak bagging analysis is significantly complicated by the large diversity of oscillation features that can be found in stars evolving from the main sequence (MS) to red giants (RGs). While analyzing a few targets, either manually or using semi-automated approaches, is still feasible, performing a peak bagging analysis on tens of thousands of stars becomes an impractical path to follow. In addition to this, in this coming decade we will face new observations from the all-sky mission ESA PLATO (Rauer et al. 2014), which will increase the expected yield of stars for which a peak bagging analysis can be done by at least one order of magnitude.

In Corsaro & De Ridder (2014) the authors introduced for the first time the so-called Bayesian multi-modal fitting for peak bagging, showing that it can be successfully used on a MS solar-like oscillator, although the approach was still not competitive in terms of computational speed. In a recent work, Corsaro (2019) (hereafter C19) presented a significant improvement of the Bayesian multi-modal approach and showed how it retains a great potential for overcoming the problem of extracting a large amount of asteroseismic information in a short time. In particular, C19 proved that this process can be automated by applying it to the case of an RGB star. However, at that time the methodology was not extended and tested to stars in different evolutionary stages, nor was the actual mode identification discussed and included as an output of the computation. The mode identification typically requires a detailed knowledge of the possible oscillation features that can be observed from a given star and is usually never returned as a direct output from the peak bagging analysis. The way the oscillation features change as a function of fundamental stellar properties, evolutionary stage, and rotation of the star, has been extensively discussed in the literature (see e.g. Gizon & Solanki 2003; Ballot et al. 2008; Huber et al. 2011; Mosser et al. 2011; White et al. 2011; Bedding et al. 2011; Mosser et al. 2012; Beck et al. 2012; Corsaro et al. 2012, 2015a; Lund et al. 2017; Gehan et al. 2018), and a detailed discussion about it is not the aim of this paper. Here we present a

Send offprint requests to: Enrico Corsaro
e-mail: enrico.corsaro@inaf.it

new pipeline, dubbed FAMED, which exploits our knowledge of the stellar oscillation features, builds on the recent development in numerical sampling presented by C19, and is based on the public Bayesian inference tool DIAMONDS (Corsaro & De Ridder 2014; Corsaro et al. 2018; Corsaro 2018)[1]. FAMED is not only capable of quickly and efficiently extracting the asteroseismic properties of the individual oscillation modes, but it also incorporates a mode identification for each of the modes extracted up to the level of the rotationally split components. Finally, using both simulated and real datasets of well characterized stars, we will show how FAMED can reliably perform the peak bagging analysis in stars ranging from hot F-type MS to the core-Helium-burning phase of stellar evolution in an automated, fast, and flexible manner.

2. Bayesian multi-modal fitting

Bayesian approaches for detailed asteroseismic analysis have become more widely adopted mostly thanks to the larger availability of computational power and to the appealing possibility of incorporating a priori information on the free parameters to fit (e.g. Gruberbauer et al. 2009; Benomar et al. 2009; Kallinger et al. 2010; Handberg & Campante 2011; Corsaro & De Ridder 2014; Corsaro et al. 2015a; Davies et al. 2016; Lund et al. 2017; Corsaro et al. 2017a; Handberg et al. 2017; Vrard et al. 2018). These Bayesian approaches are used to perform peak bagging by modeling the stellar power spectral density (hereafter PSD) with a mixture of Lorentzian profiles for as many oscillation modes as one intends to fit. Here each Lorentzian profile accounts for the free parameters of frequency, amplitude, and linewidth of a single oscillation mode to be modeled. This peak bagging analysis, which we can refer to as a standard peak bagging, is intrinsically uni-modal, meaning that the aim is to obtain a single-point solution that contains the estimates of all the free parameters of the fitting model. While this certainly allows for the highest precision on the parameter estimates, a uni-modal approach has two main disadvantages: 1) it involves many free parameters to fit and therefore implies a slow computation; 2) it requires an input list of prior hyper-parameters that are often time consuming to retrieve and problematic to properly set up. Both these disadvantages cause standard peak bagging to be difficult to automate and to perform on a large sample of targets, hence severely limiting its wide applicability.

As originally anticipated by Corsaro & De Ridder (2014) and then more thoroughly discussed by C19, the DIAMONDS code offers the possibility to perform peak bagging in an innovative way, i.e. using a Bayesian multi-modal approach. This is possible thanks to the nested sampling Monte Carlo algorithm (Skilling 2004) implemented in DIAMONDS, which is well suited to efficiently sampling distributions that contain multiple local maxima. In this case one can invert the condition presented in the uni-modal case, and model the entire PSD with just one single Lorentzian profile. This in turn produces a degenerate solution (instead of a single-point solution), where the frequency centroid of the Lorentzian profile has many different possible outcomes. This multi-modal approach can be easily set up and performed because it only requires a few input prior hyper-parameters, which are straightforward to build up. Additionally the multi-modal approach is extremely fast because of the low number of free parameters involved. In the following sections we shall introduce the reader to an improved version of the multi-modal fitting presented by C19.

[1] https://github.com/EnricoCorsaro/DIAMONDS.

2.1. Islands peak bagging model

In C19 it was shown that the so-called islands peak bagging model can be represented by a Lorentzian profile where the free parameters are its frequency centroid ν_0 and its amplitude A, with the FWHM of the profile, Γ, kept to a fixed value. The known correlation between oscillation mode height H and linewidth Γ is not a problem in this case because the FWHM is fixed, which means that A^2 and H behave as the same quantity during the fitting process, except for a constant multiplication factor. A first improvement to the multi-modal approach can thus be obtained by replacing the amplitude of the Lorentzian profile with its height. The advantage of having the height as a free parameter is that it is a direct observable in the PSD, i.e. it can be measured as the level of the PSD signal above the noise level. Conversely, the amplitude cannot be visualized in such a simple way (it corresponds to the frequency integral of the Lorentzian profile), and retrieving it from the PSD requires the height to be converted into amplitude according to the relation $A = \sqrt{\pi \Gamma H/2}$ (for a single-sided PSD, e.g. Appourchaux et al. 2014). As a result, in order to have a reliable estimate of the amplitude, one should have at least a reasonable estimate of the FWHM. When H is used instead, the corresponding prior hyper-parameters can be set up without any complication, and independently of the value chosen for Γ. If uniform prior probability density functions are adopted (as it is done for our applications), the prior hyper-parameters for H can be set to zero for the lower limit, and to the maximum height measured from the region of the stellar PSD that contains the oscillation modes as the upper limit. The new islands peak bagging model therefore reads as

$$P_{\rm isla}\left(\nu, \Gamma; \nu_0, H\right) = \frac{H}{1 + 4\left(\frac{\nu - \nu_0}{\Gamma}\right)^2} \tag{1}$$

with ν_0 and H the free parameters specifying the frequency centroid and height, respectively, of the oscillation peak, and with Γ the FWHM to be fixed to a specific value, which changes depending on the level of resolving power that is needed to fit the stellar PSD (see Sect. 4.1 and 5.1 for more details). This is because fitting the islands peak bagging model to the PSD can be considered analogous to the effect obtained by smoothing the actual PSD signal at a resolution imposed by the FWHM of the Lorentzian profile.

2.2. Averaged Shifted Envelope Function

A second important improvement to the multi-modal approach is made in relation to the counts histogram (CH) originally introduced by C19. The CH represents the histogram built from the sampling obtained with DIAMONDS when applying the islands peak bagging model to the stellar PSD. This sampling is the set of points that was collected from the parameter space explored during the nested sampling process. The set of sampling points is sorted by increasing value of the likelihood function (Skilling 2004; Sivia & Skilling 2006), meaning that as the sampling evolves, i.e. the nested iteration increases, we approach more closely to better solutions. In C19 it was shown that the CH can be used to automatically extract the individual oscillation mode frequencies because each oscillation mode will pop up as a peak in the CH. However, using a simple CH as shown in Fig. 1 of C19 presents a couple of drawbacks: 1) it requires that the sampling obtained during the first iterations be removed because it is contaminated by the noise structures in the PSD; 2) it may be subject to fluctuations depending on how the sampling is distributed with respect to the choice of histogram bins,

hence with respect to the total number of bins, and to the actual density of the sampling for a given local maximum in the distribution. Here we propose a different tool that gets rid of the previous drawbacks, termed the averaged shifted envelope function (ASEF), which can be introduced with the following two steps:

1. In the first step, instead of computing a simple CH from the sampling, we obtain an averaged shifted histogram (ASH, Härdle et al. 2004), which already provides a more stable solution against fluctuations caused by the way the sampling points may fall into each bin. In the ASH, one considers the sum of the sampling point values (here represented by the values of the nested iterations they correspond to) falling in each bin, and shifts the bin position for a given number of realizations, thus averaging the different realizations into a single one at the end.
2. Although the ASH is more stable against the choice of the histogram bins, it can be affected by the noise structures that dominate the nested sampling at low values of the nested iterations and by the scarcity of the sampling in some regions of the parameter space. To overcome these problems, in the second step, instead of evaluating a standard ASH as explained in the first step, the value of the histogram at each bin is now taken as the maximum sampling value (in nested iteration) falling in the bin. The result is an averaged shifted histogram of the envelope function of the actual nested sampling obtained with DIAMONDS.

The resulting ASEF does not require any cut-off to be applied to the sampling at low values of the nested iterations, meaning that we can get rid of an extra configuring parameter of the multi-modal approach that was previously introduced by C19. The local maxima in the ASEF remain rather stable both in abscissa and ordinate position, even if one uses a different realization of the sampling (i.e. the fit is recomputed). This is of course a more ideal case for our purpose, since we aim at extracting the position of the different local maxima without the need to perform multiple islands peak bagging fits to have a stable solution. Another important advantage of the ASEF is that a local maximum in the sampling can be well reproduced even if the density of sampling points for that maximum is scarce as compared to that of the other maxima (see Fig. 1 for an example). Finally, the ASEF preserves the same scale and ordinate value as the nested iteration values obtained in the sampling, thus offering the possibility to make a direct comparison between ASEF and sampling distribution. In Fig. 1 we can see a comparison of these three different metrics for a pair of quadrupole and radial modes observed in a RGB star. Despite the peak on the right side being undersampled with respect to the peak on the left side (in this case because it falls closer to the edge of the frequency boundary), the final ASEF is providing the same amplitude for both peaks, as expected from the value of the nested iteration reached in the sampling. Conversely, the ASH and CH yield a much lower amplitude for the peak on the right side because they are based on the sampling counts, thus limiting the possible detection of the peak. In addition, the CH is clearly more affected by the presence of smaller structures in the sampling, hence it turns out to be less stable than the corresponding ASH.

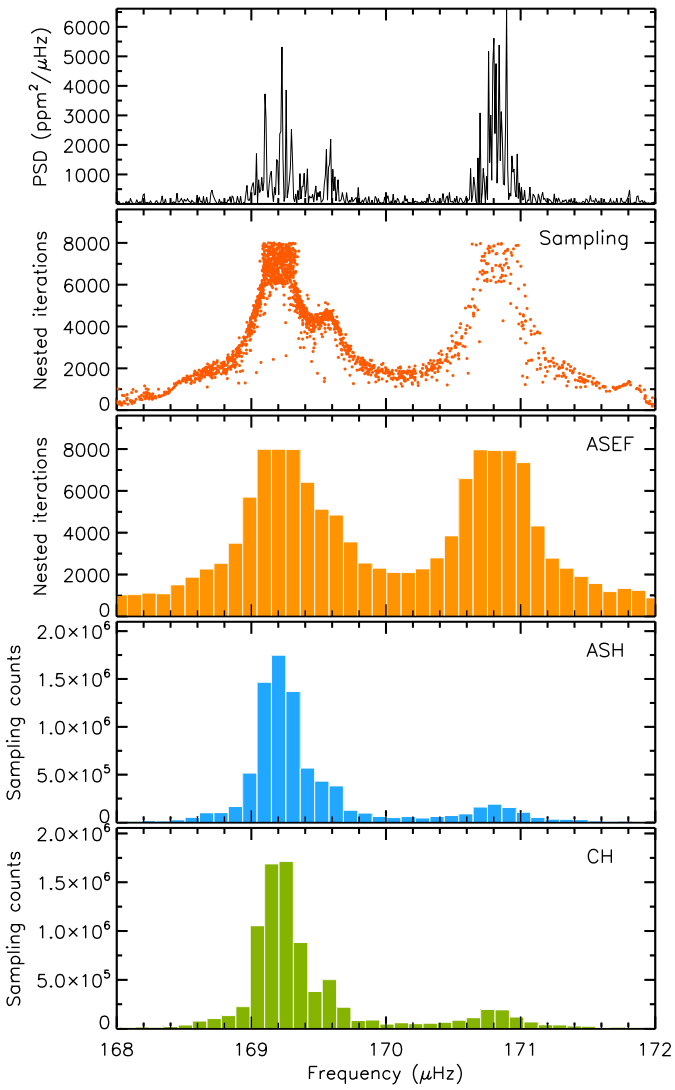

Fig. 1. The different histograms discussed in Sect. 2, computed from the multi-modal sampling obtained with DIAMONDS. The top panel depicts a portion of PSD of the RGB star KIC 12008916, where the $\ell = 2, 0$ mode pair can be clearly observed. The sampling from DIAMONDS is shown in the second panel. The resulting ASEF, ASH, and CH are shown in the bottom three panels, respectively. For the ASH and CH, the right peak is almost entirely suppressed because of the low number of sampling points.

3. FAMED pipeline

The FAMED (Fast and AutoMated pEak bagging with DIAMONDS) pipeline is a parallelized multi-platform free software aimed at performing the peak bagging analysis in low- and intermediate-mass stars that exhibit solar-like oscillations. This includes stars that range from the MS to RGs. This means that stars in the sub-giant (SG) phase of stellar evolution, as well as stars evolved towards the RGB tip, stars settled in the Helium-burning MS (or red clump, RC), and stars starting to evolve from the RC towards the asymptotic giant branch (AGB), can also be analyzed with this pipeline. In particular, FAMED extracts the characteristic oscillation mode properties of frequency, linewidth, and amplitude, and provides the corresponding mode identification and detection probability for each mode by means of a fast and fully automated procedure. FAMED exploits a combination of multi-modal and uni-modal fitting using DIAMONDS, and utilizes the free software

GNUparallel[2] (Tange 2011) to run the fits with parallel computing to improve its speed.

FAMED uses an input list of configuring parameters – with the most relevant ones introduced throughout the sections of this paper that describe the pipeline – that allows the general setup of the pipeline and the automated analysis of stars in different evolutionary stages by means of their general oscillation features. The pipeline is constituted by different modules, with modules being executed in a sequential order from the most basic up to the most detailed in an onion-like structure (see Table 1 for a summary). Each module of the pipeline performs a series of tasks, which are necessary to execute the subsequent modules. Each module aims at improving the level of detail, accuracy, precision, and reliability of the results obtained from the previous module. Finally, each module can be run separately from the others at any time, provided that the previous modules necessary for its execution have already been executed. This means that the pipeline can be run in a flexible manner, such that the user can decide where to stop depending on what kind of output is needed, and to resume later on an analysis that was stopped at a given level, in order to obtain further details.

Executing more modules of the pipeline is equivalent to adding up more layers in the analysis, which will also imply that the computation will become more time consuming. Table 1 lists an estimate of the time required to accomplish each module. Although the pipeline currently accounts for four modalities (or modules), the mandatory ones to produce usable outputs are the GLOBAL and CHUNK modalities. It is worth mentioning that one may already find interesting and useful what comes out of the GLOBAL modality alone (see Sect. 4). The ÉCHELLE and COMPLETE modalities are instead extra modules that the users may decide not to use, depending on their needs (see Table 1 for an overview of the pipeline outputs). In this work we will focus on the GLOBAL and CHUNK modalities only, while the extra modalities ÉCHELLE and COMPLETE will be presented in detail in a follow-up paper. The GLOBAL and CHUNK modalities contain the real novelty in the whole approach of peak bagging, which deserves a more extensive discussion, as already initiated in Sect. 2. By using the first two modalities of FAMED it is possible to process an entire star containing on the order of 100 oscillation modes, hence get most of the useful information contained in its asteroseismic dataset, not only in a fully automated manner but within just a few minutes of computation too (see Table 1). Figure 2 shows that the regime in which the GLOBAL and CHUNK modalities of FAMED are operating is low-dimensional, with DIAMONDS involved in computations running up to about 1 min only. The GLOBAL and CHUNK modalities therefore constitute the major strength of the FAMED pipeline. The GLOBAL and CHUNK modalities of FAMED are currently available in IDL, with a Python version already under development[3].

In the following sections we will present the necessary preparatory steps before running the pipeline. Then we will describe in detail the tasks accomplished by each of the first two modules, and how they are used to analyze stars in different evolutionary stages that have different oscillation features.

[2] GNUparallel is a shell tool that can be downloaded at https://www.gnu.org/software/parallel/.

[3] FAMED can be downloaded from the public GitHub repository https://github.com/EnricoCorsaro/FAMED. Installing documentation and tutorials are provided.

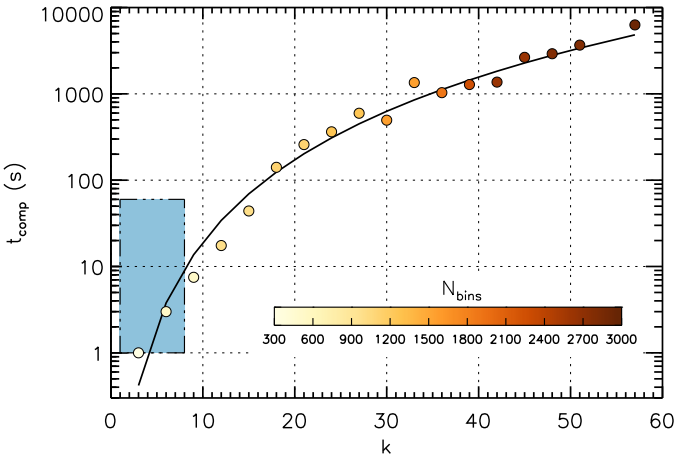

Fig. 2. The computational time t_{comp} to run a fit with DIAMONDS as a function of the number of free parameters k involved in the fit. The points correspond to the calibration performed by Corsaro et al. (2018) on the star KIC 12008916 using a 2.7 GHz single-core CPU. Each point is obtained from a uni-modal fit to the oscillation modes in the stellar PSD (see Sect. 3.4). The color of the points depicts the number of data bins involved in each computation, with the number increasing as the number of fitted oscillation modes increases (meaning a larger frequency range). The blue box represents the region where FAMED is operational when using the GLOBAL and CHUNK modalities, exploiting a low-dimensional ($1 \leq k \leq 8$), hence fast computation ($1 \lesssim t_{comp} \lesssim 60$ s) with DIAMONDS.

3.1. Estimating the background signal

It is important to point out that FAMED performs its analysis using only the original stellar PSD. While in some peak bagging applications one may decide to rely on a PSD normalized by a background level (e.g. Buysschaert et al. 2016), FAMED requires that the original signal, hence its statistics, are preserved. This is because FAMED performs model hypothesis testing aimed at assessing the significance of the oscillation modes above the level of the background. For this procedure to be reliable, as shown by Corsaro & De Ridder (2014) and by Corsaro et al. (2015a), one needs to incorporate the level of the background into the fitting models while keeping the statistics of the dataset unchanged. Therefore the user is required to perform a preliminary step before proceeding with the actual peak bagging analysis with FAMED. This step consists of estimating the background signal in the stellar PSD.

As presented by Corsaro et al. (2015a, 2017b), the background signal is typically modeled by a series of Harvey-like profiles, that account for granulation, meso-granulation, and low-frequency trends (including super-granulation, rotational modulation, and possible stellar activity), and by the instrumental noise level (either white noise or white and colored noise). To estimate the background, we recommend adopting the newest version of the Background code based on DIAMONDS[4], which is a free software (see also Corsaro 2018). In the new version of the Background code it is possible to switch from one background model to another, choosing from a series of models provided in the package that are commonly found in the literature (e.g. Kallinger et al. 2014). Once the background fit is

[4] The latest version of the Background code extension for DIAMONDS is available at the public GitHub repository https://github.com/EnricoCorsaro/Background.

Table 1. A summary of the different modules of the FAMED pipeline, with outputs and estimated computational time indicated. For the CHUNK and COMPLETE modalities the reported overall computational time refers to the analysis of a single chunk, where for one star several chunks can be present. The overall computational time is a reference time estimated by analyzing a four-years long *Kepler* dataset using FAMED on a 2.6 GHz 6-core CPU. The overall computational time is subject to vary depending on the system configuration, the data quality, and the complexity of each individual application.

Modality	Outputs	Overall computational time (min)
GLOBAL	Global oscillation frequencies and 1-σ uncertainties (n, ℓ) mode identification, with $\ell = 0, 1$ Global $\Delta\nu_{\rm ACF}$, $\Delta\nu_0$, ϵ, α_0 $N_{\rm chunks}$, frequency boundaries s_n for each chunk Flag for depressed dipole stars	1.0-2.0
CHUNK	Detailed oscillation frequencies and 1-σ uncertainties (n, ℓ) mode identification, with $\ell = 0, 1, 2, 3$ $m = 0, \pm1$ mode identification and $\cos i$ for peaks with detected rotation Local ϵ, $\delta\nu_{02}$, ΔP_1, Γ_0, Γ_3 Peak testing probabilities for detection, rotation, and duplicity Flags for peak blending and peak sinc^2 profile Frequency ranges $r_{a,b}$ and divisions $d_{a,b}$ for each oscillation frequency	0.2-1.0 per chunk
ÉCHELLE	$\Delta\nu_{\ell=0}$, $\delta\nu_{02}$, $\delta\nu_{01}$, $\delta\nu_{03}$, α_ℓ, $\beta_{0\ell}$, $\Delta\Pi_1$, q $m = 0, \pm1$ mode identification for all peaks in RGs and $\delta\nu_{\rm rot,core}$ for SG and RG Evolutionary stage (RGB vs. RC) Final validated list of oscillation modes	0.1-1.0
COMPLETE	$\ell = 0, 1, 2, 3$ frequencies with highest precision and accuracy Oscillation amplitudes and linewidths $\cos i$ and $\delta\nu_{\rm rot}$ for MS only Bayesian credible limits on all oscillation parameters	0.5-5.0 per chunk

completed, the FAMED pipeline will automatically read the resulting background outputs from Diamonds, and use the corresponding background level within its peak bagging analysis. It is however possible to feed in the background level estimated from a different fitting tool. Using a background fit from a different code than the Background code extension of Diamonds will not affect the correct functioning of FAMED, provided that the estimated background level is adequate for the dataset at hand. The only requirement is that any background fit to be used, must be provided in the form of a set of parameters that were estimated from the fit, according to one of the models that are currently implemented in the Background code (see its GitHub repository for more details). The actual background level adopted in the analysis will thus be generated by FAMED within its computation using the input parameters of the fitted model.

As previously mentioned, FAMED performs a number of model hypothesis tests based on the model comparison process with the Bayesian evidence, which is computed by Diamonds (see Sect. 5 for more details). We caution that this implies the background level adopted in the analysis should be quite accurate, especially in the region containing the oscillations. A poor background fit may hamper the quality of the model comparison process, yielding incorrect results in relation to the peak detection tests (Sect. 5.3) and the estimation of the peak amplitudes and linewidths (e.g. see the discussion in Corsaro & De Ridder 2014, Sect. 6.6).

3.2. General setup

When the pipeline is executed for the first time, it is necessary to have the PSD of the star and its background fit available. Ideally, the PSD of the star initially used by FAMED is the same that was used to fit the background level, which means that it covers a frequency range significantly larger than where the oscillation power excess is confined. FAMED will trim the input PSD using the frequency position of the Gaussian oscillation envelope, $\nu_{\rm max}$, and its standard deviation estimated from the background fit, thus preparing the folder that will contain all the outputs of the computation. The star folder created by FAMED is organized as shown in Fig. 3. In particular, the outputs are divided into groups, depending on the particular type of application that is performed.

3.3. Asymptotic fitting code

Within the analysis done by the GLOBAL modality, FAMED computes fits of the asymptotic relation of p modes (Tassoul 1980; Mosser et al. 2011; Lund et al. 2017) by means of Diamonds. Following the recent developments by Lund et al. (2017), we have implemented an asymptotic pattern for modes of angular degrees $\ell = 0, 1, 2, 3$ that incorporates the curvature term on the large frequency separation $\Delta\nu$, which we refer to as α_ℓ, and on the small frequency spacings $\delta\nu_{0\ell}$, which we term $\beta_{0\ell}$. In particular, the generalized asymptotic relation adopted here takes the form

$$\begin{aligned} \nu_{n\ell} \simeq \Delta\nu \left(n + \epsilon + \frac{\ell}{2}\right) + \\ \frac{\alpha_\ell \Delta\nu}{2} \left(n - \frac{\nu_{\rm max}}{\Delta\nu}\right)^2 - \\ \beta_{0\ell} \Delta\nu \left(n - \frac{\nu_{\rm max}}{\Delta\nu}\right) - \delta\nu_{0\ell} \, . \end{aligned} \tag{2}$$

where $\Delta\nu \equiv \Delta\nu_{\ell=0}$, and we have explicitly removed the dependency of α_ℓ and $\beta_{0\ell}$ on $\Delta\nu$, such that it is easier to set up their prior hyper-parameters for the fits. The asymptotic fits are performed by using a Gaussian likelihood function that takes the radial orders n as covariates, and as uncertainties those estimated on the observed frequencies, as obtained in Sect. 4.3. This is done by means of a new code extension of Diamonds, called Asymptotic, which has been made publicly available with the

publication of this paper[5]. The Asymptotic code allows ϵ, α_ℓ, and $\beta_{0\ell}$ to be treated as either fixed or free parameters. For example, if the condition $\alpha_\ell = \beta_{0\ell} = 0$ is used, the curvature terms on $\Delta\nu$ and $\delta\nu_{0\ell}$ of the asymptotic relation will be neglected during the fit. These features will be useful within the GLOBAL modality and will be discussed in Sect. 4.5. The ÉCHELLE modality is instead heavily based on the use the Asymptotic code, as it will be presented in a follow-up paper.

3.4. PeakBagging fitting code

A large and fundamental part of the analysis done by FAMED for the GLOBAL and CHUNK modalities (and for COMPLETE too) is through the PeakBagging code extension of DIAMONDS. This code has already been made available and updated by Corsaro & De Ridder (2014); Corsaro et al. (2015a); Corsaro (2018), but here we release a new version of it that incorporates some important additional features[6]. The new PeakBagging code can now be used in five different configurations:

1. Multi-modal fit: performs a multi-modal fit using either one or two Lorentzian profiles;
2. Sliding-pattern fit: performs a multi-modal fit using a mixture of Lorentzian profiles that are distributed in frequency according to the asymptotic pattern of p modes;
3. Peak-testing fit: performs uni-modal fits using a set of different peak testing models aimed at assessing the significance of the oscillation modes, the presence of blending between two adjacent modes, and the presence of rotational and duplicity effects;
4. Standard uni-modal fit: performs the standard uni-modal fit using a mixture of Lorentzian profiles;
5. Uni-modal fit with rotation: performs the uni-modal fit using a mixture of Lorentzian profiles with the rotational effect incorporated by using the additional free parameters of $\cos i$ and $\delta\nu_{\rm rot}$, for stellar spin-inclination angle and rotational splitting, respectively.

FAMED exploits a combination of all the different configurations provided by the PeakBagging code. In particular, configuration #1 was already presented by C19, and further discussed in Sect. 2 for the case of a single Lorentzian profile. The application of configuration #1 with two Lorentzian profiles is presented in Sect. 5.2. Configuration #2 is described in Sect. 4.4.1, while configuration #3 is addressed in Sects. 5.3 and 5.4. Lastly, configurations #4 and #5 will be discussed in a follow-up paper as they are used in the COMPLETE modality. A general description and application of configuration #4 can already be found in Corsaro & De Ridder (2014) and in Corsaro et al. (2015a).

4. The GLOBAL modality

The GLOBAL modality, or first module, is the most basic but most important module of FAMED. While subsequent modules, if wrongly performed for any reason, may affect only a small portion of the results, the GLOBAL modality, if not properly performed, will bias the entire analysis done by the pipeline, thus

[5] The Asymptotic code extension for DIAMONDS is available at the public GitHub repository https://github.com/EnricoCorsaro/Asymptotic.

[6] The latest version of the PeakBagging code extension for DIAMONDS is available at the public GitHub repository https://github.com/EnricoCorsaro/PeakBagging.

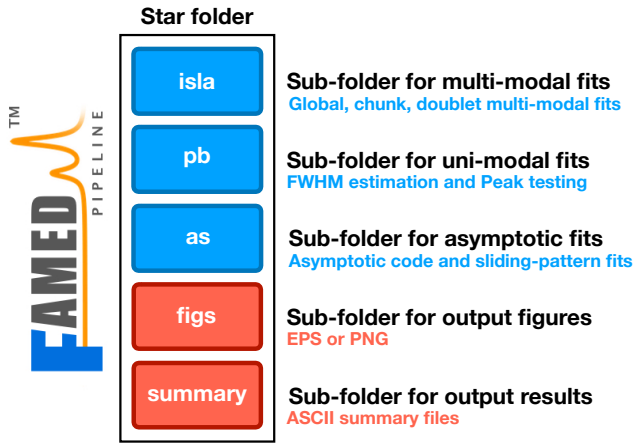

Fig. 3. A sketch of the folder content created by FAMED for each star analyzed.

all results produced will be wrong. It is therefore important to make sure that this modality is correctly executed from the very beginning. However, given that the GLOBAL modality is fast to be computed, it is quite straightforward to verify whether or not a bad result is produced.

The aim of the GLOBAL modality is to focus on the entire region of the PSD that contains the stellar oscillations and to give an approximate frequency position of the oscillation modes identified as $\ell = 0$ and as $\ell = 1$. This includes locating the frequency position of each chunk of PSD containing a pair of $\ell = 1, 0$ modes. If for some reason the oscillation mode pairs $\ell = 1, 0$ are wrongly identified (i.e. they are swapped), the chunk frequency boundaries will be affected, as well as the remainder of the analysis performed by FAMED. Executing the GLOBAL modality in a correct manner requires that the asymptotic terms $\Delta\nu$ and ϵ are properly estimated. To accomplish this task, the GLOBAL modality relies on two main parts, the multi-modal sampling and its subsequent analysis.

4.1. Global multi-modal sampling

In the first part of the GLOBAL modality, the multi-modal fit with DIAMONDS is performed using configuration #1 of the PeakBagging code by means of a single Lorentzian profile (see Sect. 3.4), over a frequency range that is centered around $\nu_{\rm max}$, as obtained from the background fit. The frequency range covers about 4-4.5$\sigma_{\rm env}$ on each side of $\nu_{\rm max}$ for MS, SG, and RG stars having $\Delta\nu > \Delta\nu_{\rm CL}$, 2.5$\sigma_{\rm env}$ for RGs having $\Delta\nu_{\rm tip} < \Delta\nu \leq \Delta\nu_{\rm CL}$, and 1.2$\sigma_{\rm env}$ for RGs having $\Delta\nu \leq \Delta\nu_{\rm tip}$. Here $\sigma_{\rm env}$ is the standard deviation of the Gaussian envelope of the oscillations that was obtained from the background fit, while $\Delta\nu_{\rm tip} = 3.2\,\mu$Hz and $\Delta\nu_{\rm CL} = 9\,\mu$Hz are set as configuring parameters of FAMED and are mainly based on the evolutionary stage classifications presented by Kallinger et al. (2012) (see Table 2). The additional constraint of having a range extending to at least 4.5$\Delta\nu$ on each side of $\nu_{\rm max}$ is used as well to make sure that even if $\sigma_{\rm env}$ is not sufficiently large (e.g. because the oscillation modes are highly peaked in the central region), the frequency range covered is still adequate to incorporate all the significant modes. In this initial part the large frequency separation $\Delta\nu$ is evaluated as a simple estimate from the $\nu_{\rm max}$-$\Delta\nu$ relation by Huber et al. (2011) (see Sect. 4.2 for more details). In this way it is possible to incorporate all useful information that can help in speeding up the analysis process, namely that the frequency range to inspect the

oscillations is narrowing as the star is evolving, going from MS stars that span about 20 radial orders, to stars placed towards the tip of the RGB, where up to only 3-4 radial orders are observable.

For performing the multi-modal fit in the GLOBAL modality of FAMED, the FWHM of the Lorentzian profile from Eq. (1) is fixed to a value obtained using one of two regimes, both requiring an input value of $T_{\rm eff}$:

- for $\nu_{\rm max} > \nu_{\rm max,thresh}$: Γ-$\nu_{\rm max}$-$T_{\rm eff}$ relation calibrated by Ball et al. (2018);
- for $\nu_{\rm max} \leq \nu_{\rm max,thresh}$: Γ-$T_{\rm eff}$ relations calibrated by Corsaro et al. (2015a).

with $\nu_{\rm max}$ given as input from the background fit and $\nu_{\rm max,thresh} = 300\,\mu$Hz set as a configuring parameter (see Table 2). The adopted linewidth relations provide an estimate of Γ for a radial mode. These relations are of course not definitive ones and can easily be updated from time to time in order to provide more accurate predictions of the oscillation linewidths for a wider range of input $\nu_{\rm max}$ and $T_{\rm eff}$. We note that having an accurate $T_{\rm eff}$ for the star to be analyzed is not a critical requirement for FAMED. We have tested that, in general, the entire analysis is not affected even if the input $T_{\rm eff}$ is off by up to about 200-300 K. For stars evolved towards the tip of the RGB and towards the AGB, having $\Delta\nu \leq \Delta\nu_{\rm tip}$, the FWHM of the islands peak bagging model is however further reduced by a factor 10 because of the very narrow peaks that are found in these cool targets.

This choice of Γ ensures that the oscillation envelope will be sampled at a resolution that is sufficiently high to distinguish $\ell = 2, 0$ mode pairs from $\ell = 1$ modes in stars from MS to RGs, but sufficiently low to avoid resolving the individual mixed modes in more evolved stars. This is done because in the GLOBAL modality our purpose is to only localize the positions of the $\ell = 2, 0$ pairs (with each pair approximated by a single $\ell = 0$ peak), and of the $\ell = 1$ peaks. In the case of stars with mixed modes, each $\ell = 1$ peak extracted from the GLOBAL modality is approximating the entire (or part of the) region of mixed modes between two adjacent $\ell = 0$ peaks. The top-left panel of Fig. 4 shows the resulting sampling from the GLOBAL modality performed on a MS star. The probing power of the global multi-modal sampling is already apparent from this example, where 31 different regions containing oscillation modes could be automatically extracted using just a single Lorentzian profile, the island peak bagging model presented in Sect. 2.1. The multi-modal fit is stored in the subfolder `isla`, as shown in Fig 3. We refer to this first multi-modal sampling as the *global multi-modal sampling* because it is performed for the GLOBAL modality.

The strength in performing a multi-modal sampling over the PSD is that, using a very simple and easy setup of the fitting model, it is able to recognize the presence of oscillation peaks without imposing any asymptotic pattern. This not only allows fitting stars in any evolutionary stage without the need to have a preliminary classification of their evolutionary stage, hence an a priori knowledge of their oscillation features, but to also automatically understand what kind of oscillation pattern we are dealing with based on how the multi-modal sampling is distributed over the frequency range.

4.2. Large frequency separation $\Delta\nu_{\rm ACF}$

Once the multi-modal fit is performed, the first task of the subsequent analysis is to use the global multi-modal sampling to measure the large frequency separation $\Delta\nu$. This parameter is of critical importance to analyze the oscillation features of the star because it is directly related to the stellar mean density (Ulrich 1986), and because it defines the characteristic frequency spacing of p modes in the asymptotic pattern (Tassoul 1980). The value of $\Delta\nu$, similarly to what is done in preparation of the global multi-modal sampling, is initially estimated by means of the $\nu_{\rm max}$-$\Delta\nu$ relation calibrated by Huber et al. (2011) and it is used as a raw guess. The multi-modal sampling is then converted into an ASEF, following the description presented in Sect. 2.2. The ASEF is first computed at high resolution, having $N_{\rm bins} = 800$. This high-resolution ASEF is used to evaluate a squared autocorrelation function (ACF^2) around the raw $\Delta\nu$ guess. The ACF^2 is then interpolated at a higher resolution and a Gaussian is fitted[7], whose centroid constitutes the final estimate $\Delta\nu_{\rm ACF}$. The right panel of Fig. 4 depicts an example of what was just described for the solar-type MS star KIC 12069424 (16 Cyg A), where the ACF^2 of the ASEF shows a very clear peak. This can be explained by the highly regular structures that are already visible in the multi-modal sampling obtained by Diamonds (Fig. 4 top-left panel) and in the obtained ASEF (visible in the bottom-left panel of the same figure), which shows the strength of using a multi-modal approach on the stellar PSD. The advantage of computing $\Delta\nu_{\rm ACF}$ from the high-resolution ASEF is that it turns out to be a reliable estimate of $\Delta\nu$ of the star (often accurate to well below 1 %), and that it is measurable both for noisy datasets and for evolved stars that have a complicated oscillation mode pattern (especially in the regimes from SG to RGs). This is because when computing the ASEF, one gets rid of the stochastic noise that is overlaid on the Lorentzian shape of each oscillation peak observed in the stellar PSD. As a result, the ASEF is significantly more sensitive to Lorentzian-like structures that can be present in the dataset, thus yielding a clearer signal to use for computing an ACF^2 than in the case of using the PSD itself.

4.3. Extracting oscillation frequencies and uncertainties

After measuring $\Delta\nu_{\rm ACF}$, the ASEF is recomputed at standard resolution, which in the GLOBAL modality is typically on the order of $N_{\rm bins} \approx 200$ for MS stars, and of $N_{\rm bins} \approx 100$ for RGs due to the smaller frequency range of their oscillation envelope. With the standard-resolution ASEF in hand, following what was explained by C19, we adopt a hill-climbing algorithm in order to locate the frequency position of each local maximum found above some input threshold. The input threshold is provided in percentage of ASEF units, i.e. nested iterations. We have found that an input threshold of 1 % is adequate for all applications involving the GLOBAL modality. Using this threshold implies that a local maximum can be located only if its ASEF amplitude is at least equal to 1 % of the ASEF global maximum (here corresponding to 8000 nested iterations) with respect to a neighboring local minimum.

4.3.1. Frequency divisions and ranges

The extracted local maxima from the ASEF represent our raw set of frequencies that will be used to obtain the final list of oscillation frequencies for the GLOBAL modality. Once the local maxima are identified, the next step consists of obtaining the so-called frequency *ranges*, $r_{a,b}$, and *divisions*, $d_{a,b}$, for each local

[7] The Gaussian fit to the interpolated ACF^2 incorporates a background term which is modeled by a second-degree polynomial. This allows obtaining a more stable and reliable fit even if the ACF^2 signal is more contaminated by noise.

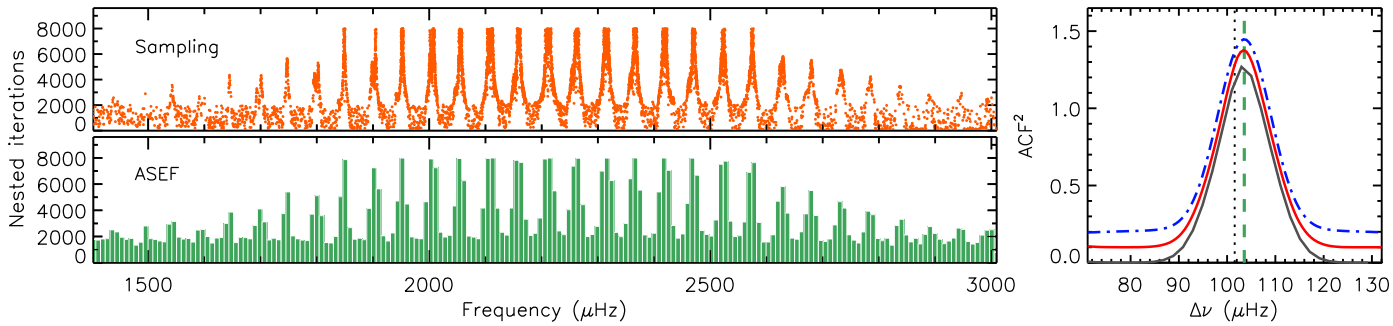

Fig. 4. Estimating $\Delta\nu_{\rm ACF}$ in the GLOBAL modality for the G-type MS star KIC 12069424. The top-left panel shows the resulting global multi-modal fit with DIAMONDS, with the rising of a clear regular structure in frequency, resembling the regular asymptotic pattern of p modes observed in the stellar PSD. The bottom-left panel represents the resulting ASEF, here in standard resolution for plotting purposes, which allows for the identification of 31 different local maxima. The right panel shows the ACF^2 (computed at the frequency resolution of the PSD) of the high-resolution ASEF (solid black line), the interpolated ACF^2 using a resolution higher than the PSD (about 100 bins in total, solid red line), and the final Gaussian fit to the interpolated ACF^2 (dot-dashed blue line). The red and blue curves have been offset by +0.1 and +0.2 in amplitude, respectively, for a clear visualization. The vertical dotted line represents the input $\Delta\nu$ guess from the $\nu_{\rm max}$-$\Delta\nu$ relation, while the vertical dashed green line is the final $\Delta\nu_{\rm ACF}$ taken as the centroid of the Gaussian fit.

maximum found in the ASEF. Both $r_{a,b}$ and $d_{a,b}$ are pairs of values (in frequency units) that define two different kinds of boundary around each local maximum, with the subscript a referring to the lower edge, and b to the upper edge of the boundary. For a given local maximum i having frequency ν_i, the frequency divisions are evaluated as

$$d_a^i = \frac{\nu_i + \nu_{i-1}}{2}$$
$$d_b^i = \frac{\nu_i + \nu_{i+1}}{2} \quad (3)$$

where ν_{i-1} and ν_{i+1} are the frequencies of the local maxima $i-1$ and $i+1$ respectively. Therefore the divisions are the midpoints between two adjacent local maxima. When either the previous or the next local maximum is not present because we are at the edge of the ASEF range, the division is set to the limit frequency of the ASEF range (either the minimum or the maximum frequency of the range).

The determination of the frequency ranges is instead more complicated, and it is initially done in two steps:

1. For a given local maximum, both left and right ranges are initially defined such that they correspond to the point on either side of the local maximum peak where the ASEF stops decreasing. The amount of decreasing ASEF values towards the tails of the local maximum peak is controlled by some tolerance, which in our applications of the GLOBAL modality corresponds to 1 % of the ASEF amplitude at the local maximum under consideration. The ranges so defined often provide a narrower boundary than that set by the divisions. This is because between two adjacent local maxima there could be a flat ASEF region, which will not be incorporated into a range. In any case, the ranges cannot exceed the divisions.
2. Using the ranges so computed, the sampling from DIAMONDS falling within each $r_{a,b}$ boundary is used to compute a weighted mean frequency value and a corresponding weighted 1-σ uncertainty. This is done using the squared value of the nested iteration of each sampling point as a weight (see the description by C19, Figure 2B). The estimated uncertainties and frequencies are then used to readjust the frequency ranges such that the range on each side of the frequency peak is falling between 1-σ and 2-σ uncertainty of the peak, and the frequency and its uncertainty are recomputed once again. This process is iterated two times to provide a range more closely centered around the peak, hence a more realistic uncertainty and accurate value of the final frequency. This range optimization procedure can however be tuned by changing the number of iterations and the number of times σ is used to define the lower and upper value of each range.

In this way, divisions, ranges, frequency estimates and their uncertainties are all extracted from the sampling and can be used for the subsequent analysis. The advantage of using frequencies and uncertainties estimated from the sampling is that they correspond to estimates computed from an actual fit to the PSD, even if obtained with a multi-modal approach. For the remainder of this paper we will refer to these estimated frequencies and their uncertainties as $\nu_{f,i}$ and $\sigma_{f,i}$, respectively, to avoid confusion with the frequencies corresponding to the local maxima of the ASEF, which we named ν_i in the first part of this section. The frequency uncertainties obtained here are used in the asymptotic fits done in the GLOBAL modality using the Asymptotic code extension of DIAMONDS (see Sect. 4.5.1).

The difference between divisions and ranges is depicted in Fig. 5 for three local maxima found in a portion of the ASEF of KIC 12069424. As it is evident, the ranges are significantly smaller than the divisions but both ranges and divisions are useful for different applications within the analysis performed by FAMED. This is especially true for the CHUNK modality, as we will discuss in Sect. 5. From the same figure, we can see that the local maxima ν_i and the estimated frequencies $\nu_{f,i}$ are in general different from one another, the latter being more accurate by definition. In addition, the local maxima do not come with any uncertainty, as this one is only a quantity estimated afterwards from the sampling itself once that the ranges are computed.

Finally, we recall that in the application of the GLOBAL modality the peaks corresponding to $\ell = 2$ modes are not resolved because of the small resolving power used to fit the PSD (see Sect. 4.1). As a result, the frequency $\nu_{f,i}$ initially estimated for an ASEF local maximum covering an $\ell = 2, 0$ mode doublet, is biased because it falls roughly halfway between the two power peaks of the doublet, as visible for example in the bottom panel

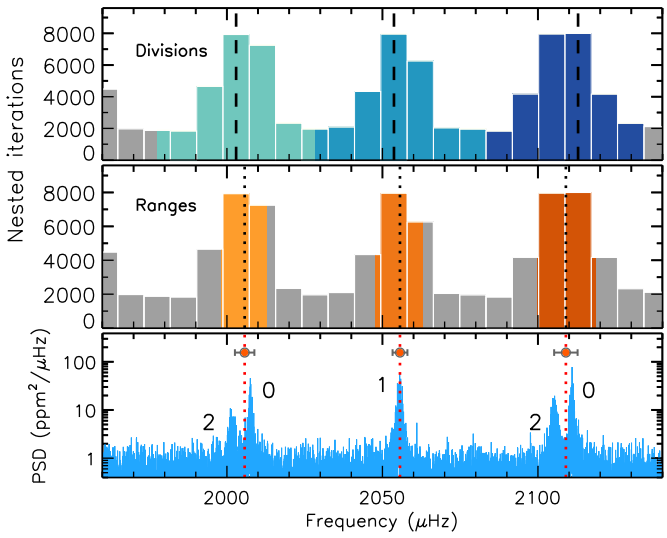

Fig. 5. Evaluation of frequency divisions and ranges, and of frequency estimates and uncertainties using the ASEF. The top and middle panels represent the standard-resolution ASEF evaluated from the GLOBAL modality for the MS star KIC 12069424, in a close-up view from the larger frequency range shown in Fig. 4. *Top panel*: the frequency divisions $d_{a,b}$ computed on three local maxima ν_i identified by the hill-climbing algorithm. The frequency interval defined by each pair of divisions is delimited using different blue-tone shading. The local maxima from the ASEF are indicated by vertical dashed lines. *Middle panel*: similar to the top panel but with the frequency ranges $r_{a,b}$ highlighted using orange-tone shading. The vertical dotted lines represent the frequencies $\nu_{f,i}$ estimated from the sampling (see Sect. 4.3.1) using the indicated frequency ranges. *Bottom panel*: the stellar PSD, with overlaid the frequencies $\nu_{f,i}$ (red bullets and vertical dotted lines) and corresponding 1-σ uncertainties $\sigma_{f,i}$ estimated using the frequency ranges from above. The frequencies corresponding to $\ell = 2, 0$ mode pairs are visibly offset with respect to the position of the corresponding $\ell = 0$ mode of each pair.

of Fig. 5. This bias is initially generated on purpose to obtain a first set of frequency estimates and a general mode identification with a high computational efficiency, but it is then improved in a later stage, as explained in Sect. 4.5.1.

4.4. Asymptotic phase term ϵ

At this stage, we have a list of frequencies $\nu_{f,i}$ that were estimated using the sampling from Diamonds. This list will contain frequencies that correspond to $\ell = 2, 0$ mode pairs (which for simplicity we will refer to as $\ell = 0$ or radial modes, for the GLOBAL modality), and frequencies that correspond to $\ell = 1$ (or dipole) mode peaks.

To distinguish between the different evolutionary stages presented it is necessary to have an estimate of the phase term ϵ of the asymptotic relation. As shown by White et al. (2011), in an échelle diagram ϵ sets the absolute position of each radial mode frequency. However, ϵ is not straightforward to obtain, especially during the MS and core-Helium-burning phase of stellar evolution, where it can be subject to large variation depending on the fundamental stellar properties of mass, temperature, metallicity (e.g. White et al. 2011), as well as on the thermodynamic state of the stellar convective envelope (Kallinger et al. 2012; Christensen-Dalsgaard et al. 2014). For our purposes it is useful to consider that in the regime of hot stars (F-type) ϵ follows a relatively tight relation with the stellar $T_{\rm eff}$, as shown by White et al. (2011) and by Lund et al. (2017), while for RGB stars ϵ can be reliably predicted by the ϵ-$\Delta\nu$ relation (Mosser et al. 2011; Kallinger et al. 2012; Corsaro et al. 2012). For solar-like oscillating stars in any evolutionary stage, one can compute ϵ by adopting the relation

$$\epsilon = \frac{\nu_0 \bmod \Delta\nu}{\Delta\nu} \tag{4}$$

which follows from evaluating the asymptotic pattern of radial modes in an échelle diagram. Here ν_0 is the frequency of the central radial mode of the star (the closest to $\nu_{\rm max}$). Given that $\Delta\nu$ is already known with good accuracy, computing ϵ requires that ν_0 is properly evaluated. This part of the analysis is particularly important for the rest of the computations performed by FAMED because the phase term ϵ uniquely sets the mode identification for each oscillation mode.

4.4.1. Sliding-pattern fit

Locating the central radial mode of the star is in general not straightforward because its position is related to the phase term ϵ, which has the effect of introducing a frequency offset in the asymptotic pattern that is given by the quantity $\epsilon\Delta\nu$. For a successful mode identification process, it is therefore important to obtain a reliable estimate of ϵ, which in turn implies that the central radial mode is correctly located. With this aim, we have developed the configuration #2 of the PeakBagging code (see Sect. 3.4), which allows fitting a so-called sliding pattern to the stellar PSD. The sliding pattern is a model defined as

$$\mathcal{P}_{\rm sliding}(\nu) = \mathcal{G}(\nu)\, R(\nu)\, [\mathcal{P}_{03}(\nu) + \mathcal{P}_{12}(\nu)] + \overline{B}(\nu)\ , \tag{5}$$

where $R(\nu)$ is the response function given by the sampling of the dataset (see Corsaro et al. 2015a, Eq. 2), and $\overline{B}(\nu)$ is the background level (fixed and without the Gaussian envelope) estimated from the background fit, and already incorporating the correction by the response function. The term $\mathcal{G}(\nu)$ is the unitary-height Gaussian used to modulate the peak heights in the sliding pattern according to $\nu_{\rm max}$ and the Gaussian envelope standard deviation estimated from the background fit. The terms $\mathcal{P}_{03}(\nu)$ and $\mathcal{P}_{13}(\nu)$ are defined as

$$\mathcal{P}_{03}(\nu) = \sum_{i=-(N_{\rm ord}-1)/2}^{(N_{\rm ord}-1)/2} \left[\mathcal{L}^i_0(\nu) + \mathcal{L}^i_3(\nu)\right], \tag{6}$$

and

$$\mathcal{P}_{12}(\nu) = \sum_{i=-(N_{\rm ord}-1)/2}^{(N_{\rm ord}-1)/2} \sum_{m=-\ell}^{\ell} \left[\mathcal{L}^i_{1m}(\nu) + \mathcal{L}^i_{2m}(\nu)\right], \tag{7}$$

while

$$\mathcal{L}^i_0(\nu) = \frac{H_0}{1 + \frac{4}{\Gamma_0^2}(\nu - \nu_0 - i\Delta\nu)^2}\ , \tag{8}$$

$$\mathcal{L}^i_{1m}(\nu) = \frac{H_0 V_1^2 \xi_{\ell \rm m}(\cos i)}{1 + \frac{4}{\Gamma_1^2}(\nu - \nu_0 - i\Delta\nu - \Delta\nu/2 + \delta\nu_{01} - m\delta\nu_{\rm rot})^2}\ , \tag{9}$$

$$\mathcal{L}^i_{2m}(\nu) = \frac{H_0 V_2^2 \xi_{\ell \rm m}(\cos i)}{1 + \frac{4}{\Gamma_0^2}(\nu - \nu_0 - i\Delta\nu + \delta\nu_{02} - m\delta\nu_{\rm rot})^2}\ , \tag{10}$$

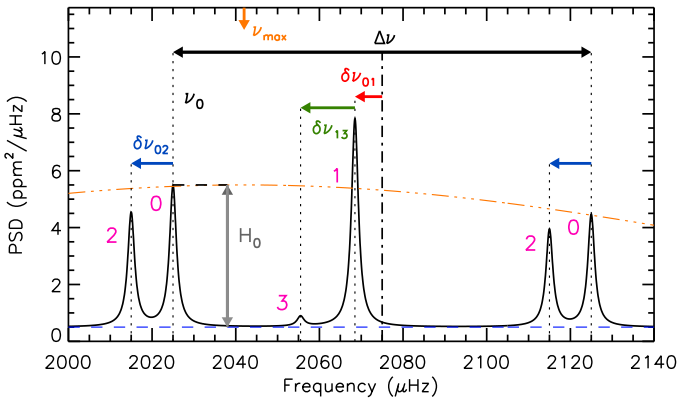

Fig. 6. A representative sliding-pattern model for a MS star, covering two consecutive radial modes. The pink numbers show the angular degree ℓ of each mode of the pattern. The free parameter ν_0 gives the location of the reference radial mode, while the frequency spacing parameters $\Delta\nu$, $\delta\nu_{02}$, $\delta\nu_{01}$, $\delta\nu_{13}$ are indicated by arrows. The vertical dotted lines mark the frequency position of each mode, while the vertical dot-dashed line is the midpoint between the two radial mode frequencies of the pattern. The free parameter specifying the radial mode height H_0 is indicated by a vertical gray arrow. The Gaussian envelope $\mathcal{G}(\nu)$, rescaled by H_0 to help in the visualization, is shown by the double dot-dashed orange line, with its centroid $\nu_{\rm max}$ indicated by the downward orange arrow. The horizontal dashed blue line is the background level estimated from the background fit. For illustration purposes, the sliding-pattern model depicted here is not including the rotational effect (i.e. $\cos i = 1$ or $\delta\nu_{\rm rot} = 0$).

$$\mathcal{L}^i_3(\nu) = \frac{H_0 V_3^2}{1 + \frac{4}{\Gamma_0^2}(\nu - \nu_0 - i\Delta\nu - \Delta\nu/2 + \delta\nu_{01} + \delta\nu_{13})^2} \quad , \quad (11)$$

are the Lorentzian profiles for $\ell = 0, 1, 2, 3$ modes, respectively, with the additional rotational effect incorporated only for the modes $\ell = 1$ and 2 through the term $\xi_{\ell m}(\cos i)$ (following the formulation by Gizon & Solanki 2003). This sliding pattern is tuned by up to eight free parameters, namely the already introduced ν_0, the corresponding radial mode height H_0, $\Delta\nu$, the small frequency spacings $\delta\nu_{02}$, $\delta\nu_{01}$, $\delta\nu_{13}$, the rotational splitting $\delta\nu_{\rm rot}$, and the inclination angle in the form of $\cos i$. The linewidth of the central radial mode, Γ_0, is instead fixed to a value predicted by the empirical relations already introduced in Sect. 4.1, and it is the same for each profile in the pattern, except for the dipole modes. Here we adopt the linewidth $\Gamma_1 \equiv \Gamma_0\eta_1$, which is thus related to Γ_0 through an input parameter η_1, termed dipole linewidth magnification factor. The term η_1, the number of radial orders to compute the sliding-pattern model, $N_{\rm ord}$, as well as the mode visibilities V^2_ℓ, are all provided as configuring parameters for the computation and are therefore not varied within the fit. An example of a sliding-pattern model not incorporating the rotational effect is shown in Fig. 6, where it can be seen how the different oscillation modes are located in frequency by combining ν_0 with the various frequency separations adopted.

The main free parameter of interest for the sliding-pattern model is ν_0, which controls the sliding of the entire pattern over the allowed frequency range. The choice of adopting the small frequency spacings to locate the non-radial modes of the pattern is essential for using the central radial mode as the only reference mode of the entire model. This in turn creates a multi-modal fitting problem, in an analogous manner as done for the multi-modal sampling at the beginning of the GLOBAL modality analysis. Similarly to the multi-modal fit performed in configuration #1, the sliding-pattern fit utilizes a high threshold as a stopping condition for Diamonds, which we have set to 4000 nested iterations in all our applications (see also the discussion in C19).

Fitting the sliding pattern to the PSD is a fundamental step for the GLOBAL modality, and has to be performed with care. The novelty of the sliding-pattern model is that it is highly configurable, where any of the free parameters ($\Delta\nu$, $\delta\nu_{02}$, $\delta\nu_{01}$, $\delta\nu_{13}$, $\delta\nu_{\rm rot}$, $\cos i$) can be arbitrarily fixed in order to either set any of them to a constant value or even completely remove one or more of them from the computation. For example, one could decide to fix the free parameter $\delta\nu_{01}$ to a constant value, meaning that the position of the dipole modes in the pattern is fixed with respect to that of the radial modes. Alternatively, it is possible to set $\delta\nu_{01}$ to a sufficiently large value (e.g. 99) in order to have the term $\mathcal{L}^i_{1m}$ completely removed from the pattern, which would therefore account for $\ell = 0, 2, 3$ modes only. A similar condition holds for the case of the rotation, where fixing $\delta\nu_{\rm rot}$ and $\cos i$ to either a constant or a sufficiently large value (e.g. 99) will either fix the shape of the rotational multiplets or completely remove the effect of rotation from the individual modes. We note that in this formulation the $\ell = 3$ modes do not incorporate the effect of rotation because of their low visibility.

Thanks to its flexibility, the sliding-pattern model can be used in different ways, depending on a very general identification of the evolutionary stage of the star. In the following we detail the different setup used to fit each type of star considered:

- For MS and early SG stars ($\Delta\nu_{\rm ACF} > \Delta\nu_{\rm thresh}$), we adopt the values $V_1^2 = 1.5$, $V_2^2 = 0.62$, and $V_3^2 = 0.07$ obtained by Lund et al. (2017), $\eta_1 = 1$, and $N_{\rm ord} = 7$ to adequately cover the large oscillation envelope of such stars;
- For late SG and RG stars ($\Delta\nu_{\rm ACF} \leq \Delta\nu_{\rm thresh}$), we adopt the values $V_1^2 = 0.7$, $V_2^2 = 0.8$, and $N_{\rm ord} = 3$ because of the smaller frequency range of the oscillations as compared to less evolved stars, with $\eta_1 = 5$ in late RGB stars. These values have been calibrated by testing the efficiency of the sliding-pattern fit on evolved stars.

We note that $\Delta\nu_{\rm thresh}$ is a configuring parameter of FAMED that for our applications has been tuned to 30 μHz. In the following we discuss how the sliding-pattern fit is applied by FAMED to stars in different evolutionary stages. The fits performed by Diamonds for the sliding pattern are all stored in the sub-folder `as` (Fig. 3). The mode visibilities adopted for evolved stars, V_1^2 and V_2^2, as well as the large value of η_1 for late RGB stars, are not to be intended as physically meaningful values but only as indicative quantities that were calibrated for obtaining a more stable solution from the sliding-pattern fit. All these values can be varied through the input configuring parameter list of the pipeline.

4.4.2. Main-sequence and early sub-giant stars

The oscillations in MS stars are characterized by a very regular pattern of p modes. As the star evolves into an early SG, the $\ell = 2, 0$ mode pairs remain regularly spaced, but some of the $\ell = 1$ modes start to undergo avoided crossings, thus becoming mixed modes (with up to two or even three mixed modes per radial order, in some cases), that is they do not follow the regular frequency pattern of p modes anymore (e.g. Benomar et al. 2013). For automatically distinguishing between the two regimes (MS vs. early SG), FAMED analyzes the regularity

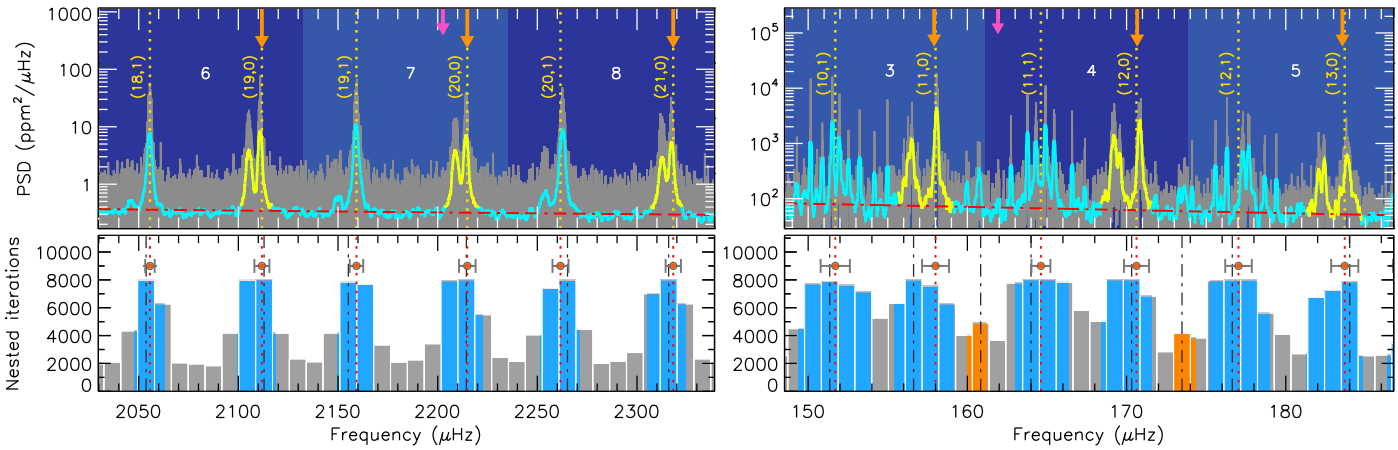

Fig. 7. The general mode identification, estimated oscillation frequencies, and chunk division of the GLOBAL modality. The left plots correspond to the MS star KIC 12069424, while the right plots are for the low-luminosity RGB star KIC 12008916. For both stars, a close-up to the region containing three PSD chunks centered around $\nu_{\rm max}$ is shown. *Top panels*: the stellar PSD (dark gray) in logarithmic scale with a smoothing proportional to $\Gamma_{\rm global}$ overlaid (thick cyan curve, with yellow chunks emphasizing the position of the $\ell = 2, 0$ pairs). The level of the background estimated from the background fit is shown by a horizontal dot-dashed red line. The vertical dotted yellow lines mark the frequencies $\nu_{f,i}$ resulting from the correction and skimming process (see Sect 4.5.1). The general mode identification (n, ℓ) automatically obtained for each $\nu_{f,i}$ (see Sect. 4.5) is indicated next to each frequency position. The orange downward-pointing arrows mark the asymptotic position of the radial modes, while the purple one shows the position of $\nu_{\rm max}$. The blue-shaded background (using alternate tonalities) indicates the different PSD chunks identified (see Sect. 4.6), with the individual chunk number (or chunk ID) shown in white. *Bottom panels*: ASEF showing the position of the local maxima ν_i from the hill-climbing algorithm (vertical dashed black lines, see Sect. 4.3). The blue-shaded regions mark the interval from the frequency ranges $r_{a,b}$ around each local maximum (see Sect. 4.3.1 and Fig. 5). The estimated frequencies $\nu_{f,i}$ shown in the top panels are indicated by vertical dotted red lines and red bullets, with their corresponding 1-σ uncertainties $\sigma_{f,i}$. The orange-shaded regions are delimited by the frequency ranges for those local maxima corresponding to the frequencies $\nu_{f,i}$ that were discarded during the skimming process.

of the frequencies $\nu_{f,i}$ that were previously extracted using the ASEF (see Sect. 4.3). The first step is to divide the set of $\nu_{f,i}$ frequencies falling within $\nu_{\rm max} \pm 2\Delta\nu_{\rm ACF}$ in two groups of odd and even frequencies. In the second step, for each frequency considered, the frequency modulo $\Delta\nu_{\rm ACF}$ is computed, and a median value for each group is obtained. In the third step, FAMED finds the maximum deviation (in units of $\Delta\nu_{\rm ACF}$) between the frequency modulo $\Delta\nu_{\rm ACF}$ and the median value in each of the two groups. If this deviation is larger than an input threshold, which we set to 6 % of $\Delta\nu_{\rm ACF}$ for our applications, the star is assumed to be an early SG. This approach is quite reliable because in the central regions of the oscillation envelope we have the highest signal-to-noise, and because the frequencies $\nu_{f,i}$ in this region are typically marking alternate positions of $\ell = 0$ and $\ell = 1$ mode peaks. For improving the chances to correctly classify stars that may contain two or three mixed modes per radial order as for SGs having $\Delta\nu$ closer to $\Delta\nu_{\rm thresh}$, the procedure described above is also performed in an analogous manner by dividing the set of estimated frequencies in three groups instead of two, with each group having as a starting frequency one offset with respect to the previous group by one step, and with each subsequent frequency taken every three steps. This helps in handling situations where the ASEF of the global multi-modal sampling is identifying two $\ell = 1$ mode peaks within the same radial order. An example of the result obtained from the GLOBAL modality by applying such classification procedure is depicted in Fig. 7 (left panels), where the pipeline was capable of correctly classifying the star as a MS just from the regularity of its $\ell = 1$ modes.

Once that the star has been assigned with a preferential classification according to the scheme presented above, FAMED proceeds with the setting up of the sliding-pattern model. For early SGs the sliding-pattern model: *i)* utilizes a $\Delta\nu$ fixed to the value of $\Delta\nu_{\rm ACF}$; *ii)* does not incorporate any $\ell = 1$ and 3 peaks; *iii)* does not account for rotation. These choices are motivated by the confusion created by the $\ell = 1$ mixed modes in the spectrum, which at the same time have linewidths comparable to those of the radial modes and may happen to fall close to, or even overlap with, the neighboring radial modes. Fitting an $\ell = 1$ peak using a regular spacing does not help in stabilizing the sliding-pattern fit in this case. Rotation and $\ell = 3$ peaks can be removed because they cannot be used to discriminate between $\ell = 1$ and $\ell = 0$ modes since the former ones are not included in the model. Moreover, it is necessary to fit the $\ell = 2$ modes through a varying $\delta\nu_{02}$ because this parameter can vary significantly from star to star in this regime (see White et al. 2011).

If the star is not classified as an early SG, then it is assumed to be a MS star. Here, despite the regular asymptotic pattern of p modes, we can find complications caused by the presence of rotation (if resolved by the observations), and by the large mode linewidths. A potential source of bias in the sliding-pattern fit could be when the star has a high spin-inclination angle, $\cos i = 0$. Here the dipole modes are split into doublets ($m = \pm 1$ components), which could create confusion with the adjacent $\ell = 2, 0$ mode pairs, thus potentially leading to the estimation of a wrong location of the central radial mode of the pattern. Including rotation on the $\ell = 1, 2$ modes, and an $\ell = 3$ peak too (which falls always to the left side of the $\ell = 1$ peak in this case) helps in getting rid of this potential degeneracy. On top of this, fitting a $\Delta\nu$, varied by ± 4 % with respect to the ACF value, further improves the stability of the fit even if the signal-to-noise ratio (SNR) is low. This can be explained by the wide frequency range covered by the sliding pattern (seven radial orders), over

which the separation between adjacent modes of different radial order could be subject to an appreciable variation. A similar condition to that mentioned for the early SG applies to MS stars in relation to the required fit of the $\delta\nu_{02}$ parameter, which is allowed to vary up to $\Delta\nu_{\rm ACF}/4$. In conclusion, the sliding-pattern for MS stars is fitted using the largest set of free parameters available for this model.

When MS stars are hot (F-type), with $T_{\rm eff} \geq T_{\rm eff,SG}$ (see Table 2 for the adopted value), even the most flexible sliding pattern may still provide a wrong result if used with low SNR conditions. This is caused by the large linewidths of hot stars, which in turn generate important blending effects on the oscillation peaks. A strong peak blending can prevent us from unambiguously distinguishing between a $\ell = 2, 0$ mode pair and a $\ell = 1$ mode peak (especially if split by rotation), which may look identical even to the most experienced eye (see also the example shown in Fig. 13). To overcome this, FAMED performs an additional check by comparing the ϵ value computed through Eq. (4) using ν_0 from the sliding-pattern fit, with ϵ obtained from a polynomial fit to the ϵ-$T_{\rm eff}$ sample estimates presented by Lund et al. (2017). If the mode identification calculated from the two values of ϵ coincides (i.e. the two ϵ values are very similar, see also Sect. 4.5), then the sliding-pattern fit is validated, otherwise the value of ϵ from the ϵ-$T_{\rm eff}$ relation is taken as the true ϵ of the star. Note that the value $T_{\rm eff,SG}$ is set as a configuring parameter of FAMED and can thus be varied, if needed.

4.4.3. Late sub-giant and red-giant stars

When a star has evolved into a late SG and RG, its oscillation pattern still presents $\ell = 2, 0$ modes regularly spaced by $\Delta\nu$, but at the same time it is populated by many dipolar mixed modes (with at least three or four of them in each radial order). Albeit the oscillation pattern is clearly more complicated than in MS and early SG stars, the advantage of having a high density of mixed modes is that one can still ignore the presence of a $\ell = 1$ peak in the pattern, thus fitting it in a similar way as done for early SG stars. This means that $\ell = 3$ modes and rotation are ignored as well. Another advantage of such evolved stars, contrary to the case of early SGs, is that the frequency position of the $\ell = 2$ mode peaks follows a tight relation with $\Delta\nu$ (Montalbán et al. 2010), meaning that $\delta\nu_{02}$ can be fixed to the asymptotic value given by the $\delta\nu_{02}$-$\Delta\nu$ relation calibrated by e.g. Corsaro et al. (2012). However, the curvature effects of the asymptotic pattern are in general more pronounced than in less evolved SGs, which calls for the need of fitting again $\Delta\nu$, here set to vary within ±4 % of the ACF value.

When the RG stars approach the RGB tip the oscillation pattern changes once again, a condition this one that we identify if $\Delta\nu_{\rm ACF} < \Delta\nu_{\rm tip}$. In this subclass of evolutionary stage, the number of dipole mixed modes that are observable in the PSD reduces to a single peak. The sliding-pattern model used to fit these stars therefore incorporates a $\ell = 1$ peak that, contrary to the case of MS stars, is set to have a large linewidth (with $\eta_1 = 5$ as already mentioned), but using a frequency centroid that is fixed from the $\delta\nu_{01}$-$\Delta\nu$ relation found by Corsaro et al. (2012), which incorporates a mass dependency as well. Any $\ell = 3$ peaks and the effect of rotation are removed because useless.

Despite ϵ following a relatively tight relation with $\Delta\nu$ for RGB stars, ϵ for RGs evolving into the Helium-burning MS has the tendency to be lower than the value predicted from the ϵ-$\Delta\nu$ relation in a way that is difficult to accurately predict (see in particular the observational results by Kallinger et al. 2012; Corsaro et al. 2012). This further motivates the choice of performing a sliding-pattern fit for evolved stars to measure their true ϵ. If requested by the user, for low-luminosity RGB and late SG stars (which we have identified as fulfilling the condition $\Delta\nu_{\rm CL} \leq \Delta\nu_{\rm ACF} \leq \Delta\nu_{\rm thresh}$) FAMED can however perform an additional check against the ϵ-$\Delta\nu$ relation calibrated by Corsaro et al. (2012) to make sure that the sliding-pattern fit yields a reliable result. This can be useful especially in low SNR or frequency resolution conditions. In addition, the user has the possibility to set the frequency of the reference radial mode ν_0 as an input value, which will be used internally by FAMED to evaluate ϵ from Eq. (4). This latter case could be exploited for very challenging datasets where the automated solutions offered by the pipeline may not be accurate enough to correctly identify the position of the radial modes. The advantage of this latter option is that the input central radial mode frequency has not to be very accurate, meaning that a simple visual inspection can perfectly suffice.

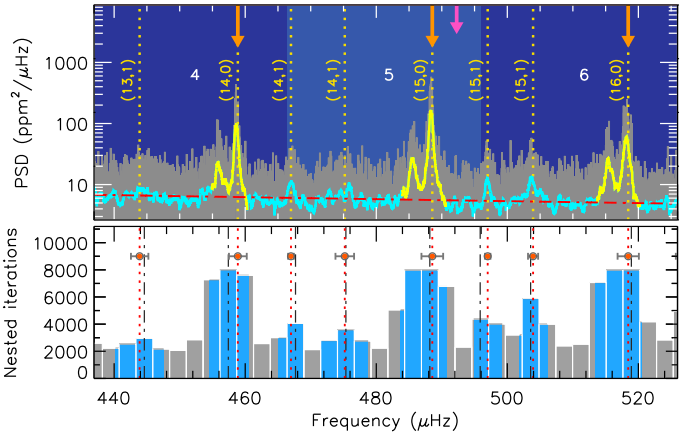

Fig. 8. Similar description as for Fig. 7 but for the depressed dipole SG star KIC 8561221. The peaks associated to dipole modes with depressed amplitudes exhibit an ASEF local maximum below 3/4 of the maximum nested iteration allowed, the latter set to 8000.

We summarize the effect of performing a sliding-pattern fit on a low-luminosity RGB star in Fig. 7 (right panels), where it is visible that the central $\ell = 0$ mode, closest to $\nu_{\rm max}$, has been properly located in the PSD.

4.4.4. Depressed dipole stars

Another interesting class that ought to be investigated is that of stars having depressed dipole mode amplitudes (García et al. 2014b; Stello et al. 2016; Mosser et al. 2017). These stars are found from the SG phase up to the RC, and exhibit a peculiar oscillation spectrum where the power corresponding to the regions of the dipole modes is significantly reduced with respect to what is expected for a standard star having similar $\nu_{\rm max}$. While the origin of this phenomenon is still under debate (e.g. Fuller et al. 2015; Mosser et al. 2017), as shown by Stello et al. (2016) these stars are not rare, especially in the intermediate-mass range, and it is therefore useful to have the opportunity to perform a peak bagging analysis even on such type of peculiar targets.

Given that the PSD of depressed dipole stars is mostly characterized by the presence of $\ell = 2, 0$ modes, FAMED checks whether there is a sufficiently large number (50 %) of estimated frequencies from the central region of the oscillation envelope, within $\nu_{\rm max} \pm 2\Delta\nu_{\rm ACF}$ for $\Delta\nu_{\rm ACF} > \Delta\nu_{\rm thresh}$ and within $\nu_{\rm max} \pm \Delta\nu_{\rm ACF}$ for $\Delta\nu_{\rm ACF} \leq \Delta\nu_{\rm thresh}$, that have ASEF values well

below the maximum nested iteration allowed in the global multimodal sampling (< 3/4). If this happens, then the star is flagged as a potential depressed dipole star. In this condition, if the star has $\Delta\nu_{\rm ACF} \leq \Delta\nu_{\rm thresh}$ the sliding-pattern model uses the same setup as for stars in the same $\Delta\nu$ range (Sect. 4.4.3). Otherwise the sliding pattern is set up in a similar way as for the early SGs (Sect. 4.4.2), with the difference that $\Delta\nu$ now varies within ±4 % instead of being fixed to the ACF value. This allows to better sample the position of the $\ell = 2, 0$ mode regions because the $\ell = 1$ modes are now missing or very low in power in the PSD, and are therefore not a source of power contamination for modes of different angular degree.

An example of the analysis of a depressed dipole star is illustrated in Fig. 8, where we can see that in most cases the ASEF peaks associated to potential $\ell = 1$ modes are significantly smaller in height (hence suppressed) with respect to those of the $\ell = 0$ modes, and always below 3/4 of the maximum nested iteration. In this case, FAMED could successfully classify the star as a depressed dipole star just by using the frequencies estimated from the ASEF, thus allowing to subsequently apply the sliding-pattern fit configuration described earlier in this section.

4.5. General mode identification

Once ϵ has been correctly evaluated using Eq. (4), and having ν_0 estimated from the sliding-pattern fit, one can couple them with $\Delta\nu_{\rm ACF}$ to obtain an automated mode identification that provides the angular degrees $\ell = 1, 0$ and radial order n for each frequency extracted from the ASEF. For this purpose, our starting point is to consider the asymptotic relations

$$\nu_{n0} \simeq \Delta\nu\,(n + \epsilon) + \frac{\alpha_0 \Delta\nu}{2}\left(n - \frac{\nu_{\rm max}}{\Delta\nu}\right)^2 , \tag{12}$$

for the radial modes and

$$\nu_{n1} \simeq \Delta\nu\left(n + \frac{1}{2} + \epsilon\right) + \frac{\alpha_0 \Delta\nu}{2}\left(n - \frac{\nu_{\rm max}}{\Delta\nu}\right)^2 - \delta\nu_{01} , \tag{13}$$

for the dipole modes, where in the latter we have removed the curvature term on the small spacing, controlled by the parameter β_{01} (see Eq. 2), and adopted the same α_0 as for the radial modes. These choices are justified because the frequencies $\nu_{f,i}$ we are dealing with in the GLOBAL modality are less accurate and precise than those that will be derived in the CHUNK modality. Since we do not have an a priori estimate of β_{01} to include in the asymptotic relation for dipole modes, and because this term is small compared to the other terms that we considered, it can be neglected without affecting the mode identification process. By inverting Eq. (12) and Eq. (13) and by replacing the asymptotic frequency predictions ν_{n0} and ν_{n1} with a generic estimated frequency $\nu_{f,i}$, we can obtain two different estimates for ϵ, namely

$$\epsilon_0 \simeq \frac{\nu_{f,i} - \Delta\nu\left[n + \frac{\alpha_0}{2}\left(n - \frac{\nu_{\rm max}}{\Delta\nu}\right)^2\right]}{\Delta\nu} \tag{14}$$

and

$$\epsilon_1 \simeq \frac{\nu_{f,i} - \Delta\nu\left[n + \frac{1}{2} + \frac{\alpha_0}{2}\left(n - \frac{\nu_{\rm max}}{\Delta\nu}\right)^2\right] + \delta\nu_{01}}{\Delta\nu} . \tag{15}$$

For a given input frequency $\nu_{f,i}$ (which could correspond to either a radial or a dipole mode), the associated radial order n_i is found as the one minimizing the difference $|\epsilon_0 - \epsilon|$ (out of a set of possible n values), with ϵ being the value obtained from the sliding-pattern fit (see Sect. 4.4.1) and ϵ_0 given by Eq. (14). The radial order evaluated with this method will be correct even if $\nu_{f,i}$ corresponds to a dipole mode. The angular degree ℓ is subsequently obtained as follows: *i)* the radial order n_i that was found is used to compute the reference values ϵ_0 and ϵ_1 through Eq. (14) and Eq. (15). The value of $\delta\nu_{01}$ used in Eq. (15) is set to the one obtained from the sliding-pattern fit in the case of MS stars as identified following Sect. 4.4.2, to the asymptotic value from the $\delta\nu_{01}$-$\Delta\nu$ relation for stars having $\Delta\nu < \Delta\nu_{\rm tip}$, and to zero otherwise; *ii)* the differences $\delta\epsilon_0 = |\epsilon_0 - \epsilon|$ and $\delta\epsilon_1 = |\epsilon_1 - \epsilon|$ are computed, with ϵ again the input value from the sliding-pattern fit; *iii)* if $\delta\epsilon_0 < \delta\epsilon_1$ then the input frequency $\nu_{f,i}$ is better approximated by a radial mode frequency, hence it is flagged as a $\ell = 0$ mode, otherwise it is flagged as a $\ell = 1$ mode. This procedure is initially performed by setting $\alpha_0 = 0$ in both Eq. (14) and Eq. (15) because its value is not known at the beginning.

The set of estimated frequencies $\{\nu_{f,i}\}$ is thus divided in two groups, namely those flagged as $\ell = 0$ and those identified as $\ell = 1$. In this subdivision, the radial modes are the most important ones for the GLOBAL modality. This is because the radial modes always fulfill the regular frequency pattern of p modes (at least to first approximation) independent of the evolutionary stage of the star. Conversely, the pattern of $\ell = 1$ modes can change significantly when stars evolve off the MS. Whether or not the dipole mode peaks are initially identified in a proper way is not a necessary condition for obtaining a successful analysis in the GLOBAL modality. This is because dipole modes are analyzed in detail in the CHUNK modality of FAMED, as it will be discussed in Sect. 5. An example of the general mode identification obtained by FAMED is illustrated in Figs. 7, 8, where we can see that all the radial modes have been correctly identified. For the SG star showing depressed dipole modes, albeit some of the PSD peaks have been identified as $\ell = 1$ modes in the GLOBAL modality, they will be converted to $\ell = 3$ modes with the CHUNK modality (see the application presented in Sect. 6.4 for the same star).

4.5.1. Improving the set of estimated frequencies

Although the general mode identification (n, ℓ), with $\ell = 0, 1$, presented in Sect. 4.5 can be applied to any of the frequencies in our set $\{\nu_{f,i}\}$, these frequencies may not always correspond to real oscillation modes or to oscillation modes that can be deemed significant. The general mode identification process does not recognize whether the given frequency is actually following the asymptotic pattern or not, with a pair (n, ℓ) being assigned in any case. For example, there could be two frequencies $\nu_{f,i}$ flagged as radial modes within the same radial order, if for some reason (such as the presence of a neighboring dipole mixed mode) the ASEF has produced more than one local maximum in a region containing the real $\ell = 0$ mode. To overcome this issue it is necessary to apply a skimming process on the set $\{\nu_{f,i}\}$ in a way that spurious frequencies can be identified and removed from the list, and that only good radial mode frequency candidates are left by the end of the analysis performed by the GLOBAL modality. The entire process of the general mode identification is thus optimized as follows:

1. once all the input frequencies $\nu_{f,i}$ have been flagged as either $\ell = 0$ or $\ell = 1$ for the first time, according to the methodology presented in Sect. 4.5, a correction to the frequencies identified as radial modes is applied. As already mentioned at the end of Sect. 4.3.1, the frequencies $\nu_{f,i}$ associated to the radial modes are initially biased because they correspond to

$\ell = 2, 0$ mode pairs in the PSD rather than to single $\ell = 0$ mode peaks. The correction $\delta\nu_0$ on the radial mode frequencies is usually a positive term (because a $\ell = 2, 0$ mode pair is biasing a corresponding $\nu_{f,i}$ frequency identified as $\ell = 0$ towards lower frequencies, see Fig. 5). This correction is defined as $\delta\nu_0 = \nu_0 - \nu_{0,f}$, where ν_0 is the reference radial mode frequency obtained from the sliding-pattern fit, as described in Sect. 4.4.1, while $\nu_{0,f}$ is its closest radial mode frequency from the set $\{\nu_{f,i}\}$. For each radial mode frequency $\nu_{f,i}$, the corrected one is evaluated as $\nu_{f,i} = \nu_{f,i} + \delta\nu_0$. If no result from the sliding-pattern fit is used, then $\delta\nu_0 = 0$;
2. the asymptotic frequency predictions ν_{n0} for the estimated frequencies $\nu_{f,i}$ flagged as $\ell = 0$, are computed by means of the asymptotic patterns given by Eq. (12) by imposing $\alpha_0 = 0$ (in the first iteration);
3. using the asymptotic frequency predictions ν_{n0} for all the radial mode frequencies in the set $\{\nu_{f,i}\}$, the differences $\delta\nu_{0,i} = |\nu_{f,i} - \nu_{n0}|$ are evaluated for each radial mode frequency available;
4. if for a given $\nu_{f,i}$ flagged as $\ell = 0$, its $\delta\nu_{0,i}$ is below an input tolerance threshold, then the frequency is kept in the list of extracted frequencies, otherwise it is temporarily removed. The input tolerance threshold is given in units of $\Delta\nu$ and in our applications it has been set to 18, 20, 25% for MS, SG and RG stars, respectively;
5. if more than one $\nu_{f,i}$ is flagged as a $\ell = 0$ mode with the same radial order n, then the one that is closer in frequency to the corresponding prediction from Eq. (12) is picked up. The other frequency is temporarily discarded from the $\{\nu_{f,i}\}$ set. This step is mandatory because only a maximum of one radial mode frequency for each radial order can be allowed according to the asymptotic theory of the oscillations;
6. using the corrected and skimmed $\ell = 0$ frequencies obtained from the previous steps, as well as their corresponding radial orders n_i and uncertainties $\sigma_{f,i}$ – obtained from the frequency ranges introduced in Sect. 4.3.1 – the Asymptotic code based on Diamonds is adopted to fit the asymptotic pattern of radial modes. The asymptotic fit now incorporates the curvature term α_0 as a free parameter, while ϵ is fixed to the value given by the sliding-pattern fit. In this way a more accurate estimate of $\Delta\nu$ than $\Delta\nu_{\rm ACF}$ is obtained, which we refer to as $\Delta\nu_0$ (see also Table 1). The asymptotic fit results are stored in the sub-folder `as` (Fig. 3);
7. the general mode identification is computed once again using the new set of estimated frequencies (corrected and skimmed) and adopting the values of $\Delta\nu_0$ and α_0 that were obtained from the asymptotic fit;
8. all the steps from #1 to #7 are repeated by re-starting each time from the original set of frequencies $\nu_{f,i}$ (uncorrected and unskimmed) in order to progressively improve the set, and for obtaining more reliable estimates of $\Delta\nu_0$ and α_0. In particular, step #2 is subsequently performed by imposing the values of α_0 obtained from the asymptotic fit performed on step #4 of the previous iteration.

The number of iterations to skim the actual set of frequencies can be tuned from a configuring parameter of FAMED, and is set to two for all our applications. In this way the estimated frequencies originally obtained as in Sect. 4.3.1 are compared to progressively more accurate asymptotic predictions, so that in the end the skimming process becomes more reliable than if not iterating. An example of the effect of the skimming process can be seen in the ASEF plotted in the bottom-right panel of Fig. 7. Here the ASEF corresponds to the PSD of a low-luminosity RGB, where the oscillation pattern is clearly more complicated than in the case of the MS star shown on left side of the same figure. For the RGB star two of the frequencies extracted from the ASEF in the selected frequency range – indicated by the regions marked with orange shading – are not retained in the final set of estimated frequencies. This is because these two frequencies, initially identified as radial modes because of their proximity to adjacent radial modes, despite possibly corresponding to real oscillation modes (in this case dipole and octupole modes), do not match the limiting threshold condition imposed at step #4 of the skimming process.

We note that by increasing the tolerance threshold used to skim the set of frequencies with subsequent evolutionary stages (step #4 of the skimming process), the overall result improves. This is because for more evolved stars, the curvature α_0 of the asymptotic pattern becomes more important, and because the actual multi-modal sampling from Diamonds is more irregular than in the case of MS stars due to the presence of mixed modes (e.g. see the right panels of Fig. 7). Choosing an appropriate value of the tolerance threshold for the frequency skimming requires the star to be classified based on its evolutionary stage. Since the stellar evolutionary stage is not known a priori, in the GLOBAL and CHUNK modalities FAMED distinguishes between MS, SG, and RG stars based on a combination of input thresholds on $\Delta\nu$ and $T_{\rm eff}$ (see Table 2 for a summary), namely:

- MS stars are identified by having either $\Delta\nu \geq \Delta\nu_{\rm SG}$ or at the same time $\Delta\nu_{\rm RG} \leq \Delta\nu \leq \Delta\nu_{\rm SG}$ and $T_{\rm eff} \geq T_{\rm eff,SG}$;
- SG stars are identified by having at the same time $\Delta\nu_{\rm RG} < \Delta\nu \leq \Delta\nu_{\rm SG}$ and $T_{\rm eff} < T_{\rm eff,SG}$;
- RG stars are identified by having $\Delta\nu \leq \Delta\nu_{\rm RG}$.

The thresholds used for MS and SG regimes are based on the $\Delta\nu$-$T_{\rm eff}$ diagram presented by Appourchaux et al. (2012) (see their Fig. 4), while that of RGs represents an approximated value of $\Delta\nu$ where the stars start to exhibit at least three or four mixed modes per radial order. This classification is of course simple and schematic, and is not intended to provide the real evolutionary stage of the star. For example, stars classified as SGs but having $\Delta\nu$ close to $\Delta\nu_{\rm RG}$ (e.g. < 20-30μ Hz) could already be early RGB stars. However, the adopted classification scheme can be used by FAMED to apply some general constraints on the expected stellar oscillation features that significantly improve the overall analysis and computational efficiency. The thresholds on $\Delta\nu$ presented here are not definitive values and can be changed by the user in the list of configuring parameters for the pipeline.

After the skimming process is completed, the subset of estimated radial mode frequencies $\nu_{f,i}$ is replaced by the corresponding asymptotic predictions in order to obtain more accurate positions of the radial orders in the stellar PSD (see Sect. 4.6 below, and Figs. 7, 8). This usually leads to an improvement that is more evident towards the tails of the Gaussian envelope of the oscillations, where the ASEF peaks become smaller in amplitude and the contamination from neighboring mixed modes (if any) and/or noise peaks is more pronounced.

4.6. Finding the chunks

The final task performed by the GLOBAL modality is to estimate the frequency separations s_n that set the boundaries for each radial order n in the PSD of the star. This is a necessary step prior to running the CHUNK modality, where chunks will be analyzed individually. More precisely, these separations delimit chunks of PSD, each one containing a single pair of $\ell = 0, 1$ modes. Each chunk is therefore approximately as wide as $\Delta\nu$

Table 2. Main configuring parameters of FAMED that are adopted for the peak bagging applications presented in this work. The left column shows the parameter name, while the right column lists its value. Each of these parameters can be tuned by the user from an input configuring parameter file.

Configuring parameter	Value
$\nu_{\rm max,thresh}$	$300\,\mu$Hz
$\Delta\nu_{\rm thresh}$	$30\,\mu$Hz
$\Delta\nu_{\rm tip}$	$3.2\,\mu$Hz
$\Delta\nu_{\rm CL}$	$9\,\mu$Hz
$\Delta\nu_{\rm RG}$	$15\,\mu$Hz
$\Delta\nu_{\rm SG}$	$90\,\mu$Hz
$T_{\rm eff,SG}$	6350 K

but contains modes having different radial orders, depending on their actual angular degree (see below). The number of chunks contained in the stellar PSD, $N_{\rm chunks}$, is uniquely estimated from the difference between the maximum and minimum radial order found from the skimmed frequency set.

To locate the frequency position of each chunk, the radial mode asymptotic frequencies are computed from Eq. (12) for each radial order covered by the set of frequencies $\nu_{f,i}$. The upper frequency boundary (or upper separation) of each chunk is thus given by the asymptotic frequency of the radial mode plus a fraction of $\Delta\nu$, which is set to 20% for MS stars, and to 25% for SG and RGs (but this value can be tuned as well). The larger range in evolved stars is motivated by their more pronounced curvature effects in the asymptotic pattern of p modes. The curvature effect could make the predicted position of the radial mode frequencies less accurate towards the tails of the Gaussian envelope of the oscillations.

The upper separation of a given chunk will correspond to the lower separation of the subsequent chunk, with the first and last chunk of the PSD being defined by the minimum and maximum frequency of the PSD range, respectively. In the way chunks are defined, the estimated frequencies contained inside a chunk corresponding to the radial order n will thus comprise one $\ell = 0$ frequency of radial order n, and one or more $\ell = 1$ mode frequencies of radial order $n - 1$ (thus placed to the left side of the radial mode). For evolved stars one could in general expect to have more than one $\ell = 1$ mode frequency identified in a single chunk. Figure 7 (top panels) shows an example of the chunk division obtained in both a MS and a RG star in a frequency range covering three radial orders around $\nu_{\rm max}$, while Fig. 8 (top panels) shows the same process but for a SG star that has depressed dipole modes.

Each chunk will be identified by its frequency separations even if no $\ell = 0$ and/or $\ell = 1$ modes have been found in it. This is possible because the evaluation of the chunk separations is based on the asymptotic radial mode frequencies, which are in turn computed for all radial orders from the minimum to the maximum of the frequency range considered, independent of whether or not we identify a $\ell = 0, 1$ frequency from the ASEF. To understand this feature, let us suppose we have three radial orders from the general mode identification covered by a set of $\ell = 0$ frequencies $\nu_{f,0}$, $\nu_{f,1}$ and $\nu_{f,2}$, which have radial order $n - 1$, n, and $n + 1$, respectively. If the frequency $\nu_{f,1}$, corresponding to the central radial order of the set, is removed during the skimming process because is does not adequately fulfill the expected asymptotic pattern, we end up with the frequencies $\nu_{f,0}$ and $\nu_{f,2}$, corresponding to radial orders $n - 1$ and $n + 1$. This means that the radial mode of the central radial order is not kept in our list of radial modes. Nonetheless, when the chunks are identified, it is still possible to analyze the chunk corresponding to the central radial order of our example, and it is still possible to locate the $\ell = 0$ mode of the chunk during the CHUNK modality. The minimum condition to analyze the chunk, however, is that it contains at least one frequency from the GLOBAL modality, i.e. at least one $\ell = 0$ or $\ell = 1$ mode.

All the output results produced by the GLOBAL modality (summarized in Table 1) are stored in the subfolder `summary`, while the figure showing the general mode identification, the ASEF, the multi-modal sampling, and the ACF^2 for $\Delta\nu$ is stored in the subfolder `figs` (Fig. 3).

5. The CHUNK modality

In Sect. 4 we have seen that the GLOBAL modality of the FAMED pipeline performs a series of different operations in order to provide a set of identified $\ell = 0, 1$ frequencies, and the frequency positions of each chunk in the stellar PSD. Although this information is already useful for understanding what kind of general oscillation features the star possesses and what is the mode identification scheme to follow, the GLOBAL modality output comes with some major limitations:

- the general mode identification is usually reliable for the radial mode frequencies, but the radial mode frequencies may not be very accurate because they approximate the $\ell = 2, 0$ mode pairs instead of representing the single $\ell = 0$ mode peaks in the PSD;
- the $\ell = 1$ modes identified are not thoroughly inspected, and may be unreliable;
- the $\ell = 2$ modes are not extracted because from the global multi-modal sampling they appear as joint peaks with their adjacent $\ell = 0$ modes;
- the $\ell = 3$ modes are not even contemplated because they are too small in amplitude with respect to radial and dipole modes, such that a global multi-modal sampling will usually not be able to recognize them, if present;
- no peak significance tests are performed, meaning that at this stage the output frequency list is not yet validated in terms of detection against the noise level.

Overcoming these aspects requires an additional level of detail in analyzing the dataset. This is achieved by investigating each chunk of the PSD, as identified from the first module of FAMED. This will require a series of tasks that we implement in the CHUNK modality, which we thoroughly describe in the sections below.

The mode identification procedure carried out by the CHUNK modality allows for identifying radial and quadrupole modes in stars spanning all evolutionary stages from MS (with particular remark on the powerful capability of the pipeline to disentangle modes in stars that exhibit a strong peak blending) up to RC stars and even beyond to early AGB (Sects. 5.2, 5.3). The quadrupole modes are however not inspected neither from the point of view of rotation nor in terms of quadrupole mixed modes composition. This means that quadrupole modes are treated as single peaks, as it is usually done in the standard peak bagging analysis, and that all radial and quadrupole modes extracted with FAMED have a mode identification tag of the type (n, ℓ). In addition, for each chunk a local value of the ϵ parameter of the asymptotic pattern as evaluated from the frequency of the chunk radial mode, and of the frequency separation between $\ell = 2, 0$ modes, $\delta\nu_{02}$, are also provided.

In addition in the CHUNK modality the identification of the dipole modes is done independently of the evolutionary stage of the star and of any theoretical asymptotic pattern by combining the frequencies extracted from the multi-modal sampling of the chunk (see Sect. 5.1) with the subsequent peak detection testing (Sect. 5.3.3). This data-driven approach is very efficient in obtaining a fast and automated extraction of dipole modes for stars in any evolutionary stage because it does not rely on the actual frequency location of any of the peaks. This is especially useful for evolved stars such as SG and RGs, where the presence of mixed modes can significantly complicate the oscillation pattern in each chunk of the PSD. Interestingly, the same data-driven approach allows handling without difficulties the analysis of RGs with depressed dipole mode power because each candidate dipole mode is tested separately from the others and independently of quadrupole and radial modes. We refer to Sect. 6 for several applications showing the capabilities of this data-driven approach for evolved stars and to Sect. 7 for a concluding discussion.

5.1. Chunk multi-modal sampling

Similarly to the GLOBAL modality, the CHUNK modality requires that an initial multi-modal sampling is performed. This is done by using again the PeakBagging code with configuration #1 and one Lorentzian profile (Sect. 3.4), hence adopting the same high-threshold stopping criterion described by C19 and already presented for the GLOBAL modality. The main differences with respect to the global multi-modal sampling are that: 1) the prior for the frequency centroid of the island peak bagging model is now constrained by the frequency range of the chunk to analyze, as obtained from the frequency separations s_n evaluated from the GLOBAL modality (see Sect. 4.6); 2) different values of the FWHM of the islands peak bagging model defined in Eq. (1) are used, depending on the evolutionary stage classification of the star. Concerning point 1), in Sect. 4.6 it was shown that the frequency separations s_n delimit the frequency region of each chunk without any overlap between consecutive chunks. Nonetheless one should note that having no overlap between two consecutive chunks poses a risk in the detection of potential oscillation peaks that are unluckily falling at the edge of the chunk frequency range. To overcome this issue, FAMED applies an extension to each frequency separation s_n, such that the lower frequency boundary of each chunk is moved to slightly smaller frequencies, thus becoming smaller than the upper frequency boundary of the previous chunk. The amount of chunk overlap is tuned as a configuring parameter, and it has been set to be 15 % of $\Delta\nu$ for MS stars, and to 25 % of $\Delta\nu$ for SG and RG stars. A larger overlap in evolved stars is certainly motivated by the presence of dipolar mixed modes, which can span all over the frequency range between two consecutive radial modes. The chunk overlap is especially useful for chunks that are located towards the tails of the Gaussian envelope of the oscillations, where the global frequencies corresponding to radial modes may be less accurate because of the low SNR of the dataset.

For the point 2) presented above, the FWHM of the islands peak bagging model for the multi-modal sampling to be performed in the CHUNK modality, which we refer to as $\Gamma_{\rm chunk}$, is initially computed from the same relations presented in Sect. 4.1 using $\nu_{\rm max,thresh}$ as a control parameter. By naming the FWHM used for the global multi-modal sampling as $\Gamma_{\rm global}$, the one used for the multi-modal sampling in the CHUNK modality can be obtained as follows depending on $\Delta\nu$ and $T_{\rm eff}$ of the star:

- for $\Delta\nu_{\rm RG} < \Delta\nu \leq \Delta\nu_{\rm SG}$ and $T_{\rm eff} \geq T_{\rm eff,SG}$, or for $\Delta\nu \geq \Delta\nu_{\rm SG}$: $\Gamma_{\rm chunk} = \Gamma_{\rm global}/10$. This corresponds to MS stars;
- for $\Delta\nu_{\rm RG} < \Delta\nu < \Delta\nu_{\rm SG}$ and $T_{\rm eff} < T_{\rm eff,SG}$: $\Gamma_{\rm chunk} = \Gamma_{\rm global}/2$. This corresponds to SG and early RGB stars;
- for $\Delta\nu_{\rm CL} < \Delta\nu \leq \Delta\nu_{\rm RG}$: $\Gamma_{\rm chunk} = \Gamma_{\rm global}/5$. This corresponds to low-luminosity RGB stars;
- for $\Delta\nu_{\rm tip} < \Delta\nu \leq \Delta\nu_{\rm CL}$: $\Gamma_{\rm chunk} = \Gamma_{\rm global}/8$. This corresponds to RC stars (both 1$^{\rm st}$ and 2$^{\rm nd}$ RC) and to more evolved RGB stars;
- for $\Delta\nu \leq \Delta\nu_{\rm tip}$: $\Gamma_{\rm chunk} \lesssim \Gamma_{\rm global}$. This corresponds to stars towards the RGB tip but can also include stars that have evolved off the RC towards the AGB;

where the parameters $\Delta\nu_{\rm SG}$, $\Delta\nu_{\rm RG}$, $\Delta\nu_{\rm CL}$, $\Delta\nu_{\rm tip}$, and $T_{\rm eff,SG}$ have already been defined in the GLOBAL modality (see Table 2 for a summary). The reference value for $\Delta\nu$ used in the CHUNK modality is $\Delta\nu_0$ estimated from the asymptotic fit in the GLOBAL modality (see Sect. 4.5.1). All the rescaling factors here presented can be modified by the user from the configuring parameter list.

The general condition $\Gamma_{\rm chunk} < \Gamma_{\rm global}$ is necessary for obtaining a higher resolving power of the islands peak bagging model with respect to the case of the GLOBAL modality. In addition, the new multi-modal sampling, henceforth termed *chunk multi-modal sampling*, is performed over a frequency range that is about one order of magnitude smaller than that used in the GLOBAL modality, which given that the number of nested iterations is the same of that used for the global multi-modal sampling, implies that the frequency sampling is much denser in terms of number of points. This condition of high resolving power and high frequency resolution of the sampling is required to maximize the number of detections of potential oscillation peaks, especially for those peaks having the narrowest linewidths. The output results from the chunk multi-modal fit performed by Diamonds are stored in the sub-folder `isla` (Fig. 3).

The large rescaling factor for computing $\Gamma_{\rm chunk}$ in MS stars (set to 10) stems from the large oscillation mode linewidths found in these stars. For stars evolved toward the tip of the RGB instead, the oscillation modes are the narrowest observed because of the cool temperatures of these stars and of their late stage of evolution. Here the adopted linewidth for the multi-modal fitting is the smallest among the different regimes to allow for the identification of even the narrowest peaks in the PSD, although a value slightly smaller than the one used for the global multi-modal sampling proves to be already enough. The scaling values for RG stars have been obtained using observations from the *Kepler* nominal mission, spanning up to more than four years, which until today provide the highest-resolution datasets available for red giant stars that exhibit oscillations (Corsaro et al. 2015a).

Given that the chunk multi-modal sampling is obtained independently for each chunk, this process can be parallelized to improve the computational speed of the pipeline. In the automated analysis sequence operated by FAMED, the procedure is to first perform the chunk multi-modal sampling for all the chunks found in the GLOBAL modality using a parallel computation, and then to analyze each chunk separately in progressively decreasing PSD SNR order. In this way chunks having the best and most clear asteroseismic signal in the PSD are analyzed first. This choice is further discussed in the following section. The chunk multi-modal sampling is analyzed by FAMED using a series of tasks that are quite different with respect to those adopted in the GLOBAL modality. The preliminary step of the

analysis, however, is to exploit the multi-modal sampling for computing a standard resolution ASEF ($N_{\rm bins} \approx 100$), with local maxima ν_i, frequency ranges $r_{a,b}$ and divisions $d_{a,b}$, frequency estimates $\nu_{f,i}$ and 1-σ uncertainties $\sigma_{f,i}$, all evaluated following the same description presented for the GLOBAL modality (Sect. 4.3). The threshold used for the hill-climbing algorithm to identify the local maxima of the ASEF now varies as a function of the evolutionary stage classification described in Sect. 4.5.1. In particular, our applications of FAMED consider for the hill-climbing algorithm a 3 % ASEF amplitude threshold for MS stars, and a 5 % one for SG and RG stars. These thresholds help in minimizing the effect caused by the presence of noise peaks, thus their adoption can significantly speed up the overall computation.

Conversely to the case of the GLOBAL modality, where the only preliminary information available was the background level, as well as $\nu_{\rm max}$ and $T_{\rm eff}$ of the star, the analysis of the oscillation peaks in the CHUNK modality has at its disposal the frequencies identified from the GLOBAL modality (henceforth referred to as global frequencies), as well as the asymptotic parameters $\Delta\nu_0$, ϵ, α_0. This information will be essential for obtaining a detailed mode identification of the newly extracted frequency peaks.

5.2. Radial and quadrupole modes

An important task for a successful analysis in the CHUNK modality is to obtain an accurate estimate of the frequency of the $\ell = 0$ and $\ell = 2$ modes contained in the chunk, if they are detectable. For this reason, FAMED performs a series of operations that we shall describe in the following two sections.

5.2.1. Finding the radial mode

In Sect. 4.6 we have seen that a chunk can in general be defined independently of whether or not a global radial mode frequency is found from the GLOBAL modality. However, a single chunk can be analyzed in the CHUNK modality only if at least one global mode frequency is found, which can correspond to either a $\ell = 0$ or a $\ell = 1$ mode, otherwise the chunk is skipped. From now on, we will assume that this latter condition is always fulfilled.

At the beginning, the CHUNK modality attempts to improve the global radial mode frequency that is found in the chunk to analyze, or to obtain one if it is not available. For this purpose the CHUNK modality searches for a possible solution from the same CHUNK modality that was previously performed on a neighboring chunk. We recall that the analysis of the chunk multi-modal sampling is done for one chunk per time by proceeding in a sequential decreasing SNR order. This means that, with the exception of the first chunk that is analyzed, i.e. the one with the highest SNR, all the remaining chunks can potentially exploit a solution from a neighboring chunk that was previously analyzed because having a higher SNR. For understanding how FAMED is using this information, let us suppose we have a solution from the CHUNK modality from the highest SNR chunk of the entire set, and we label this chunk as c_i. Very likely this chunk will be centered around $\nu_{\rm max}$ because this value corresponds by definition to the position of the maximum oscillation power (hence highest SNR) of the PSD region containing the oscillations. We thus consider that the CHUNK modality solution for this chunk contains the chunk radial mode frequency $\nu_{n_i,0}$, corresponding to the radial order n_i, and that this frequency is more accurate than a global radial mode frequency because it is a solution from the CHUNK modality. If the new chunk that is analyzed after c_i is located next to the right side, which we term chunk c_{i+1}, then the mean frequency of the chunk will be higher than $\nu_{\rm max}$. FAMED can improve the value of the global radial mode frequency of the chunk c_{i+1} by using the chunk radial mode frequency estimated for chunk c_i. The improved global radial mode frequency $\nu_{n_{i+1},0}$ of the chunk c_{i+1}, corresponding to the radial order n_{i+1}, can thus be written as

$$\nu_{n_{i+1},0} = \nu_{n_i,0} + \Delta\nu_0 \left[1 + \alpha_0 \left((n_{i+1} - 0.5 - \frac{\nu_{\rm max}}{\Delta\nu_0}\right)\right], \qquad (16)$$

as follows from Eq. (12), where $\Delta\nu_0$, α_0 are our estimates of the asymptotic fit to the radial modes from the GLOBAL modality (see Sect. 4.5.1, step #6), while the radial order n_{i+1} is provided by the general mode identification (Sect. 4.5). In the unfortunate case that the previous chunk c_i does not contain any $\ell = 0$ mode solution, FAMED checks for the presence of a $\ell = 0$ mode solution in the chunk c_{i-1}, previous to c_i, and corresponding to radial order n_{i-1}. If a radial mode frequency $\nu_{n_{i-1},0}$ is thus obtained from the chunk c_{i-1}, the improved global radial mode frequency $\nu_{n_{i+1},0}$ of the chunk c_{i+1} is calculated as

$$\nu_{n_{i+1},0} = \nu_{n_{i-1},0} + 2\Delta\nu_0 \left[1 + \alpha_0 \left(\frac{2n_{i+1} - 1}{2} - 0.5 - \frac{\nu_{\rm max}}{\Delta\nu_0}\right)\right], \qquad (17)$$

A similar argument can be applied for the specular case of a chunk c_{i-1}, falling to the left side of chunk c_i, hence having an average frequency lower than $\nu_{\rm max}$. This approach is thus building upon those radial mode frequencies extracted from a higher SNR region of the stellar PSD, and that are therefore assumed to be more reliable in both frequency position and mode identification tag. The advantage of this approach is threefold: 1) it is able to maintain the accuracy of the location of the global radial mode frequencies as we move away from $\nu_{\rm max}$ towards lower SNR regions; 2) it allows avoiding misidentification of $\ell = 0$ modes into $\ell = 2$ (and vice versa) as we approach to the tails of the Gaussian envelope where the curvature effects of the asymptotic relation of p modes are stronger; 3) it allows computing a reliable global radial mode frequency even if this is not available from the GLOBAL modality, thus opening the possibility to find quadrupole and radial modes contained in the chunk. As a side note, if no global dipole mode frequency is found from the GLOBAL modality, this approach provides a guess for a global dipole mode frequency based on the global radial mode frequency of the chunk.

If no global radial mode frequency can be obtained from the procedure explained above, for example because the chunk has no close neighbors and the GLOBAL modality did not return a global radial mode frequency, then the radial mode of the chunk is assumed to be obtained from the asymptotic relation computed from the radial order of the adjacent dipole increased by one. In this condition the pipeline will not proceed further in estimating the chunk radial mode frequency (see below) and in searching for a possible adjacent quadrupole mode. Dipole modes will be inspected and analyzed even if no radial mode is found.

Subsequently to the re-estimation of a global radial mode frequency, FAMED is using it as a reference to locate the actual radial mode of the chunk using the ASEF computed out of the chunk multi-modal sampling. This is done by finding the frequency $\nu_{f,i}$ estimated from the new ASEF that is considered to be the most reliable candidate in representing the radial mode frequency of the chunk. The degree of reliability for the candidate chunk radial mode frequency is computed as the combination

of different reliability indicators, which include the proximity of $\nu_{f,i}$ to the global radial mode frequency, the amplitude of the corresponding ASEF local maximum (in nested iterations), the number of sampling points falling within the ASEF local maximum (in logarithmic units), and the height of the peak from a smoothed PSD, previously computed using a smoothing factor given by $\Gamma_{\rm chunk}$ (defined in Sect. 5.1). With the candidate chunk radial mode identified, it is then possible to establish an upper limit to the frequency range that will be used for the subsequent analysis described in Sect. 5.2.2, as well as a lower limit frequency that delimits the starting point of the chunk in a way that it does not incorporate the previous radial mode frequency. These limiting frequencies will thus ensure that the oscillation peaks to be identified inside the chunk are not placed beyond the actual chunk radial mode frequency and that at the same time are confined above the lower limit frequency imposed by the previous radial mode.

After the procedure to locate the radial mode of the chunk from the ASEF is completed, FAMED performs two additional checks. The first one is to assess whether the selected ASEF peak flagged as the chunk radial mode is not the adjacent quadrupole mode by checking that there is no prominent ASEF peak next to the right side. The second check is to test that the lower limit frequency of the chunk does not contain the previous radial mode. This check is applied only if the chunk has a mean frequency larger than $\nu_{\rm max}$, i.e. it belongs to the right-hand side of the Gaussian envelope of the oscillations. This check can be useful in low SNR conditions, when for example the radial mode identified from the previous chunk(s) may turn out to be inaccurate (this could happen if there is a dipole mixed mode very close to the previous radial mode). The test is performed by assuming that if a radial mode from the previous chunk(s) is visible, its ASEF peak is generally prominent and at least comparably as high as that of the radial mode of the current chunk investigated.

5.2.2. Finding the quadrupole mode

In most stars that are less evolved, such as early SG and MS, the $\ell = 2, 0$ oscillation mode pairs may often fall relatively close to one another with respect to their mode linewidth, at the risk of being partially or almost entirely blended if the star has a high $T_{\rm eff}$ (hence large mode linewidths). Despite the chunk multi-modal sampling is in principle able to distinguish peaks that are close to one another, it is usually not able to reliably separate and identify an $\ell = 2$ from an $\ell = 0$ peak if a significant level of blending is found. The small frequency separation $\delta\nu_{02}$ is not known a priori in such stars, and it is not straightforward to predict accurately, especially during the MS phase of stellar evolution (e.g. White et al. 2011). As a consequence, the effect produced by the peak blending on the multi-modal sampling is not known, such that it is not possible to understand whether the sampling will produce two separate maxima in the distribution or just a single broader one. To overcome this problem and solving any possible ambiguity, for all stars classified as SG and MS, having $\Delta\nu \geq \Delta\nu_{\rm RG}$, FAMED performs an additional multi-modal fitting on the sole region containing the $\ell = 2, 0$ mode pair, which can be located using the estimated chunk radial mode frequency from the previous section. This time the new multi-modal sampling, which we shall refer to as *doublet multi-modal sampling*, is performed using configuration #1 of the PeakBagging code presented in Sect. 3.4 but with two Lorentzian profiles. Similarly to what done for the chunk multi-modal sampling, the output results are stored in the sub-folder `isla` shown in Fig. 3. This configuration of the PeakBagging code utilizes the so-called two-Lorentzian islands peak bagging model, which in analogy to Eq. (1) can be defined as

$$P_{\rm isla}\,(\nu, \Gamma; \nu_0, H, \delta\nu_{02}) = \frac{H}{1 + 4\left(\frac{\nu-\nu_0}{\Gamma}\right)^2} + \frac{HV_2^2}{1 + 4\left(\frac{\nu-\nu_0+\delta\nu_{02}}{\Gamma}\right)^2} \quad (18)$$

where the first term on the right-hand side is the same as the single-Lorentzian islands peak bagging model – here used to model the $\ell = 0$ mode of the chunk – while the second term represents the second Lorentzian profile that is modeling the $\ell = 2$ mode adjacent to the $\ell = 0$. The height of the $\ell = 2$ peak is modulated by the visibility of quadrupole modes, which is set in the same way as explained in Sect. 4.4.1. The linewidth Γ is the same for both peaks, and it is fixed to the value predicted using the empirical relations from Sect. 4.1 for the chunk radial mode frequency. Conversely to Eq. (1), Eq (18) accounts for three free parameters, ν_0, H, and $\delta\nu_{02}$, the latter allowing locating the position of the quadrupole mode with respect to its adjacent radial mode. Adopting the formulation with $\delta\nu_{02}$ as a free parameter in the fit is forcing the model to have a $\ell = 2$ peak displaced to the left side of the $\ell = 0$ peak, which is therefore limiting the potential multi-modality of the fitting problem, thus improving the reliability of the fit solution. Figure 9 (left panels) shows an example of the powerful capability of the doublet multi-modal sampling in estimating an accurate position of quadrupole and radial modes even in the case of a simulated MS star PSD having a strong peak blending effect, where each of the oscillation modes in the pair has a linewidth larger than $4\,\mu$Hz and with $\delta\nu_{02} \simeq 2\,\mu$Hz. Here the oscillation frequencies are known from stellar modeling because they were used to simulate the dataset (Ball et al. 2018), otherwise it would be impossible to visually distinguish the two oscillation peaks from the PSD. The frequencies estimated by FAMED have an excellent agreement with those obtained from the simulations, significantly below 0.1 %. In conclusion, for stars identified as SG and MS, the chunk radial mode frequency initially obtained as described in Sect. 5.2, is here re-estimated using the solution from the doublet multi-modal fit, which is used at the same time to estimate the chunk quadrupole mode frequency and to obtain a more accurate value of the lower limit frequency of the chunk.

For stars classified as RGs instead, having $\Delta\nu < \Delta\nu_{\rm RG}$, the two-Lorentzian islands peak bagging model is not used. This is because 1) the quadrupole and radial modes are now well separated in frequency, given that their linewidth is smaller than $\delta\nu_{02}$, hence the chunk ASEF can properly distinguish them (see Fig. 1 for an example); 2) the frequency separation $\delta\nu_{02}$ can be predicted with good accuracy from the $\Delta\nu$-$\delta\nu_{02}$ relation (e.g. Huber et al. 2011; Corsaro et al. 2012). Consequently, the chunk quadrupole mode frequency corresponds to the frequency $\nu_{f,i}$ estimated from the chunk ASEF that is closest to the predicted quadrupole mode frequency $\nu_{n-1,2} = \nu_{n,0} - \delta\nu_{02}$, where $\nu_{n,0}$ is the chunk radial mode frequency and $\delta\nu_{02}$ is obtained from the $\Delta\nu$-$\delta\nu_{02}$ relation from Corsaro et al. (2012). If no $\nu_{f,i}$ frequency is found to be closer to the asymptotic position of the $\ell = 2$ mode than that of the chunk $\ell = 0$ mode, then the pipeline assumes that no quadrupole mode is found in the chunk.

Another useful consideration for $\ell = 2$ modes in evolved stars regards the potential presence of quadrupole mixed modes, whose pattern in the PSD could be further complicated by the effect of rotation on the individual $\ell = 2$ mixed modes (e.g. see Deheuvels et al. 2017). The result is that when performing the chunk multi-modal sampling, the ASEF could contain more than one local maximum in the region of the $\ell = 2$ mode (e.g. see Fig. 9, right panels). We note that the current version of the

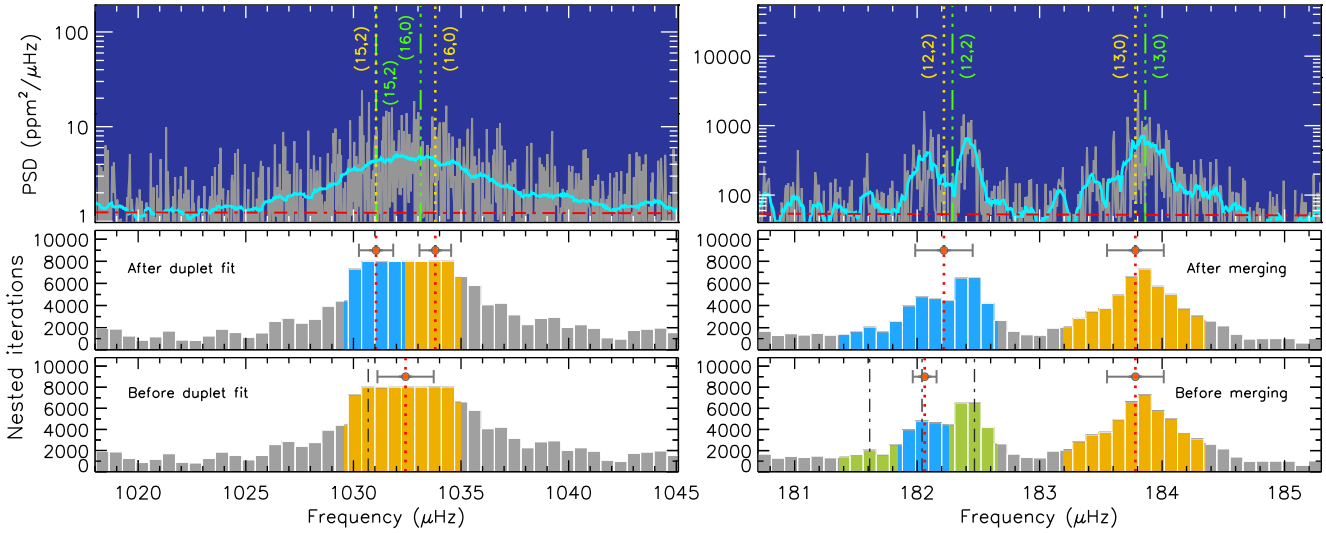

Fig. 9. The identification of the chunk quadrupole mode for the simulated F-type MS star 06550, having $T_{\rm eff}$ = 6416 K (Ball et al. 2018) and corresponding to a 1-year length observation with TESS (left panels), and the RGB star KIC 12008916 observed with *Kepler* for more than four years (right panels). *Top panels*: similar to Fig. 7, top panels, but now showing a PSD region containing a $\ell = 2, 0$ mode pair of one of the chunks analyzed, where the frequencies estimated from the CHUNK modality are indicated by vertical dotted yellow lines, with included the corresponding (n,ℓ) mode identification obtained by FAMED. The cyan curve is the PSD smoothed by a factor proportional to $\Gamma_{\rm chunk}$. The vertical double-dot dashed green lines, and their mode identification, correspond to the oscillation modes computed by Ball et al. (2018) for the MS star, and to those extracted by Corsaro et al. (2015a) for the RGB star. *Middle and bottom panels*: the chunk ASEF showing the frequency ranges (blue shading for $\ell = 2$ and yellow for $\ell = 0$), frequency estimates, and 1-σ uncertainties, obtained after and before applying a two-Lorentzian multi-modal fit for the MS star, and a quadrupole mixed modes merging for the RGB star. The local maxima originally found in the ASEF that are considered for obtaining the ultimate chunk quadrupole mode frequency are marked by the vertical dot-dashed black lines, with green shading indicating the frequency ranges of those ASEF peaks that are merged.

pipeline does not deal with the detection and analysis of $\ell = 2$ mixed modes and therefore assumes that there is only one $\ell = 2$ peak, at most, in each chunk analyzed. For improving the estimation of the chunk quadrupole mode frequency, FAMED checks whether there are frequencies estimated from the ASEF that fall inside the control range $[\nu_{n-1,2} - \phi_2\delta\nu_{02}/2, \nu_{n-1,2} + \phi_2\delta\nu_{02}/2]$, where the parameter ϕ_2 can be changed from the configuring parameter list and allows to vary the extent of the control range, with $\phi_2 = 1$ for all our applications. If the condition is satisfied, the frequencies falling in the control range are removed from the set of estimated frequencies and the corresponding ASEF peaks are merged to that of the identified $\ell = 2$ mode of the chunk. In this way the chunk quadrupole mode frequency and its associated 1-σ uncertainty are recomputed using a larger frequency range $r_{a,b}$, which now incorporates the frequency ranges of the estimated frequencies falling inside the control range. This approach allows to take more accurately into account the $\ell = 2$ power barycenter in estimating the quadrupole mode frequency, while at the same time yielding an enlarged uncertainty with respect to the case of no merging because of the larger frequency range involved. A clear example of this procedure can be seen in the right panels of Fig. 9, where the extra ASEF peaks originally identified and later on merged into a single $\ell = 2$ peak are shown in green shading. Here the chunk quadrupole mode frequency identified in the bottom-right panel is clearly offset with respect to the one shown in the middle panel, the latter matching within 0.04% to the value obtained by Corsaro et al. (2015a) using a standard (non-automated) peak bagging analysis. Nonetheless, we consider that the multi-modal approach used by FAMED retains potential for incorporating the analysis of quadrupole mixed modes in future developments of the pipeline.

Once that the chunk quadrupole mode frequency is estimated, as expected from the asymptotic theory of p modes the associated radial order will correspond to the radial order of the adjacent radial mode, already obtained in the GLOBAL modality, but decreased by one. This therefore completes the frequency estimation and mode identification of radial and quadrupole modes of the chunk.

5.3. Peak detection and blending tests

With the identification of quadrupole and radial modes, the remaining frequencies estimated from the chunk ASEF local maxima are initially flagged as dipole modes, independently of how many frequencies are found, with the only constraint of being located in the region comprised between the current radial mode and that of the previous radial order, such that no repeated frequencies from one chunk to another are found. The mode identification of all the remaining frequencies other than $\ell = 2, 0$ is therefore obtained by assuming an angular degree $\ell = 1$ and a radial order given by that of the chunk radial mode frequency decreased by one. However, we notice that all the frequencies estimated and identified until this stage, including the chunk $\ell = 0, 2$ modes, are still only candidate oscillation modes. This is because none of them has yet been validated against the level of noise in the PSD. As a result, an important fraction of the estimated frequencies may turn out to be not significant, hence degraded from potential modes to noise peaks and discarded from further analysis and from the final output of the pipeline. The following step of the analysis, which is crucial for the reliability of the results

produced by the CHUNK modality, is therefore to test whether or not each of the identified frequency peaks of the chunk, of any given ℓ, is significant against the level of the background noise of the star.

As shown by Corsaro & De Ridder (2014); Corsaro et al. (2015a), testing the significance of a frequency peak in the stellar PSD can be done by performing a Bayesian model comparison that exploits the so-called Bayesian evidence, which is a direct computation output for Diamonds. The Bayesian evidence can be interpreted as a statistical weight to the fitting model, which can therefore be confronted with that of another model attempting to reproduce the same dataset. The advantage of the Bayesian evidence with respect to e.g. a standard χ^2 minimization or a Maximum Likelihood Estimation is that it takes into account both the model complexity and the fit quality such that the choice of the individual assumptions on the model free parameters can be tested and assessed in the light of the available data. Given that the Bayesian evidence is a comparative quantity and that taken as a single value has no meaning, the significance of a frequency peak that is assumed to be an oscillation mode has to be evaluated by confronting two fitting models, one incorporating the peak with a typical oscillation mode profile on top of a varying background level, and another one incorporating only the background level (hence excluding the peak). This working scheme can be extended to test the significance of a pair of frequency pxeaks that are blended because of their proximity. If a peak blending occurs, by testing the peak significance for only one peak we would clearly ignore the hypothesis that the observed peak is in reality constituted by two different ones that are partially merged. This is the typical condition verified for $\ell = 2, 0$ mode pairs in less evolved stars. Performing a Bayesian model comparison process therefore implies that: 1) the correct model at interpreting the data is among the fitting models that are considered in the comparison; 2) the assumptions on the model hypothesis, i.e. the prior probability distributions on the model free parameters, are part of the outcome, meaning that the obtained Bayesian evidence of each model will also reflect the way we set up the prior hyper-parameters.

For managing this first phase of the peak testing, FAMED makes use of an useful facility provided by the new version of the PeakBagging code, namely a set of peak fitting models that can be used for different applications in relation to peak significance, and which are listed below:

- $\mathcal{M}_{\rm A}$ is a model to test the hypothesis that the frequency peak is consistent with noise. It has one free parameter, the background level amplitude $\sigma_{\rm noise}$, which is a dimensionless quantity changing the level of the background estimated from the background fit;
- $\mathcal{M}_{\rm B}$ is a model to test that the frequency peak is an oscillation peak with a resolved lifetime, i.e. a Lorentzian profile. It has four free parameters, namely the background level amplitude as for model $\mathcal{M}_{\rm A}$, and frequency centroid, amplitude, and linewidth of the Lorentzian profile ($\nu_{i,0}, A_i, \Gamma_i$, respectively);
- $\mathcal{M}_{\rm C}$ is a model to test that the frequency peak is an oscillation peak with an unresolved lifetime, i.e. a sinc^2 profile (Corsaro et al. 2015a). It has three free parameters, namely the background level amplitude as for model $\mathcal{M}_A$, and frequency centroid and height of the sinc^2 profile ($\nu_{i,0}, H_i$, respectively);
- $\mathcal{M}_{\rm D}$ is a model to test the presence of a blended $\ell = 2, 0$ mode pair, assuming that the two frequency peaks are oscillation modes with a resolved lifetime, i.e. two Lorentzian profiles. It has seven free parameters, namely the background level amplitude as for model $\mathcal{M}_{\rm A}$, and the frequency centroids, amplitudes, and linewidths of the two Lorentzian profiles ($\nu_{i,0}^{\ell=0}, A_i^{\ell=0}, \Gamma_i^{\ell=0}$ for the radial mode, and $\nu_{i,0}^{\ell=2}, A_i^{\ell=2}, \Gamma_i^{\ell=2}$ for the quadrupole mode, respectively).

The choice of fitting amplitudes instead of heights for models $\mathcal{M}_{\rm B}$ and $\mathcal{M}_{\rm D}$ is motivated by the known correlation between height and linewidth, which would increase the computational time needed to conduct each fit. The height is instead a free parameter for model $\mathcal{M}_{\rm C}$ because the sinc^2 profile does not require the fitting of a linewidth.

Depending on the angular degree of the candidate oscillation mode we are dealing with, FAMED performs uni-modal fits using the PeakBagging code by utilizing pairs of models from the above list and by comparing their Bayesian evidences to test whether the peak is significant above the level of noise (peak detection test), and whether the peak is actually a blended structure containing two peaks (peak blending test). The peak detection tests are divided in two groups, those for the candidate $\ell = 2, 0$ modes, and those for the candidate $\ell = 1$ modes, while the peak blending test is only done for the candidate $\ell = 2, 0$ mode pairs. All the results from the peak detection and blending tests are stored in the sub-folder `pb`, as shown in Fig. 3. It is useful to note that all the fits conducted within the peak detection and blending testing are uni-modal, using 1000 live points and with an imposed low-threshold termination condition on the nested sampling with Diamonds that is set to 0.1, i.e. 10 times smaller than the one given according to the new calibration provided by Corsaro et al. (2018) for standard uni-modal fits. This lower threshold allows to obtain a more accurate value of the Bayesian evidence and to reduce its fluctuations from fit to fit as arising from the adoption of a Monte Carlo sampling approach. This configuration is essential for a successful conduction of the peak testing phase.

5.3.1. FWHM of the chunk radial mode

The first frequency peaks to be assessed in terms of significance are the radial and quadrupole modes of the chunk. In this section we shall assume that a candidate radial mode frequency has been identified. If this is not the case, then FAMED skips the part related to the peak testing of the $\ell = 2, 0$ mode pairs and goes directly to the peak testing of the $\ell = 1$ modes (Sect. 5.3.3).

Before performing the actual peak testing on the $\ell = 2, 0$ modes, and on the $\ell = 1$ modes afterwards, FAMED evaluates the FWHM of the radial mode of the chunk by fitting the corresponding PSD peak by means of a Lorentzian profile. The FWHM of the chunk radial mode is an useful parameter to set up the peak testing that will be discussed in Sects. 5.3.2, 5.3.3, 5.4, 5.5.

If the star is sufficiently evolved, with $\Delta\nu < \Delta\nu_{\rm thresh}$ (see Table 2), the radial mode is treated as a single peak and the free parameters of the fitting model are those of a single Lorentzian profile, namely frequency centroid, amplitude, and linewidth, with the background level fixed to the value of the background fit for obtaining a more stable solution of the FWHM (this is done using the fitting model $\mathcal{M}_{\rm E}$ presented in Sect. 5.4). For less evolved stars, $\Delta\nu \geq \Delta\nu_{\rm thresh}$, the radial mode peak is fitted simultaneously to its adjacent quadrupole mode peak, meaning that the fitting model accounts for two Lorentzian profiles, again using a fixed background level (this is done using the fitting model $\mathcal{M}_{\rm G}$ presented in Sect. 5.4). For performing the Bayesian inference with Diamonds, our pipeline adopts uniform prior distributions for all the free parameters. This choice

is primarily motivated by the fast computation that is guaranteed with the adoption of this type of priors, but it is also supported by previous testing and published results (e.g. Corsaro & De Ridder 2014; Corsaro et al. 2015a, 2017a) that are based on the use of Diamonds as a fitting code. In this regard, it is useful to mention that the nested sampling algorithm implemented in Diamonds allows to efficiently sample likelihood distributions that may contain pronounced degeneracies, and to properly discover local maxima that may be hidden inside these degeneracies. This ensures that the adoption of uniform priors will neither hamper the sampling quality nor the capability of Diamonds to obtain reliable estimates of the free parameters, especially in the low-dimensional regime adopted by FAMED. The uniform prior hyper-parameters on the frequency centroid of the Lorentzian profiles are obtained from the frequency ranges $r_{a,b}$ of the corresponding chunk frequencies, while those on the amplitude (and therefore on the linewidth) are obtained by computing an amplitude estimate using the peak heights measured from a PSD smoothed by $\Gamma_{\rm chunk}$, and a linewidth estimate from the empirical Γ-$\nu_{\rm max}$-$T_{\rm eff}$ relations (see also Appendix A for more details).

The peak fit utilizes a portion of the dataset that is centered around the peaks. If one Lorentzian profile is used, the dataset spans up to the boundaries set by the frequency divisions $d_{a,b}$ of the chunk radial mode frequency. If two Lorentzian profiles are used, the dataset spans from the frequency division d_a of the quadrupole mode up to the frequency division d_b of the radial mode. This kind of prior setting up shows how the frequency ranges and divisions, where in general $r_{a,b} < d_{a,b}$ (see Sect 4.3.1 for a definition), are now being used for two different purposes. This is because on one hand it is useful to have a dataset range that is as wide as possible to make sure that the frequency peak is entirely contained inside this range, while on the other hand the prior boundaries on the frequency centroid should be relatively narrow to obtain a more accurate frequency centroid from the fit. We also note that for obtaining a more reliable estimate of the peak linewidth, the peak fit on the chunk radial mode is performed multiple times in parallel, and the final FWHM estimate, henceforth Γ_0, is the median value of the set of FWHM estimates. The number of FWHM estimates to compute, which is set to three, is controlled from a configuring parameter.

5.3.2. Radial and quadrupole modes

Once the FWHM of the chunk radial mode frequency is estimated, FAMED proceeds with the peak detection and blending tests for the $\ell = 2, 0$ peaks. According to the findings by Corsaro et al. (2015a), a peak is tested against the level of noise only if its height in the smoothed PSD is lower than 10 times the local level of the background, otherwise the peak is automatically considered as detected. This will speed up the CHUNK modality because if the peak is sufficiently prominent, the Bayesian model comparison process will yield a detection probability of 100 %, which makes the peak testing a useless step to perform. In the following we shall discuss the case of peaks that are not sufficiently prominent to be excluded from a peak detection and blending test.

For stars having $\Delta\nu < \Delta\nu_{\rm thresh}$ (see Table 2), the peak blending test is not performed and the peak detection test on the $\ell = 2, 0$ peaks is done separately for each peak. This is because, as already anticipated, for such evolved stars the two peaks are well separated from one another, their relative separation $\delta\nu_{02}$ can be predicted with good accuracy, and the chunk multi-modal sampling is able to properly disentangle them. As anticipated, for testing the detection of each peak two fits are executed, one using model $\mathcal{M}_{\rm A}$, and the other using model $\mathcal{M}_{\rm B}$. Here the priors are again uniform and the hyper-parameters for the Lorentzian peak are set in a similar way as done for the fit to the FWHM of the chunk radial mode, but are this time based on the chunk radial mode linewidth Γ_0, which is obviously more accurate than an empirical prediction. A detailed list of all the prior ranges is presented in Appendix A, Table A.1. The adequateness of uniform prior distributions for conducting successful peak detection tests using Diamonds was already proved by Corsaro & De Ridder (2014); Corsaro et al. (2015a). The resulting Bayesian evidences $\mathcal{E}_{\rm A}$ and $\mathcal{E}_{\rm B}$ for models $\mathcal{M}_{\rm A}$ and $\mathcal{M}_{\rm B}$, respectively, are then used to obtain the peak detection probability

$$p_{\rm BA} = \frac{\mathcal{E}_{\rm B}}{\mathcal{E}_{\rm A} + \mathcal{E}_{\rm B}}\,, \tag{19}$$

with the probability of non-detection being $p_{\rm AB} = 1 - p_{\rm BA}$. As presented by Corsaro et al. (2015a), the peak is considered to be significant if $p_{\rm BA} \geq 0.993$ (see also Trotta 2008). This is equivalent to considering a strong evidence condition in the Jeffreys' scale of strength (Jeffreys 1961) in favor of model $\mathcal{M}_{\rm B}$, that is the model containing the peak. We notice that the adoption of a Monte Carlo fitting approach such as that implemented in Diamonds can produce variations on the output Bayesian evidence of the fit that translate into fluctuations up to the order of 10^{-3} in probability. For improving the stability of the peak detection test against these potential fluctuations the fits can be repeated multiple times in parallel. Multiple values of the detection probability $p_{\rm BA}$ can therefore be obtained, with the final $p_{\rm BA}$ of the peak taken as the maximum of the entire set. The number of peak tests can be adjusted from the configuring parameter list and has been set to two for our applications. If the peak is not deemed significant it is discarded from the set $\{\nu_{f,i}\}$ of estimated frequencies of the chunk and it will not be analyzed further.

For less evolved stars, having $\Delta\nu \geq \Delta\nu_{\rm thresh}$, on top of the peak detection test that is carried out in a similar way as for evolved stars, FAMED performs a peak blending test as well. For conducting this latter test, an additional fit using model $\mathcal{M}_{\rm D}$ is done. Here the two Lorentzian profiles of model $\mathcal{M}_{\rm D}$ will combine together the same prior hyper-parameters adopted to fit each of the two individual profiles by means of model $\mathcal{M}_{\rm B}$. The corresponding probability of having two peaks detected at the same time is defined as

$$p_{\rm DA} = \frac{\mathcal{E}_{\rm D}}{\mathcal{E}_{\rm A} + \mathcal{E}_{\rm D}}\,, \tag{20}$$

with $\mathcal{E}_{\rm D}$ the Bayesian evidence of model $\mathcal{M}_{\rm D}$. The probability of having only one peak detected is instead the same as Eq. (19). Finally, we can compute a peak blending flag based on the probability

$$p_{\rm DB} = \frac{\mathcal{E}_{\rm D}}{\mathcal{E}_{\rm B} + \mathcal{E}_{\rm D}}\,, \tag{21}$$

which only plays the role of a discriminant factor between model $\mathcal{M}_{\rm D}$ and $\mathcal{M}_{\rm B}$, and has not to be interpreted as a detection probability. The probabilities $p_{\rm BA}$, $p_{\rm DA}$, and $p_{\rm DB}$, are then used according to two different cases:

- for $p_{\rm DB} \geq 0.5$ the $\ell = 2, 0$ peaks are treated as a blended structure. Here if $p_{\rm DA} \geq 0.993$, both quadrupole and radial modes are considered detected at the same time. If instead $p_{\rm DA} < 0.993$, then $p_{\rm BA} < 0.993$ and neither the $\ell = 0$ nor the $\ell = 2$ peaks are considered anymore in the subsequent analysis;
- for $p_{\rm DB} < 0.5$ no blending is assumed and only one peak of the $\ell = 2, 0$ pair can in principle be tested in terms of

significance. Here if $p_{\rm BA} \geq 0.993$, the peak corresponding to the estimated frequency $\nu_{f,i}$ that is closest to the Lorentzian frequency centroid obtained from the fit to the model $\mathcal{M}_{\rm B}$ is considered as the detected peak. This means that the detected peak can be either the chunk quadrupole or the radial mode, but not both. If instead $p_{\rm BA} < 0.993$ both the $\ell = 0$ and $\ell = 2$ peaks are considered as non detected and are not analyzed further.

5.3.3. Dipole modes

We have already mentioned that all estimated frequencies $\nu_{f,i}$ that are not marked as either radial or quadrupole modes, are initially flagged as dipole modes. FAMED therefore performs a peak detection test on these frequency peaks in order to be able to select only those that are statistically significant.

If the star is classified as either SG or MS, i.e. having $\Delta\nu \geq \Delta\nu_{\rm RG}$ (see Table 2 and Sect. 4.5.1), the peak detection test is performed following the approach used for an individual peak discussed in Sect. 5.3.2. This means that for each candidate dipole peak, FAMED performs two fits using models $\mathcal{M}_{\rm A}$ and $\mathcal{M}_{\rm B}$, hence computes the detection probability $p_{\rm BA}$ given by Eq. (19). Once again the peak tests are repeated two times for each peak, hence selecting the resulting maximum $p_{\rm BA}$ of the set as the final detection probability of the peak.

For stars classified as RGs instead, with $\Delta\nu < \Delta\nu_{\rm RG}$, FAMED takes into account an additional complication to the peak detection testing. As shown by Corsaro et al. (2015a), stars that are already in the low-luminosity RGB exhibit a large fraction of dipole mixed modes that are unresolved even if observed for more than four years. This suggests that a sinc^2 could be a more adequate model than the Lorentzian profile in fitting these narrow peaks. For this purpose, additionally to fitting models $\mathcal{M}_{\rm A}$ and $\mathcal{M}_{\rm B}$, also model $\mathcal{M}_{\rm C}$ is fitted, where the prior hyperparameters are presented in Appendix A, Table A.1. The detection probability of a sinc^2 peak is therefore given as

$$p_{\rm CA} = \frac{\mathcal{E}_{\rm C}}{\mathcal{E}_{\rm A} + \mathcal{E}_{\rm C}}\,, \tag{22}$$

where clearly $\mathcal{E}_{\rm C}$ is the Bayesian evidence of model $\mathcal{M}_{\rm C}$. For assessing whether the peak is better represented by a sinc^2 or a Lorentzian profile FAMED computes the probability

$$p_{\rm CB} = \frac{\mathcal{E}_{\rm C}}{\mathcal{E}_{\rm C} + \mathcal{E}_{\rm B}}\,, \tag{23}$$

which similarly to $p_{\rm DB}$ presented in Eq. (21) plays the role of a discriminant factor between models $\mathcal{M}_{\rm C}$ and $\mathcal{M}_{\rm B}$ and has not to be interpreted as a detection probability. Therefore FAMED identifies two possibilities:

- if $p_{\rm CB} > 0.5$ the peak is flagged as a sinc^2 profile. Then if $p_{\rm CA} \geq 0.993$ the peak is deemed significant, otherwise it is discarded from any further analysis;
- if $p_{\rm CB} \leq 0.5$ the peak is flagged as a Lorentzian profile. Then if $p_{\rm BA} \geq 0.993$ the peak is deemed significant, otherwise it is discarded from any further analysis.

The sinc^2 profile test so introduced will ensure that even in cases where real oscillation peaks are present in the form of narrow mixed dipole modes, their statistical significance is not underestimated by erroneously assuming that their lifetimes are temporally resolved, i.e. by fitting them as Lorentzian profiles. The sinc^2 profile test becomes of increasing importance for decreasing durations of the observing length of the datasets in use. This is because as the observing length decreases, it is less likely that a given oscillation mode can be temporally resolved, meaning that the corresponding PSD peak loses progressively its Lorentzian-like structure to become more similar to a sinc^2 (see our application in Sect. 6.6).

At the end of the peak detection tests, a list of detected candidate dipole modes of the chunk is obtained. These are still considered as candidate dipole modes because one may want to look for additional fine-structure effects such as the presence of rotational multiplets or duplicity inside each peak, as it will be discussed in Sect. 5.4, and because one peak among them could be a $\ell = 3$ oscillation mode, as it will be explained in more detail in Sect. 5.5.

5.4. Peak rotation and duplicity tests

A second phase in the peak testing focuses on the candidate dipole modes that were deemed significant according to the peak detection test presented in Sect. 5.3.3. When analyzing these peaks, where each one has been identified from a local maximum in the chunk ASEF, the resolving power of the chunk multimodal sampling may not be enough to recognize the presence of a possible fine structure within the peaks. This resolving power issue could show up in two different situations:

1. for SG and especially MS stars because the dipole mode linewidths are comparable with or even significantly larger than the frequency splitting among the rotationally split components. For hotter stars this often makes it difficult, if not impossible, to detect the effect of rotation on the oscillation mode using a simple, however careful, visual inspection;
2. for low-luminosity RGB and especially RC stars because of the low $\Delta\nu$ values and high dipole mixed mode density. Here the dipole mixed modes that exhibit a dominant p character are significantly condensed in frequency range, exhibit larger linewidths than the g-dominated $\ell = 1$ mixed modes, hence are more difficult to resolve. According to this explanation, a single chunk ASEF peak could be represented by: *a)* a single mixed mode that is split by rotation; *b)* two mixed modes that are not split by rotation but are sufficiently close to one another to partially blend; *c)* two neighboring rotational components, each one belonging to a different mixed mode; *d)* two of the three rotational components of the same dipole mixed mode that were extracted separately from the remaining third component.

In summary, a frequency peak identified using the chunk ASEF as a potential $\ell = 1$ mode could happen to be characterized by the effect of rotation or by the presence of a duplicity. For exploring these different occurrences, FAMED exploits another set of peak fitting models. Similarly to the set for peak detection and blending tests, these models are provided within the PeakBagging code and are listed below:

- $\mathcal{M}_{\rm E}$ is a model to test the hypothesis that the frequency peak is an oscillation peak represented by a single Lorentzian profile, meaning that it does not contain any fine structure inside. This model is similar to model $\mathcal{M}_{\rm B}$ (Sect. 5.3) but has a fixed background level, that is it accounts for the three free parameters of frequency centroid, amplitude, and linewidth of the Lorentzian profile ($\nu_{i,0}$, A_i, Γ_i, respectively);
- $\mathcal{M}_{\rm F}$ is a model to test that the frequency peak is a dipole oscillation peak split by the effect of rotation. It has five free parameters, namely the frequency centroid, amplitude, and linewidth of the Lorentzian profile, as well as the rotational

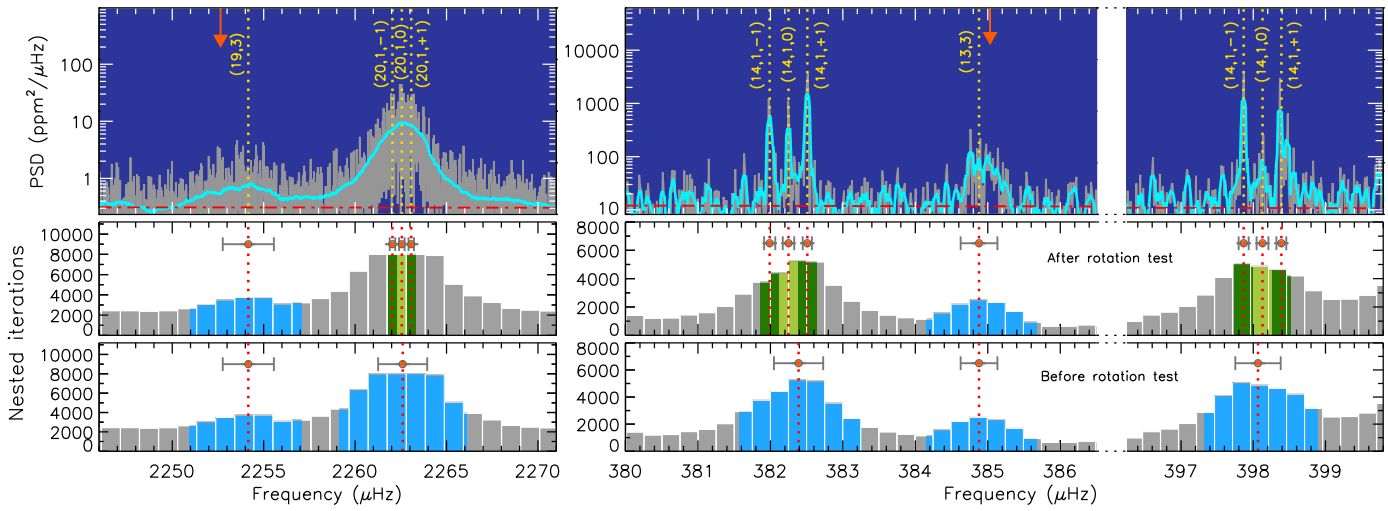

Fig. 10. The detection of rotation and of octupole modes in the MS star KIC 12069424 (left panels) and in the late SG star KIC 4351319 (right panels) using a diagram scheme similar to that shown in Fig. 9. *Top panels*: a close-up to the chunk $\ell = 1$ rotational triplet and its adjacent $\ell = 3$ for the MS star, and to the $\ell = 1$ rotational triplets of two mixed modes of the same chunk (one for each segment of the chunk PSD) for the late SG star, with the $\ell = 3$ mode included. The complete mode identification (n, ℓ, m) of the rotational components as obtained by FAMED is indicated. The orange downward arrows mark the asymptotic position of the $\ell = 3$ modes. *Middle and bottom panels*: the ASEF showing the estimated frequencies, 1-σ uncertainties, and corresponding frequency ranges, before and after the peak rotation tests.

splitting and stellar spin inclination angle of the rotational multiplet ($\nu_{i,0}, A_i, \Gamma_i, \delta\nu_{\rm rot}, \cos i$, respectively, where the spin inclination angle i is in the form of $\cos i$ to flatten out the sin law of the isotropic distribution such that a uniform prior on $\cos i$ can be used, see Corsaro et al. 2017a). The rotational multiplet accounts for $2\ell + 1 = 3$ (azimuthal) m components, and changes its shape following the formulation by Gizon & Solanki (2003). Similarly to model $\mathcal{M}_{\rm E}$, this model has a fixed background;

– $\mathcal{M}_{\rm G}$ is a model to test that the frequency peak is constituted by two adjacent dipole oscillation peaks (either different mixed modes or individual rotational components), each one represented by a Lorentzian profile. It is analogous to model $\mathcal{M}_{\rm D}$ but has six free parameters, namely the frequency centroid of the left-side Lorentzian profile, the (positive) frequency separation between the two Lorentzian profiles, and the amplitudes and linewidths of the two Lorentzian profiles ($\nu^1_{i,0}, \delta\nu_{\rm split}, A^1_i, A^2_i, \Gamma^1_i, \Gamma^2_i$, respectively, with superscripts 1 and 2 indicating the left- and right-side peaks of the duplet, and with the centroid frequency of the right-side peak given as $\nu^1_{i,0} + \delta\nu_{\rm split}$). Similarly to models $\mathcal{M}_{\rm E}$ and $\mathcal{M}_{\rm F}$, this model uses a fixed background level.

Following our discussion for the fitting models adopted in the peak detection and blending tests (Sect. 5.3), we have privileged fitting amplitudes instead of heights also for these additional models. These peak testing models do not require that the background level is varying because this hypothesis was already tested during the peak detection test. The purpose of this second set of peak testing models is to assess whether a candidate dipole mode is either split by rotation (peak rotation test) or constituted by two different oscillation peaks (peak duplicity test). The prior distributions are uniform even for these fitting models, following the discussions in Sects. 5.3.1 and 5.3.2. The prior hyper-parameters adopted on the model free parameters are detailed in Appendix A, Table A.2. Similarly to the peak detection and blending tests, all the results from the peak rotation and duplicity tests are stored in the sub-folder pb (Fig. 3). For each peak test, the portion of PSD used for the fit is always delimited by the frequency divisions $d_{a,b}$ of the given peak. If the frequency resolution of the dataset is comparable to the upper prior bound on the rotational splitting the rotation test is not performed because we cannot resolve the fine-structure of the peak. A similar discussion is applied to the peak duplicity test.

Another aspect to take into account is that the fitting model $\mathcal{M}_{\rm F}$ does not incorporate any asymmetry in the splitting components, meaning that: 1) the rotational splitting $\delta\nu_{\rm rot}$ between the central azimuthal component ($m = 0$) and the side ones ($m = \pm 1$) of the rotational multiplet, is the same on either side; 2) the linewidth is the same for all the rotational components of the multiplet. A more careful inspection of the rotational components aimed at reaching a higher level of accuracy on the estimated frequencies is in charge of the COMPLETE modality of FAMED, where the rotational multiplets will have the possibility to account for different rotational splittings and linewidths, depending on the azimuthal number of their individual components (e.g. see Benomar et al. 2018).

While the peak detection and blending tests based on the Bayesian evidence were already introduced by Corsaro & De Ridder (2014) and by Corsaro et al. (2015a), although in a slight different formulation, the peak rotation and duplicity tests performed by FAMED represent an entirely novel application of the Bayesian model comparison process done with Diamonds. The peak rotation test, in particular, allows identifying in a complete automated manner the azimuthal components for those dipole modes that are split by rotation in stars from MS to late SGs and low-luminosity RGB, with some cases extending up to RC stars (see our application in Sect. 6.3), hence to obtain an estimate of the spin inclination angle of the star directly from the parameter estimation of $\cos i$ in the fitting model $\mathcal{M}_{\rm F}$.

For stars in any evolutionary stage, following the approach used for the peak detection and blending tests, we can define the probability that a peak is split by rotation as

$$p_{\rm FE} = \frac{\mathcal{E}_{\rm F}}{\mathcal{E}_{\rm E} + \mathcal{E}_{\rm F}}\,, \tag{24}$$

where $\mathcal{E}_E$ and $\mathcal{E}_F$ are the Bayesian evidences of models $\mathcal{M}_E$ and $\mathcal{M}_F$, respectively. FAMED therefore considers that the peak is better represented by a rotational multiplet if a weak evidence condition is met, which according to the Jeffreys' scale of strength translates into $p_{FE} \geq 0.75$. The weak evidence condition is less stringent than that used for the peak detection test because we want to maximize the possibility to have the rotational effect detected in the peak. If however preferred by the user, one could strengthen the condition on the evidence by increasing the threshold on p_{FE} to that of e.g. a moderate evidence (≥ 0.923) or a strong evidence (≥ 0.993). As shown in our applications in Sect. 6, a weak evidence threshold appears to represent a favorable condition for testing the presence of rotation.

As discussed earlier in this section, for stars evolved into RG on top of the peak rotation test the candidate dipole peaks are checked against mode duplicity. The probability that a peak is a doublet is defined as

$$p_{GE} = \frac{\mathcal{E}_G}{\mathcal{E}_E + \mathcal{E}_G}\,, \tag{25}$$

with $\mathcal{E}_G$ the Bayesian evidence of model $\mathcal{M}_G$. For assessing whether the peak is better represented by a dipole rotational triplet or by a doublet, FAMED uses a flag based on the probability

$$p_{GF} = \frac{\mathcal{E}_G}{\mathcal{E}_F + \mathcal{E}_G}\,, \tag{26}$$

which is once again not to be interpreted as a detection probability, but only as a discriminant factor between models $\mathcal{M}_G$ and $\mathcal{M}_F$, following the procedure already used for the peak blending flag (Sect. 5.2) and the peak sinc^2 flag (Sect. 5.3.3). We can thus identify two conditions:

- if $p_{GF} > 0.5$ the peak is considered as a potential doublet. In this condition the duplicity is confirmed if $p_{GE} \geq 0.75$, using again a weak evidence condition as it is done for the peak rotation test.
- if instead $p_{GF} \leq 0.5$ the peak is considered as a potential dipole rotational triplet. Then, the peak rotation test is carried out in the same way as presented above using Eq. (24), namely by verifying the condition $p_{FE} \geq 0.75$.

Another useful aspect to consider in these evolved stars is that if the peak to be tested is significant but it has been flagged as a sinc^2 profile during the peak detection test ($p_{CB} > 0.5$ and $p_{CA} \geq 0.993$) then it is excluded from the peak rotation and duplicity tests. This is because if the peak is well represented by such a narrow profile, whose FWHM is comparable to the frequency resolution of the dataset, there is no point to inspect a possible fine-structure of the peak itself.

The left panels of Fig. 10 show an example of the peak rotation test conducted on a chunk dipole mode of the MS star 16 Cyg A. Here the frequency corresponding to the central azimuthal component ($m = 0$), automatically extracted by FAMED, has a remarkable agreement (on the order of 10^{-3} %) with the frequencies published by Davies et al. (2015) and by Lund et al. (2017) for the same oscillation mode. Davies et al. (2015) has also inferred a global spin inclination angle for 16 Cyg A of $i = 56^{+6}_{-5}$ deg, which is in good agreement with the value of about 59 deg obtained by FAMED from the peak rotation test of the single dipole mode shown in Fig. 10. Another application of the peak rotation test, but this time for an evolved SG star observed by *Kepler* for more than four years, KIC 4351319, and having $\Delta\nu \simeq 24\,\mu$Hz, is shown in the right panels of the same figure. Here we can see how the clear rotational triplets of two different mixed modes belonging to the same chunk have been correctly extracted and identified. The stellar spin inclination angle obtained by FAMED, averaged over the chunk mixed modes having rotational multiplets identified by the pipeline, is of about 77 deg, in line with an expected high-inclination configuration as already visible from the prominent $m = \pm 1$ components of the rotational multiplets (see our application in Sect. 6.2 and Fig. 15 too).

For RG stars instead, we can see an example of the application of both the rotation and duplicity tests in Fig. 11 for the low-luminosity RGB star KIC 12008916 (see also Sect. 6.3). On the PSD segment shown in the left panels, Corsaro et al. (2015a) has detected and identified two rotationally split dipole mixed modes (four peaks in total), corresponding to a configuration of high stellar spin inclination (hence only $m = \pm 1$ components). The ASEF obtained by FAMED is not resolving the two close peaks in the central region, where each peak is the rotational component of a different mixed mode. By means of the peak duplicity test FAMED is able to recover the actual frequency positions of the two peaks ($p_{GF} > 0.5$ and $p_{GE} \geq 0.75$), which show excellent agreement with those obtained in the literature. In the other PSD segment illustrated in the right side of Fig. 11 we can see the opposite situation, with a single ASEF peak decomposed after rotation has been detected, meaning that the probability of the duplicity test is lower than that of the rotation test ($p_{GF} \leq 0.5$ and $p_{FE} \geq 0.75$). The mode identification obtained with the peak rotation test for this oscillation mode is in agreement with that found by Corsaro et al. (2015a) using a manual approach. In addition, Corsaro et al. (2015a) did not report the $m = 0$ component of the rotational triplet because not well visible as they did not fit rotational multiplets but individual peaks only. This frequency component is instead delivered by FAMED thanks to the peak rotation test. The peak rotation test used in conjunction to the peak duplicity test has therefore the potential of distinguishing an actual peak doublet, i.e. constituted by two different mixed modes, from a single mixed mode having only $m = \pm 1$ azimuthal components visible. This is because in the latter case the peak profile has a structure that requires less free parameters to be modeled than that of the former case (five for model $\mathcal{M}_F$ versus six for model $\mathcal{M}_G$), meaning that in this example a corresponding Bayesian evidence will likely be higher for model $\mathcal{M}_F$, provided that the dataset is of sufficiently quality to allow discriminating between the two hypotheses. The subsequent ÉCHELLE modality of FAMED will however allow assigning an azimuthal number identification even to peaks that have been originated from peak doublets, i.e. not associated to any rotational multiplet during the CHUNK modality.

In conclusion to this section, one should note that the fits conducted for the peak rotation and duplicity tests are all unimodal and make use of the same nested sampling configuration presented in Sect. 5.3 for the fits of the peak detection and blending tests. However, the strong correlation between spin inclination angle and rotational splitting that arises when adopting model $\mathcal{M}_F$, translates into a larger computational time to conduct the peak rotation test with respect to the case of the peak detection and blending tests. As a result, this second peak testing phase can have a significant impact on the computational speed of the pipeline during the CHUNK modality. Nevertheless, conversely to the peak detection test that is a mandatory step for FAMED for attaining a reliable peak bagging analysis, if requested by the user the peak rotation (and as a consequence also the duplicity) test(s) can be deactivated, meaning that the output produced by FAMED will be simplified by excluding any information on the azimuthal number mode identification, and on

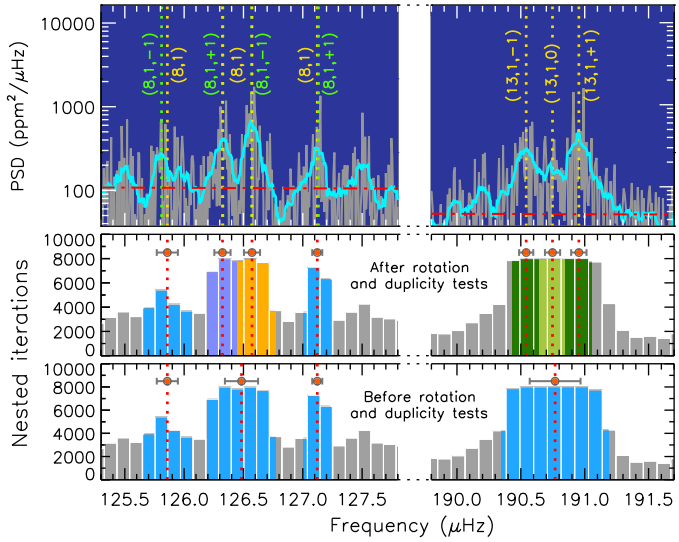

Fig. 11. The detection of rotation and mode duplicity in the RG star KIC 12008916. Similar description to Fig. 10 but showing the case of two different portions of the stellar PSD where both the peak rotation and duplicity tests have been performed. In the left panels one of the ASEF local maxima was split in two peaks because the duplicity test yielded a higher probability than the rotation test. The result is reverted for the ASEF local maximum shown in the right panels. The mode identification in green shows the azimuthal numbers for the individual peaks as identified by Corsaro et al. (2015a).

the stellar spin inclination angle. This condition could be useful if, for example, we need to speed up the computation when we know a priori that the datasets do not allow us to infer the rotation from the oscillation modes (for example if the rotation period is large compared to the time the star was observed), or because we want to perform a subsequent stellar modeling without taking into account any effect on the modes arising from stellar rotation. This latter choice is preferable for less evolved stars, such as MS and SGs, where the peak duplicity test is not even used.

5.5. Octupole modes

The last task in the analysis performed during the CHUNK modality is that of searching for the presence of a possible $\ell = 3$ mode within the chunk. This task is accomplished only after the peak detection tests of dipole modes are completed, and independently of whether the peak rotation and duplicity tests are carried out, although we recommend having the latter tests performed for late SG and RG stars to further improve the reliability of their octupole mode detection.

If the star is classified as either a MS or SG, having $\Delta\nu \geq \Delta\nu_{\rm RG}$, the search for an octupole mode is conducted only if at least two estimated frequencies are obtained from the set of significant candidate dipole modes presented in Sect. 5.3.3. This is because in cases where only one candidate dipole mode is present, FAMED privileges the mode identification of a dipole mode over that of an octupole mode given the higher mode visibility of the former. However, if the star has been flagged as a potential depressed dipole mode star during the GLOBAL modality (see Sect. 4.4.4), the octupole mode search will be executed even if only one candidate dipole mode is found. This allows incorporating the case of SG stars having depressed dipole mode power, in which no or few dipole modes could be detectable, but where octupole modes may still be clearly visible because not suppressed (see our application in Sect. 6.4).

If the star is classified as a RG, $\Delta\nu < \Delta\nu_{\rm RG}$, then the search for an octupole mode is done if at least one estimated frequency is obtained from the set of significant candidate dipole modes. This means that even if a single estimated frequency is available, and it is initially flagged as a dipole mode, after this task of the CHUNK modality it could be transformed into an octupole mode if the required conditions are met. Similarly to the case of less evolved stars, this will guarantee that octupole modes in RGs can still be found even if no dipole modes are present, which clearly incorporates stars that have depressed dipole modes.

In all cases introduced, not all the estimated frequencies flagged as candidate dipole modes can be retained for octupole mode inspection. For this selection FAMED computes a frequency range within which the potential octupole mode could be located. This frequency range is calculated from the asymptotic pattern of p modes, which shows that in MS stars the octupole mode of a chunk is always placed to a frequency below that of its neighboring dipole mode, and that the frequency position of the octupole mode is correlated with the value of $\delta\nu_{02}$ for all stars from MS to RGs. In particular, the expected frequency position of the octupole mode is given by the small frequency separation $\delta\nu_{03}$ of the asymptotic relation presented in Eq. (2). While in RGs the asymptotic position of the octupole modes is predictable with quite good accuracy, especially along the RGB, because it follows a tight $\Delta\nu$-$\delta\nu_{03}$ relation as the one calibrated by Huber et al. (2011), in MS and SG stars it is more uncertain because of the large variation of $\delta\nu_{02}$ found for these stars. In this latter case, however, we can exploit an useful approximation that allows rewriting the small frequency spacings $\delta\nu_{0\ell}$ presented in Eq. (2) as a function of $\delta\nu_{02}$ (e.g. see Bedding & Kjeldsen 2003), namely

$$\delta\nu_{0\ell} \simeq \frac{\ell\,(\ell+1)}{6}\delta\nu_{02}\,. \tag{27}$$

From this relation it follows that $\delta\nu_{03} \simeq 2\delta\nu_{02}$. By assessing $\delta\nu_{03}$ from mock samples prepared by Ball et al. (2018) we have experienced that $\delta\nu_{03}$ can vary between 1.5 and 4 times $\delta\nu_{02}$ in MS stars, and between 1.8 and 3 times $\delta\nu_{02}$ in SG stars. We have therefore implemented these limiting bounds to define a lower and upper frequency value to search for the octupole mode inside each chunk. For RG stars instead, we adopt as frequency range that obtained by varying $\delta\nu_{03}$ obtained from the $\Delta\nu$-$\delta\nu_{03}$ relation by Huber et al. (2011) between +12 and −16 %, allowing for a wider lower range to account for the reduction in $\delta\nu_{02}$ found in RC stars (e.g. see Kallinger et al. 2012). The frequency range to search for the octupole mode can however be tuned by the user from the configuring parameters list.

After this preliminary phase, FAMED checks whether inside the search frequency range for octupole modes there is at least one estimated frequency $\nu_{f,i}$ fulfilling two constraints: 1) it corresponds to a detected peak according to the peak detection test (Sect. 5.3); 2) it is not flagged as a sinc^2 profile according to the sinc^2 profile test (Sect. 5.3.3). The second constraint clearly applies to stars evolved into RGs, with $\Delta\nu < \Delta\nu_{\rm RG}$, but its meaning deserves some discussion. If a sinc^2 profile is better at reproducing the peak, assuming that the observation is sufficiently long to allow resolving the radial mode peaks of the star, then the FWHM of the mode is significantly smaller than that of an expected octupole mode, which should instead be comparable to Γ_0, the linewidth of the chunk radial mode (see Corsaro et al. 2015a). It is then obvious that in such case there is no

point of proceeding further. However, this condition has the tendency to manifest more frequently as the frequency resolution of the dataset degrades. This is because with the worsening of the frequency resolution the oscillation peaks become progressively less temporally resolved, thus resembling more closely a sinc^2 profile in the PSD (see our application in Sect. 6.6). As a result the detection of octupole modes becomes less likely with the shortening of the observations. If any of the two aforementioned requirements are not met then the search for an octupole mode stops here and no detection can be claimed. If instead at least one estimated frequency is found, FAMED proceeds by evaluating the FWHM of each corresponding peak found inside the search range, by fitting model $\mathcal{M}_E$ to the peak similarly to what has been done to obtain Γ_0 (see Sect. 5.3.1 and Appendix A, Table A.2). Even in this case, each fit is performed three times, with the resulting FWHM of each candidate octupole mode taken as the median value of each set. This procedure has the purpose of finding out the candidate octupole mode having the largest FWHM of the set, hereafter referred to as Γ_3.

At this stage, the octupole mode test can be executed on the candidate octupole mode that has the largest FWHM, through the following steps:

1. if the peak rotation and duplicity tests have been performed, FAMED checks whether the peak is either a dipolar rotational triplet or a doublet, or none of the two. For RG stars
   (a) if the peak is a dipolar rotational triplet ($p_{\rm GF} \leq 0.5$ and $p_{\rm FE} \geq 0.75$), then its mode identification remains that of a $\ell = 1$ mode by definition, and the peak is discarded from being a candidate octupole mode;
   (b) if the peak is neither a rotational multiplet nor a doublet ($p_{\rm FE} < 0.75$ and $p_{\rm GE} < 0.75$), then FAMED activates a further control check imposed on step #2.
   (c) if the peak is a doublet ($p_{\rm GF} > 0.5$ and $p_{\rm GE} \geq 0.75$) the FWHM of each peak of the doublet, as obtained from fitting model $\mathcal{M}_{\rm G}$, is compared to Γ_0. If at least one of the two peaks of the doublet has a FWHM comparable to Γ_0, then similarly to point (b) FAMED executes step #2. If none of the two peaks has a FWHM comparable to Γ_0, then the doublet is considered as a pair of $\ell = 1$ modes and the octupole mode test is stopped.

   When the star is classified as either SG or MS, only steps #1(a) and (b) hold, with (b) discarding the information on $p_{\rm GE}$ because the peak duplicity test is not done for such stars. If instead the peak rotation test was not performed because either deactivated by the user, or because the frequency resolution did not allow to resolve any fine-structure inside the peak, then FAMED proceeds directly with step #2 independently of the evolutionary stage classification of the star;
2. as a final check, the ASEF value of the local maximum corresponding to the estimated frequency of the candidate octupole mode is checked to make sure that it is smaller ($< 3/4$) than the limiting value imposed by the number of nested iterations. This is done because of the low mode visibility of octupole modes, which prevents the chunk multi-modal sampling from producing ASEF peaks that saturate to the limit. If Γ_3 of the candidate octupole mode is comparable to Γ_0, and it satisfies the condition on the ASEF maximum, the mode is finally flagged as a real $\ell = 3$ oscillation mode, having radial order given by that of the chunk radial mode minus two. Otherwise the octupole mode test is terminated without any $\ell = 3$ mode detection.

At the end of the octupole mode test we are left with either the detection of a $\ell = 3$ oscillation mode or only the $\ell = 1$ mode(s). In case we have an octupole mode detection and the mode is a doublet peak as verified according to step #1(c), before terminating the CHUNK modality the peak is split up in its two components. Here the peak of the doublet that has the largest FWHM is kept as the real $\ell = 3$ mode of the chunk, while the other peak of the doublet is flagged as a $\ell = 1$ oscillation mode with radial order given by that of the chunk radial order minus one. In this regard step #1(c) can be useful for the case of a RG star in which the octupole mode is falling very close to an adjacent dipole mixed mode, the latter being sensibly narrower than the $\ell = 3$ mode because of its partial g-mode character. The octupole mode test so introduced is therefore not only a method to detect octupole modes in the stellar PSD but to also disentangle them from possible $\ell = 1$ mixed modes that happen to be very close in frequency.

An example of the application of the octupole mode test for a chunk in both a MS and an evolved SG star is shown in Fig. 10. The asymptotic prediction for the octupole mode in the MS star is accurate to within 0.1 %, and the allowed octupole mode search range is sufficiently wide to locate the real $\ell = 3$ peak in the PSD. The frequency estimated by FAMED for the $\ell = 3$ oscillation mode of the MS star thus agrees on the order of 10^{-2} % with those extracted by Davies et al. (2015) and by Lund et al. (2017) for the same oscillation mode, with also the radial order n matching the literature value, showing that the accuracy obtained with this automated approach can be high even for these higher angular degree modes. For the evolved SG star presented in the same figure, the extracted octupole mode is found within 0.04 % from the predicted asymptotic value (see the arrow in the top right-hand panel), and has a structure that is clearly different than that of the adjacent dipole rotational multiplets, thus yielding an unambiguous detection. Other examples of the effectiveness of the octupole mode test in different stellar evolutionary stages, as well as SNR and frequency resolution conditions of the datasets, can be found in most of the applications shown in Sect. 6.

5.6. Detailed asteroseismic information

Thanks to the peak rotation test presented in Sect. 5.4, the CHUNK modality can even apply a mode identification to each dipole mode that is of the type (n, ℓ, m) in all stars ranging from MS up to late SGs and early RGB, having $\Delta\nu \geq \Delta\nu_{\rm RG}$, with some occurrences in stars evolved up to the RC as well. The additional azimuthal number tag attached to the corresponding oscillation component frequency as provided by the pipeline can be used for obtaining estimates of core-to-envelope rotation in SG and early RGB stars (depending on the degree of mixing between p and g modes for those dipole mixed modes whose rotation is detected), as well as of stellar spin inclination angle from single rotational multiplets (see Fig. 10 and the application in Sect. 6.2). For RG stars instead, the dipole mixed modes usually have a mode identification that does not include the azimuthal component, hence of the type (n, ℓ). This is because in more evolved stars the rotational components of each dipole mixed mode may have frequency separations comparable to the spacing between adjacent mixed modes. This means that these rotational components are usually detected separately from one another from the chunk ASEF. In addition, the large rotational splitting can yield confusion when the rotational components of different dipole mixed modes cross to one another in frequency (so-called crossing effects, e.g. Gehan et al. 2018). This implies that obtaining the azimuthal numbers for all the dipole mixed modes detected in RG stars requires a dedicated analysis on the individual oscillation

frequencies, which is in charge of the subsequent ÉCHELLE modality of FAMED, as it will be discussed in a forthcoming paper. Some exceptions to the mode identification scheme obtained by the CHUNK modality for RGs may however occur when a rotational multiplet is contained within a single ASEF peak like for less evolved stars. This condition could be verified for p-dominated mixed modes, especially at high oscillation frequency, where the linewidth is larger, and in general for those RG stars where the linewidths are increased because of their higher $T_{\rm eff}$, for example the 2$^{\rm nd}$ RC stars. In these scenarios FAMED can still deliver an azimuthal component identification for some of the oscillation modes, hence provide an estimate of the inclination angle of the star (see Sect. 6.3 for an application). The rotational components of the $\ell = 1$ modes are computed at the end of the CHUNK modality, and only after the octupole mode test has been performed. For their extraction, FAMED evaluates the corresponding frequencies and uncertainties $\nu_{f,i}$ and $\sigma_{f,i}$ from the chunk multi-modal sampling by using the modified frequency ranges, as illustrated in Figs. 10 and 11.

Another interesting quantity that is provided as an ouput of the computation in the CHUNK modality is the observed period spacing of the mixed dipole modes, ΔP_1, which is computed locally for each chunk only if at least two $\ell = 1$ mixed modes are found within the same chunk. If more than two $\ell = 1$ modes are found, the local ΔP_1 is computed as the mean value among the set of ΔP_1 values that can be obtained, each one calculated using a pair of adjacent mixed modes, but excluding possible $\ell = 1$ mixed modes that are placed between the $\ell = 2$ and $\ell = 0$ modes of the chunk. The value of ΔP_1 can of course be used to understand whether a star is a RGB or a RC following the same approach presented by e.g. Bedding et al. (2011) using the $\Delta\nu$-ΔP_1 diagram (see also Kallinger et al. 2012; Corsaro et al. 2012; Stello et al. 2013). ΔP_1 is computed before the rotational split components arising from the peak rotation tests are separated from one another, in order to minimize the contamination from the presence of rotation.

The CHUNK modality, thanks to the octupole mode testing presented in Sect. 5.5, is also capable of extracting and identifying octupole modes, for which a mode identification of the type (n, ℓ) is applied. As we have shown, octupole modes are extracted only under some specific circumstances because of their low mode visibility as compared to that of modes of smaller angular degree. The occurrence of octupole modes identified by FAMED can vary significantly from star to star, and it is to a large extent a strong function of the SNR of the oscillations in the stellar PSD (see the applications in Sects. 6.5 and 6.6). Once again the search for and detection of octupole modes is largely facilitated by the adoption of a data-driven approach based on the multi-modal sampling.

Another useful point to keep in mind is that that the oscillation mode frequencies extracted at the level of the CHUNK modality, especially in the case of $\ell = 1$ mixed modes, are not yet tested in the light of the theoretical asymptotic patterns. This assessment is afterwards carried out by the ÉCHELLE modality, and it is used by FAMED to provide an additional level of support to the extracted oscillation frequencies.

In summary, the CHUNK modality offers a detailed set of oscillation mode frequencies for each star, which thanks to their high level of precision and accuracy (often well below 0.1 %) can already be suitable for subsequent stellar and asteroseismic modeling purposes. The information extracted for each individual oscillation mode includes mode identification (n, ℓ, m) as discussed in this section, frequency estimate $\nu_{f,i}$ and uncertainty $\sigma_{f,i}$, frequency ranges $r_{a,b}$ and divisions $d_{a,b}$, sampling counts, ASEF maximum and smoothed PSD maximum, probabilities for peak detection, rotation, and duplicity, flags indicating whether or not the peak has a blending and whether it is a sinc^2 or a Lorentzian profile, and finally an estimate of $\cos i$ for each rotational multiplet detected. Additional parameters provided by the CHUNK modality are the chunk local values for the asymptotic parameters ϵ, $\delta\nu_{02}$, ΔP_1, as well as Γ_0 and Γ_3 if available (see also Table 1 for an overview). All these quantities are stored in an output summary file, one for each chunk, in the sub-folder `summary` (see Fig. 3). Similarly to the GLOBAL modality, a plot showing the chunk-multi modal sampling, the chunk ASEF, as well as the PSD with the extracted frequencies, uncertainties, and mode identification overlaid, is stored in the sub-folder `figs` for each one of the chunks analyzed.

6. Applications

In this section we will show different applications of the FAMED pipeline by using the GLOBAL and CHUNK modalities that were presented in Sects. 4 and 5, respectively. These applications comprise stars in a variety of evolutionary stages (both real stars and simulated ones), spanning from F-type MS up to RC. These stars have results are already available from the literature, so that a direct comparison with standard peak bagging analysis approaches and with simulated oscillation frequencies from stellar models can be made. Some of the stars shown in the following were already used in previous sections of the paper for illustrating the relevant features of the analysis procedure done by FAMED. The configuring parameters of the pipeline described in this paper are the same for all the applications shown in this section, indicating that the current setup can already cover the analysis of a wide range of stellar fundamental properties and evolutionary stages. Where possible, the applications will be illustrated in the form of échelle diagrams (Grec et al. 1983) for a direct visual comparison between the frequencies and mode identification extracted by FAMED and those available from the literature, otherwise a direct visualization of the stellar PSD will be given. For all the stars considered in this section, we have performed a preliminary background fit by means of the Background code (Sect. 3.1) following Corsaro et al. (2015a, 2017b). All the datasets for the stars observed with NASA *Kepler* that are used in this paper were optimized for asteroseismic analysis following García et al. (2011, 2014a) and Pires et al. (2015).

6.1. Main-sequence stars

The first application that we present is that of the G-type MS star 16 Cyg A, which we have already exploited for different illustrations presented in the paper. This star, classified as a solar analog and having $\Delta\nu \simeq 104\,\mu$Hz and $T_{\rm eff} = 5825$ K, is one of the best known and accurately analyzed dwarfs in terms of peak bagging analysis (Metcalfe et al. 2012; Lund et al. 2017). This is because this star has been observed by NASA *Kepler* for more than four years with high duty cycle, and exhibits excellent SNR oscillations in the stellar PSD that allow for the identification of a large number of oscillation modes. The peak blending caused by the mode linewidth becomes visible only for high frequencies, while most of the $\ell = 2, 0$ modes are well disentangled from one another. Many $\ell = 3$ modes can be identified as well through the oscillation envelope, making it an ideal target to show the capabilities of the pipeline in extracting and identifying octupole modes in MS stars. As shown in the top panel of Fig. 12 for this star, FAMED can extract oscillation modes of

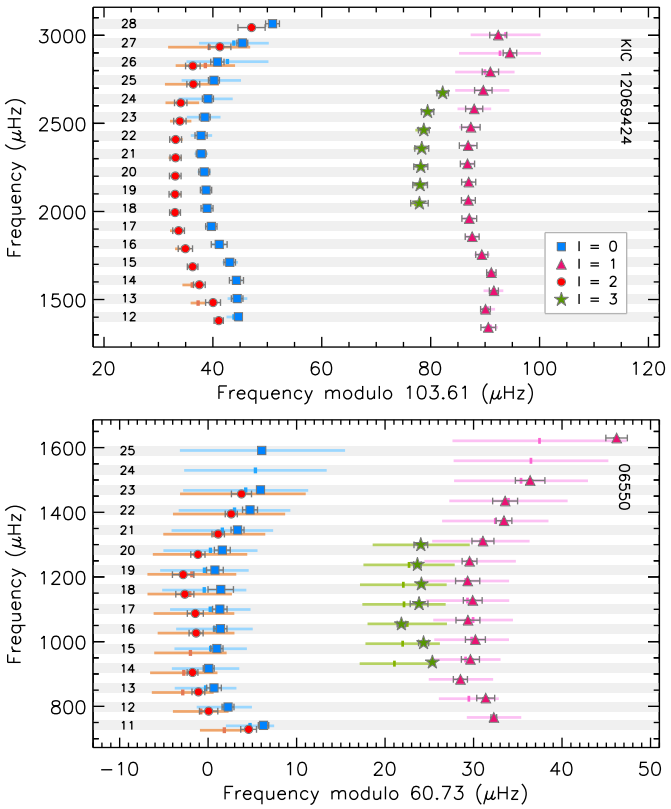

Fig. 12. The échelle diagrams for the MS stars KIC 12069424 and the simulated one 06550. The colored symbols represent the frequencies extracted by FAMED for angular degrees $\ell = 0, 1, 2, 3$ (see legend), with their associated 1-σ uncertainties, while the colored horizontal bars indicate the reference values from the literature varied by ± 1 FWHM of each peak, with the centroid marked by a vertical tick. For KIC 12069424, the adopted FWHM for the comparison values are the same for all the angular degrees within a single radial order, as provided by Lund et al. (2017). The numbers on the left side of each panel indicate the radial order n of the corresponding radial mode as obtained by FAMED. The folding value of $\Delta\nu$ is $\Delta\nu_0$ obtained from the GLOBAL modality for the real star, and the one computed by Ball et al. (2018) for the simulated one. The x-axis range is adjusted to have the $\ell = 2, 0$ ridges appearing on the left side.

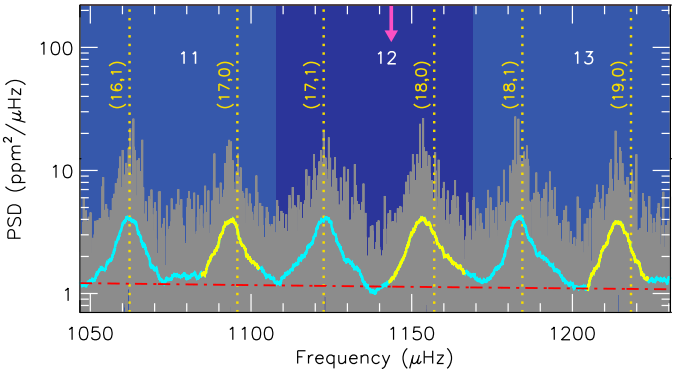

Fig. 13. The three most central chunks of the stellar PSD of the MS star 06550 as seen from the GLOBAL modality, with similar description as in Fig. 7. The position of the radial modes appears slightly offset to the right side of the corresponding $\ell = 2, 0$ peaks (marked with yellow smoothing) as the result of the correction $\delta\nu_0$ from the reference radial mode frequency obtained from the sliding pattern fit (see Sect. 4.5.1). The position of the global radial modes obtained by FAMED is in this case more realistic than that of the corresponding peak maxima in the smoothed PSD because each of these peaks also contains the adjacent $\ell = 2$ modes in an almost entirely blended structure with the $\ell = 0$ modes.

different angular degrees throughout the frequency range investigated by Lund et al. (2017), for a total of 58 oscillation mode frequencies correctly identified over 18 different radial orders. In all cases, the estimated frequencies match within the literature value of the peak FWHM, which is often smaller than the size of the symbol plotted in the figure. Additionally, FAMED identifies and extracts two $\ell = 3$ modes for radial orders 18 and 19, one $\ell = 2$ mode for radial order 11, and two more $\ell = 2, 0$ modes for radial orders 27 and 28, respectively, that are not in the list published by Lund et al. (2017). We note that the discrepancies between the FAMED and literature set of frequencies may have the tendency to increase for very high and/or very low frequency modes. For these modes, which are at the limit of detectability, the discrepancy can be explained by a combination of very large mode linewidth and low oscillation amplitudes for high frequency modes, and by the low amplitudes and high noise level for low frequency modes, which make it difficult to accurately locate the actual oscillation peak centroids independently of the approach that is used.

The second application is that of the F-type MS star 06550, which has been simulated by Ball et al. (2018) to reproduce a one year-length NASA TESS-like observation. The peculiarity of this target is that it has $T_{\rm eff} = 6416$ K, hence it exhibits large oscillation mode linewidths throughout the oscillation envelope. The large mode linewidths coupled to $\Delta\nu \simeq 61\,\mu$Hz, hence a relatively small $\delta\nu_{02}$, cause a strong peak blending for both $\ell = 2, 0$ and $\ell = 3, 1$ modes in most cases. As one could expect, the general mode identification performed by the GLOBAL modality is made challenging in this target because of the confusion caused by the peak blending, which does not allow to understand whether any of the peak structures are either a $\ell = 2, 0$ or a $\ell = 3, 1$ mode pair. This effect is well observable in Fig. 13, where the shape of the peaks associated to the two different mode pairs ($\ell = 2, 0$ and $\ell = 3, 1$) are very similar to one another and cannot be distinguished using only a visual inspection. Here the adoption of the powerful sliding-pattern fit calibrated for a MS star allows estimating the true reference radial mode frequency of the star, which is therefore used to correct the corresponding radial mode frequencies estimated from the ASEF (see the explanation in Sect. 4.5.1). The final peak bagging result for this star, obtained after executing the CHUNK modality, is instead shown in the bottom panel of Fig. 12. The comparison set used for this application is that of the theoretical frequencies and of their simulated linewidth. Despite the strong blending effects, as visible by the prominent superposition of mode linewidth for adjacent oscillation peaks, FAMED correctly distinguishes the $\ell = 2, 0$ mode pairs from those containing the $\ell = 3, 1$ modes throughout the stellar PSD. The $\ell = 0$ and $\ell = 1$ modes with radial order 24, and the $\ell = 2$ mode with radial order 23, were not found because they did not pass neither the peak blending test nor the peak detection test, while the $\ell = 2$ mode of radial order 14 was not detected because it did not pass the peak blending test. All the $\ell = 0, 1, 2$ oscillation modes presented here have been extracted in agreement with the expected theoretical fre-

quencies. Moreover, FAMED can correctly locate and identify seven different $\ell = 3$ modes, thus providing for this simulated target a total of 47 oscillation mode frequencies covering 15 different radial orders.

Another interesting aspect to discuss is that the value of the large frequency separation estimated from the GLOBAL modality, $\Delta\nu_0$ (see Sect. 4.5.1), is accurate enough to vertically align the extracted mode frequencies in the échelle. In particular, for KIC 12069424, $\Delta\nu_0$ computed by FAMED agrees within 0.3 % with the one estimated by Lund et al. (2017), while for the simulated star 06550 we find an agreement of about 0.8 %. This is a clear demonstration that the GLOBAL modality can be used to compute accurate values of $\Delta\nu$ in MS stars independently of whether the CHUNK modality is performed or not. In this way, the GLOBAL modality alone offers the opportunity to compute reliable estimates of stellar mass and radius for MS stars from scaling relations by means of the global asteroseismic parameters $\nu_{\rm max}$ and $\Delta\nu$.

6.2. Sub-giant and early red-giant stars

Sub-giant stars and stars that have recently entered the RGB are challenging targets to analyze in terms of their oscillations. The period spacing of dipole g modes, $\Delta\Pi_1$, in these stars can be significantly larger than that of stars that are more evolved along the RGB. In addition $\Delta\Pi_1$ can change sensibly from star to star depending on stellar mass and mean density, making it difficult to identify a simple $\Delta\nu$-$\Delta\Pi_1$ relation (Benomar et al. 2013). This can in turn cause the dipolar mixed modes to be displaced all over the frequency range of a given radial order, and as a result these mixed modes can even be found inside the regions containing $\ell = 2, 0$ modes, thus partially or entirely blending with them in some cases. The identification of $\ell = 2, 0$ mode pairs is further complicated for sub-giant stars, because the dipole modes displaced by the avoided crossings may still exhibit a linewidth comparable to that of pure p modes, thus yielding potential confusion in the general mode identification process as well as particularly messy oscillation patterns in some cases.

For showing the capabilities of FAMED in handling these tough asteroseismic targets, we have selected four different stars covering the regime of sub-giants and early RGB. In the first case, we consider the simulated late F-type star 05416, which similarly to the example given in the previous section, corresponds to a one-year length NASA TESS-like observation (Ball et al. 2018). Given that this sub-giant is not significantly evolved, with $\Delta\nu \simeq 58\,\mu$Hz, most of the chunks of its PSD contain only one mixed dipole mode each. However, the mixed modes are often displaced all over the range between two consecutive radial modes. Performing a peak bagging analysis is made more difficult by the relatively high temperature of this target, $T_{\rm eff} = 6139$ K, which causes a partial peak blending for the $\ell = 2, 0$ mode pairs and in one case with an adjacent $\ell = 1$ mixed mode as well. The top panel of Fig. 14 shows the comparison between the frequencies extracted and identified by FAMED, for a total of 39 over 12 radial orders, and those computed by Ball et al. (2018). We can see that there is a remarkable agreement between the two sets, including the $\ell = 1$ mixed mode having radial order 10 identified next to the $\ell = 2$ mode of the same chunk. Three different $\ell = 3$ modes could be identified too, albeit the large mode linewidths and low octupole mode visibilities make them difficult to be clearly recognized in the PSD.

The second example is that of another sub-giant simulated by Ball et al. (2018), 00123, having $\Delta\nu \simeq 49\,\mu$Hz and $T_{\rm eff} = 6097$ K. Although this star is slightly cooler than the previous

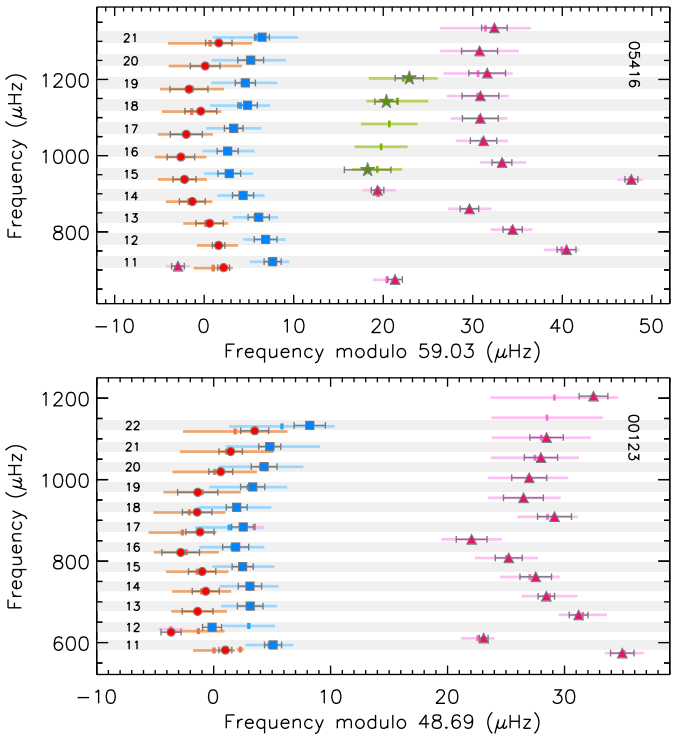

Fig. 14. The échelle diagrams for the simulated sub-giant stars 05416 and 00123. with literature values from Ball et al. (2018). Same description as for the bottom panel of Fig. 12. The folding $\Delta\nu$ values are those from the literature.

target, here the peak blending for $\ell = 2, 0$ and $\ell = 3, 1$ mode pairs is more pronounced because of the smaller values of $\Delta\nu$ and $\delta\nu_{02}$. Nevertheless, FAMED can perform the peak bagging analysis in an efficient way by providing correct oscillation frequency estimates and mode identification for all of the 37 peaks extracted over 14 radial orders. The only $\ell = 2, 0$ mode pair that appears offset with respect to its expected position from the theoretical frequencies is that corresponding to radial order 12, which is significantly affected by the presence of a $\ell = 1$ mixed mode next to it. The peak blending causes a bias in the estimation of these two modal frequencies. This is also visible from the middle panel of Fig. 14. No $\ell = 3$ modes could be detected in this target, because either affected by peak blending or not enough significant with respect to the noise level.

In the third case we consider a late SG star observed with *Kepler* for more than four years, KIC 4351319, having $\Delta\nu \simeq 24\,\mu$Hz and $T_{\rm eff} = 4842$ K. Thanks to its clear oscillation features, this star has been utilized in Fig. 10 to present the effectiveness of the peak rotation and octuole mode test. The peak bagging analysis may result computationally demanding and challenging to perform on this target because it contains a very large number of $\ell = 1$ mixed modes with a clear rotational effect, and with mixed modes displaced all over the frequency range between consecutive radial orders. As a comparative set for our application we adopt the results from a standard peak bagging analysis performed with Diamonds following the method presented by Corsaro et al. (2015a), where the individual rotational components have been extracted and identified with the aim of investigating the internal angular momentum transport of the star (Di Mauro et al. in prep.). The automated approach performed by FAMED yields a total of 86 oscillation mode frequencies covering 10 different radial orders, with the azimuthal numbers of 20

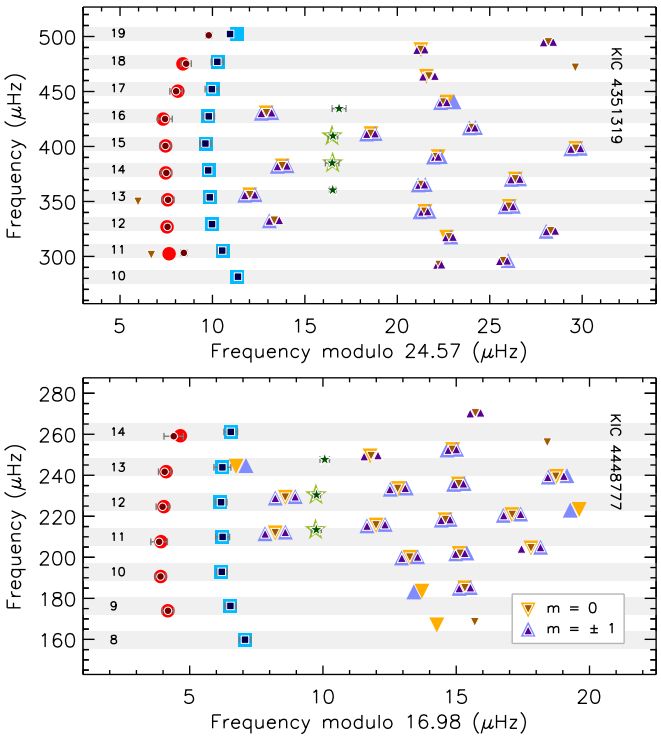

Fig. 15. The échelle diagrams for the late SG star KIC 4351319 and for the early RGB star KIC 4448777. Similar symbol description as for the top panel of Fig. 12. The frequency values obtained with the standard peak bagging approach by Corsaro et al. (2015a) for KIC 4351319 (Di Mauro et al. in prep) and for KIC 4448777 (Di Mauro et al. 2018) are shown using big symbols and light colors, with only detected oscillation modes considered. The values obtained by FAMED are instead indicated by small symbols and dark colors. The azimuthal components of the $\ell = 1$ rotational triplets are distinguished with different colors and symbols (see legend). No uncertainties are shown for the $\ell = 1$ modes because smaller than the symbol sizes in most cases.

dipole rotational multiplets correctly identified. The agreement with the comparative set is evident, although FAMED appears to outperform the standard peak bagging approach by identifying all the rotational components of seven additional $\ell = 1$ mixed modes, one new $\ell = 2$ mode for radial order 18, and two more $\ell = 3$ modes for radial orders 12 and 15. The average value of ΔP_1 estimated from the CHUNK modality is ~ 45 s, well in line with the $\Delta\Pi_1$ measured for stars in this $\Delta\nu$ regime (e.g. Mosser et al. 2012; Benomar et al. 2013).

The last example of this section is the star KIC 4448777, which has also been observed by *Kepler* for more than four years. This star is an early RGB, with $\Delta\nu \simeq 17\,\mu$Hz and $T_{\rm eff} = 4750$ K, that exhibits clear rotational effects on its dipolar mixed modes and a significant core-to-envelope differential rotation. For this reason this star constitutes an ideal target for studies of internal angular momentum transport (Di Mauro et al. 2016, 2018). From the work by Di Mauro et al. (2018) a standard peak bagging analysis done with Diamonds, again following the approach presented by Corsaro et al. (2015a), is available for a direct comparison that includes the $\ell = 1$ rotationally split components as well. In the échelle diagram shown in the bottom panel of Fig. 14 we can see an excellent agreement between the individual frequencies and mode identification obtained with FAMED and those from the literature. This is especially remarkable for all the $\ell = 1$ azimuthal components that were extracted by FAMED using the peak rotation test described in Sect. 5.4, with not even a single component misidentified with respect to the literature values. Only few differences arise in relation to those $\ell = 1$ mixed modes that were not found by our pipeline because not deemed significant, as well as for some other $\ell = 1$ mixed modes that were either not reported or reported but without detection by Di Mauro et al. (2018), and which are instead detected with our analysis. Interestingly, FAMED is also capable of detecting three $\ell = 3$ modes, one more with respect to those deemed significant by Di Mauro et al. (2018). The overall set of frequencies provided by the pipeline therefore accounts for 67 different oscillation modes (including the m components of 16 different dipole rotational triplets), spanning seven different radial orders. From ΔP_1 computed for the different chunks in the CHUNK modality, we find an average value of about 57 s, well compatible with the expected $\Delta\Pi_1$ for a star in this evolutionary stage.

The agreement between $\Delta\nu_0$ computed by FAMED with the GLOBAL modality and the reference values from the literature may vary from star to star depending on how much the frequency pattern of the oscillation modes is irregular. For the simulated stars 05461 and 00123 we find an agreement of about 1.2 % and 0.3 %, respectively, while for KIC 4351319 we have about 0.4 %, and a remarkable ~ 0.01 % for KIC 4448777, within the quoted uncertainty provided by Di Mauro et al. (2018).

6.3. Red giant branch and red clump stars

The peak bagging analysis of RG stars has to face the presence of a large number of $\ell = 1$ mixed modes. In this section we will demonstrate how FAMED can adequately extract and identify oscillation modes up to $\ell = 3$ in such evolved stars, independently of whether there is the effect of rotation. The applications that will be presented in the following comprise a star in the low-luminosity RGB, one star evolving towards the tip of the RGB, and one star in the RC. It is worth mentioning that according to the evolutionary stage classification proposed by Kallinger et al. (2012) (but see also the peculiar cases discussed by Corsaro et al. 2012), high-luminosity stars having $\Delta\nu \lesssim 3.2\,\mu$Hz, could even be stars that have recently left the RC to evolve toward higher luminosities, and may therefore comprise early AGB stars as well. Given the similarity of the stellar PSD between the high-luminosity RGB and the evolved RC and early AGB stars, we will not illustrate the pipeline analysis for such additional classes. Potentially evolved RC and early AGB stars are analyzed by FAMED in the same way as high-luminosity RGB by relying on the multi-modal sampling conditions imposed for the regime $\Delta\nu \leq \Delta\nu_{\rm tip}$, as already presented in Sect. 5.1.

Stars that are evolving along the RGB have a higher core-envelope density contrast as compared to RGs that are settled in the RC. As a consequence, the coupling between g- and p-mode cavities in the former stars is weaker than in the latter ones, meaning that the dipole mixed modes are more condensed in frequency during the RGB phase, and with a power barycenter that is regularly following the asymptotic position of pure $\ell = 1$ p modes (Montalbán et al. 2010; Corsaro et al. 2012). In these stars the $\ell = 1$ mixed modes are thus less contaminating the regions containing $\ell = 2, 0$ modes, and the mode extraction and identification process is in principle more accessible. As noted by Corsaro et al. (2015a), RG stars placed in the lower part of the RGB are optimal targets to study oscillations because their dipole mixed modes, even if rotational effects are at play, are in

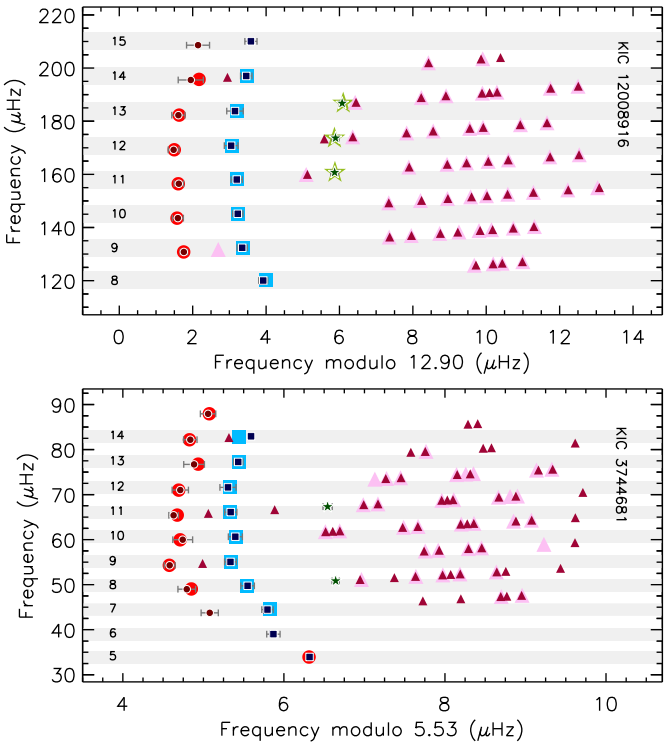

Fig. 16. The échelle diagrams for the low-luminosity RGB KIC 12008916 and the 2nd RC KIC 3744681. The literature values for the frequencies and mode identification are those from Corsaro et al. (2015a) for the RGB star and from Kallinger (2019) for the RC. Same description as for the bottom panel of Fig. 14, but without azimuthal number mode identification. Only statistical significant frequencies are shown, as indicated from the detection probabilities available in the literature. No uncertainties are shown for the $\ell = 1$ modes because smaller than the symbol sizes in most cases. For both stars, the folding $\Delta\nu$ is $\Delta\nu_0$ estimated by FAMED.

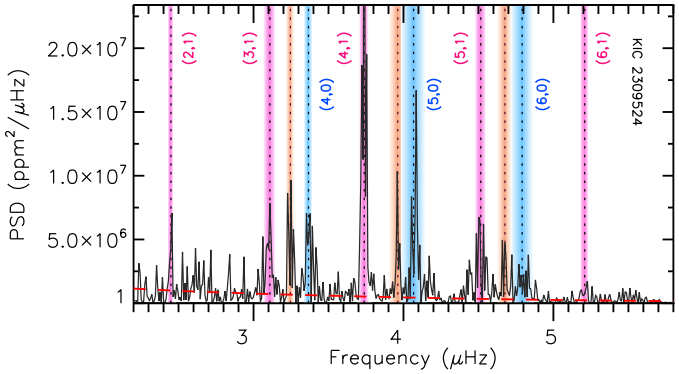

Fig. 17. The peak bagging analysis of the high-luminosity RGB KIC 2309524. The vertical dotted lines mark the oscillation modes identified by FAMED on the PSD of the star (black curve). The vertical colored bands, which are as wide as 3-σ uncertainty on each side of the estimated frequencies, indicate the angular degree of the mode (blue, red, and pink for $\ell = 0, 2, 1$ modes, respectively). The mode identification (n, ℓ) is also overlaid for $\ell = 0, 1$ modes and it has been omitted for $\ell = 2$ modes for visualization purposes only. The background level corresponds to the dashed red line.

general well separated in frequency from one another. This is because of their large values of $\Delta\nu$, on the order of 10-15 μHz, and of their high $\nu_{\rm max}$, around 100-200 μHz, which often allows to analyze several or even many consecutive radial orders. The low-luminosity RGB star considered for our application is KIC 12008916, which has been widely adopted in the literature as a benchmark RG for peak bagging analysis thanks to its high SNR and clear oscillation pattern (Corsaro et al. 2015a; Davies & Miglio 2016; García Saravia Ortiz de Montellano et al. 2018). This star has $\Delta\nu \simeq 13\,\mu$Hz and $T_{\rm eff} = 5454$ K, with a high spin-inclination angle that makes $\ell = 1$ mixed modes appear as rotational doublets in most cases. Although the CHUNK modality of FAMED is not identifying by default all the azimuthal numbers for each $\ell = 1$ rotational component if the star is classified as a RG (see the discussion in Sect. 5.6), the corresponding oscillation frequencies are all extracted and identified using a pair (n, ℓ). In the échelle diagram shown in Fig. 16 we find a remarkable agreement between the oscillation frequencies detected and identified by Corsaro et al. (2015a) (where we have ignored their information on the azimuthal number) and those extracted by FAMED, with a total of 67 oscillation frequencies covering eight radial orders. According to our analysis, FAMED was capable of detecting a new $\ell = 0$ mode for radial order 15, a new $\ell = 2$ mode for radial order 14, as well as the three $\ell = 3$ modes that were reported in the literature. Thanks to the octupole mode test presented in Sect. 5.5, the correct extraction and identification of the $\ell = 3$ mode frequencies was possible even if for some of them $\ell = 1$ rotational components are found to be very close in frequency, thus potentially leading to confusion. Finally, the value of the observed period spacing obtained as an average from the different chunks is $\Delta P_1 \simeq 33$ s, which based on the $\Delta\nu$-ΔP_1 diagram presented by Bedding et al. (2011) confirms that the star is a RGB.

Stars that are evolving towards the tip of the RGB, also referred to as high-luminosity RGB, can be rather cool and are thus classified as late K-type and early M-type giants (e.g. see Stello et al. 2014). For these stars only a handful of oscillation modes could be observed because of their very low $\nu_{\rm max}$, on the order of a few μHz, with no $\ell = 3$ modes expected to be found because of the prominent high-power noise at low frequency. In these stars the oscillation pattern is substantially simplified, with just one $\ell = 1$ mode peak per radial order as the result of the small $\Delta\nu$ and $\Delta\Pi_1$ values from the high core density and core-envelope density contrast. The difficulty in applying a Bayesian multi-modal approach for performing a peak bagging analysis in these cool but luminous targets is represented by: 1) the lack of available radial mode linewidth estimates for stars of types later than mid-K; 2) the very low values of $\nu_{\rm max}$ and $\Delta\nu$, the latter being below 1 μHz, resulting in just a few radial orders and a few to several oscillation modes that can be observed; 3) the frequency resolution that can be achieved to resolve the individual oscillation peaks, which even in the best case of observations from the full *Kepler* nominal mission often proves to be just enough to reach down to about $\nu_{\rm max} \simeq 1\,\mu$Hz. In the current version of FAMED, following the results by Corsaro et al. (2015a), Lund et al. (2017), and Handberg et al. (2017) on RGs, for stars having $T_{\rm eff} < 4900$ K we have adopted a constant value of the FWHM of radial modes, which is set to 0.12 μHz (new empirical relations connecting the mode linewidth to $\nu_{\rm max}$, $T_{\rm eff}$, and metallicity in stars from F-type MS to M-type RGs will be presented in a separate paper, Corsaro et al. in prep.). The test target that was considered for our application is the late K-type star KIC 2309524, which was observed by *Kepler* for more than four years, having $\Delta\nu \simeq 0.7\mu$Hz, and $T_{\rm eff} = 3938$ K (Pinsonneault et al. 2018).

Given that only four radial orders can be observed in this star, instead of presenting the results through an échelle diagram, the extracted frequencies are this time overlaid on top of the stellar PSD as shown in Fig. 17. We can clearly see that FAMED was capable of correctly locating the position of the $\ell = 0$ modes from the GLOBAL modality, and to subsequently identify the $\ell = 1, 2$ modes in the CHUNK modality, for a total of 11 oscillation frequencies extracted. The ϵ value obtained from the GLOBAL modality is 0.57, in line with the ϵ-$\Delta\nu$ trend reported by Kallinger et al. (2012) for stars with similar $\Delta\nu$ (see their Fig. 4). This star was also analyzed by Kallinger (2019) with an automated peak bagging approach, therefore its oscillation mode frequencies are publicly available. The author detects the same three $\ell = 0$ modes found by FAMED, with frequencies that agree on average around 0.3 %, and four $\ell = 2$ modes, three of which were also detected by our pipeline, with a very good average agreement for those in common, about 0.03 %. No $\ell = 1$ modes were however reported by Kallinger (2019) for this star.

For RGs that are settled in the core-helium-burning phase of stellar evolution, the oscillation mode pattern and therefore the mode identification process are probably the most complex among all the evolutionary stages discussed until now. This is caused by four main aspects: 1) a value of ϵ of the asymptotic relation that does not follow the ϵ-$\Delta\nu$ relation found for hydrogen-shell burning RGs, calling for the need of an independent evaluation on a star by star basis (Kallinger et al. 2012; Corsaro et al. 2012); 2) larger oscillation mode linewidths with respect to their RGB counterparts because of their higher $T_{\rm eff}$ (Corsaro et al. 2012), which can often yield important blending effects between neighboring oscillation peaks; 3) large values of $\Delta\Pi_1$ and strong coupling between the p- and g-mode cavities because of the lower core density and ∼10 times smaller core-envelope density contrast than in RGB stars of similar luminosity, resulting in $\ell = 1$ mixed modes that are significantly more displaced in frequency range; 4) rotational splittings comparable to the frequency separation between adjacent $\ell = 1$ mixed modes, which could often lead to strong crossing effects. The result is an asteroseismic signal that is usually rather messy, especially if the star has an intermediate-mass and is therefore settled in the 2nd RC. These difficulties may prevent from performing a reliable peak bagging analysis in many cases, which also explains the lack of published oscillation frequencies for RC stars until only very recent times (Kallinger 2019). In this paper we show an application to the intermediate-mass 2nd RC star originally analyzed by Deheuvels et al. (2015), KIC 3744681, and recently peak bagged by Kallinger (2019). This star is suited for the analysis of core-to-envelope differential rotation because it shows a wealth of $\ell = 1$ rotational multiplets throughout its PSD. This star has $\Delta\nu \simeq 5.5\,\mu$Hz, and $T_{\rm eff} = 5084$ K, which produces relatively large mode linewidths and therefore partial peak blending effects in many cases. By means of the automated analysis done by FAMED it was however possible to identify a total of 76 oscillation frequencies that cover 10 radial orders, as shown in the bottom panel of Fig. 16. The échelle diagram shows a comparison with the frequencies extracted and identified by Kallinger (2019), which do not have identification of the azimuthal number. The agreement for $\ell = 0$ and $\ell = 2$ modes is very good, with just one $\ell = 0$ mode likely misidentified as a $\ell = 2$ by Kallinger (2019). FAMED can even detect a $\ell = 2$ and a $\ell = 0$ mode, both corresponding to radial order 6, that were not reported in the literature set. We can see a remarkable agreement between the two sets of frequencies for those $\ell = 1$ mixed modes that are in common, although FAMED delivers 19 more significant frequencies with respect to Kallinger (2019). Furthermore,

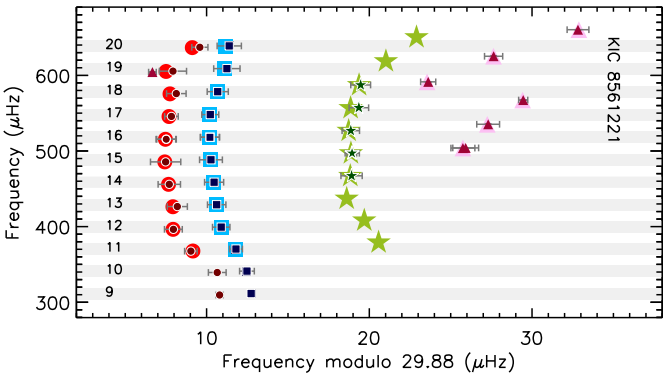

Fig. 18. The échelle diagram for the depressed dipole sub-giant star KIC 8561221. Same description as for Fig. 16. The value of $\Delta\nu$ used for the échelle is that published by García et al. (2014b).

FAMED reports the detection of two $\ell = 3$ modes, which are not listed in the literature. Another strength point of our approach is that despite most of the $\ell = 1$ mixed modes remain without an azimuthal number identification, thanks to the peak rotation test facility of the pipeline it was possible to detect rotation for three of these modes. This information extracted by FAMED is already enough to compute an average inclination angle of the star, corresponding to about 70 deg, well compatible with the value estimated by Deheuvels et al. (2015) using a dedicated approach that focused on the $\ell = 1$ rotational multiplets of the star. The observed period spacing estimated by FAMED has an average of about 146 s, which is in agreement with the expected ΔP_1 of a 2nd RC star (Bedding et al. 2011). The ϵ value obtained from the GLOBAL modality is 0.98, once again in line with the trend reported by Kallinger et al. (2012).

In conclusion, for the RG stars presented in this section, by estimating $\Delta\nu_0$ from the GLOBAL modality FAMED reaches a level of agreement of about 0.3 % for KIC 3744681, and a remarkable one of 0.03 % for KIC 12008916, as compared to the literature values. For KIC 2309524, our $\Delta\nu_0$ agrees around 0.1 % with that obtained by Kallinger (2019), thus confirming that the GLOBAL modality can reliably estimate $\Delta\nu$ for evolved RGB stars as well.

6.4. Depressed dipole stars

In Sects. 4.4.4 and 5.6 we have discussed how the GLOBAL and CHUNK modalities are suited for performing a peak bagging analysis even in RGs that show dipole mixed modes with depressed amplitudes. For ensuring that a peak bagging analysis is correctly performed in these targets, they have to be identified as potential depressed dipole mode stars during the GLOBAL modality. According to the present literature, these stars range from sub-giants to RGs, and are characterized by a dipole mode amplitude suppression affecting either a portion or the entire oscillation frequency range. For an application to this class of stars we have selected the late G-type star KIC 8561221, a sub-giant having $\Delta\nu \simeq 30\,\mu$Hz and $T_{\rm eff} = 5290$ K. This star was initially studied by García et al. (2014b), who discovered the presence of a strong gradient in the amplitude of its $\ell = 1$ modes in moving from low to high oscillation frequencies. The challenge for the peak bagging analysis of this star is that no clear global asymptotic pattern can be applied to the $\ell = 1$ mixed modes, although the $\ell = 2, 0$ mode pairs are regularly spaced in frequency throughout the PSD. As shown in Fig. 18, FAMED is capable of detecting a large set of oscillation mode frequencies,

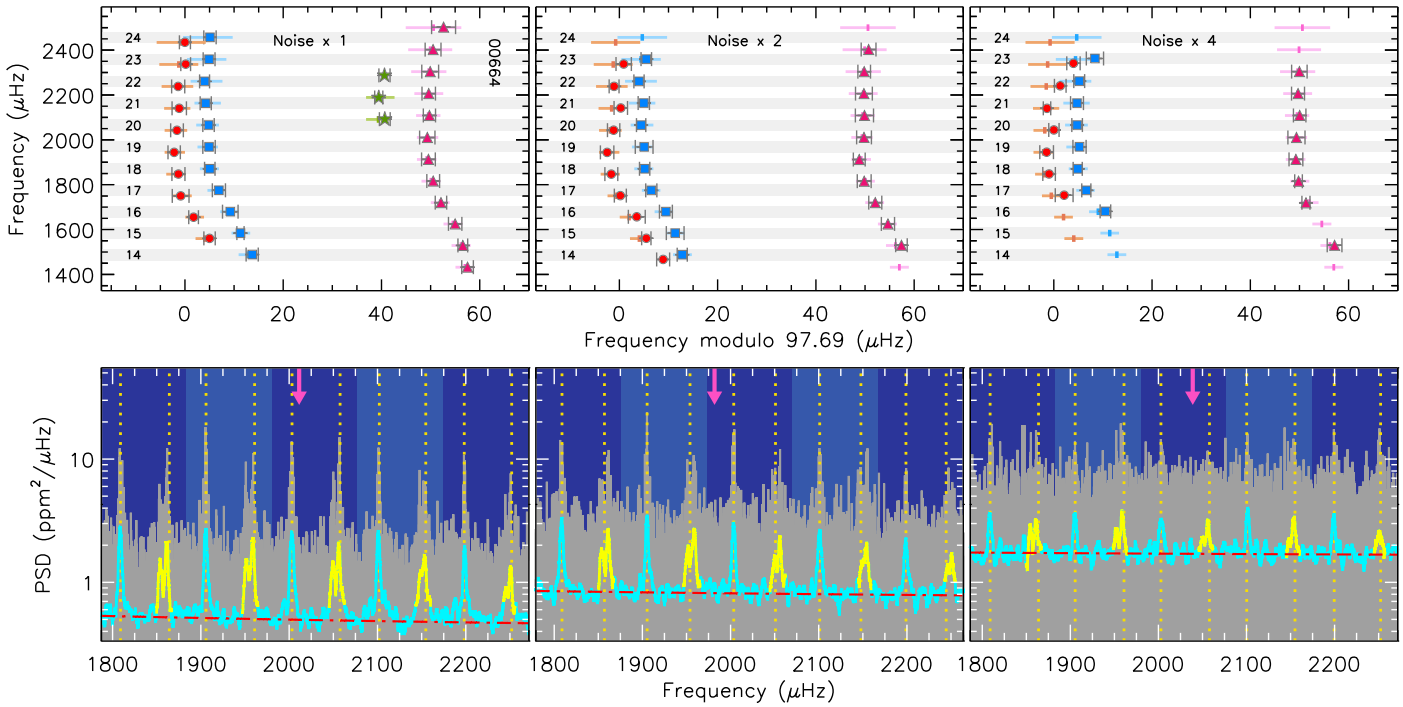

Fig. 19. The peak bagging analysis of the simulated MS star 00664 by degrading the instrumental noise in the stellar PSD. *Top panels*: the échelle diagrams obtained for three different noise levels, with same description as that used in Fig. 12. The folding $\Delta\nu$ value is that provided by Ball et al. (2018). *Bottom panels*: The five most central chunks of the stellar PSD as seen from the GLOBAL modality, with similar description as in Fig. 7. The purple arrow marks the position of $\nu_{\rm max}$ obtained from an independent background fit to each PSD.

36 over 13 radial orders, including all the $\ell = 1$ modes previously identified by García et al. (2014b), and five $\ell = 3$ modes, thus reaching a fine level of agreement with the literature values. Additionally, FAMED detects a new $\ell = 1$ mode for radial order 18, which is located just next to a $\ell = 2$ mode. The presence of this dipole mixed mode could explain why the adjacent $\ell = 2$ mode reported in the literature appears suspiciously offset to lower frequencies with respect to the expected $\delta\nu_{02}$ of the star. Finally, our pipeline could detect two new $\ell = 2, 0$ mode pairs in the two most low-frequency and low-SNR chunks. On top of the capabilities of FAMED, we consider that the new modes identified by our pipeline in the low SNR chunks were more likely to be found because of the better quality dataset used in this work, spanning from *Kepler* quarter 5 to 17, which corresponds to almost one year more observations with respect to the dataset used by García et al. (2014b). Nonetheless, all the frequencies reported by García et al. (2014b) do not come with detection probabilities, which may also explain the surprisingly large number of $\ell = 3$ modes reported by the authors, most of which located in low SNR chunks where no detectable signal could be found by FAMED. Finally, the agreement on $\Delta\nu$ obtained by the GLOBAL modality is also rather good, with a deviation of about 0.8 % only with respect to the literature value.

6.5. Noise degradation

Performing the peak bagging analysis in non-optimal SNR conditions is an important requirement to be able to maximize the yield of stars for which oscillation mode frequencies can be extracted. A larger stellar yield including stars with low SNR data can therefore account for both stars that are deemer and stars that are less evolved, hence showing smaller oscillation amplitudes (e.g. Corsaro et al. 2013). This means that if a peak bagging analysis can be conducted in low SNR conditions, one is able to extend the asteroseismic probing potential to both stars that are placed more far away in our Galaxy and to stars that are younger, with direct implications on the study of galactic populations (e.g. Miglio et al. 2013; Silva Aguirre et al. 2020; Chaplin et al. 2020) and of stellar dynamo and magnetic activity (e.g. García et al. 2010; Bonanno et al. 2014, 2019), respectively.

In the previous applications we have seen that the pipeline yields trustworthy results for a large variety of stars also for those PSD chunks having the lowest SNR within the oscillation envelope. This is a clear demonstration that the multi-modal sampling is sensitive to the presence of oscillation peaks even when these could be confused with noise from a simple visual inspection. In this section we want to prove the global effect produced on the extracted oscillation frequencies when reducing the SNR not only in a single chunk but throughout the stellar oscillation envelope. While the best data quality reference currently available corresponds to that of the observations carried out by the nominal *Kepler* mission, other photometric missions, both current and future ones allowing to observe and detect stellar oscillations, may not be able to reach similar SNR conditions as *Kepler*. In this section we will therefore show how FAMED can perform by varying the level of instrumental noise in the stellar PSD. For our application we select the simulated star 00664 from the mock sample of Ball et al. (2018). This star is a late F-type MS, having $\Delta\nu \simeq 98\,\mu$Hz and $T_{\rm eff} = 6078$ K. The outcomes from the pipeline for three different levels of the instrumental noise, namely x1, x2, and x4, are presented in Fig. 19. We can clearly see that FAMED is capable of locating the correct position of the radial modes even in the lowest SNR case. Here the oscillation modes are not anymore well observable from the

PSD and a smoothing is required to be able to see them more clearly. It is noticeable that the extracted oscillation mode frequencies remain in general rather accurate even if the noise level is increased by four times, going from a total of 36 oscillation frequencies extracted in the best SNR case (noise x1), where three $\ell = 3$ modes could be detected and properly identified too, to 23 oscillation frequencies in the worst SNR scenario (noise x4), where no $\ell = 3$ modes could be found because completely hidden by the noise. We thus have an overall decrease of about 36 % in the number of frequencies that could be extracted for this target when increasing the level of noise by four times.

The net result with decreasing SNR is, as expected, a progressive lowering of the number of oscillation modes detected by the pipeline, with the modes first disappearing from those radial orders with the lowest SNR, namely towards the tails of the oscillation envelope. This effect is explained by the drop of the detection probabilities obtained when performing the peak detection tests (Sect. 5.3), because when the background noise increases it is more likely that the peak is confused with the background level in its proximity. Another effect produced by the noise degradation that is worth to be mentioned is a progressive lowering of the frequency accuracy of $\ell = 2$ modes, which, after the $\ell = 3$ modes, are the most affected due to their lower visibility as compared to those of $\ell = 0$ and $\ell = 1$ modes. Furthermore, the estimation of $\Delta\nu$ from the GLOBAL modality reaches an accuracy level between 0.9 and 0.6 %, with no clear dependency on the actual noise level of the dataset. This means that as long as the oscillation modes can be sampled through the island peak bagging model presented in Sect. 4.1, the large frequency separation can be measured with high reliability, independently of the SNR of the stellar PSD.

6.6. Frequency resolution degradation

Another critical feature to consider when performing the peak bagging analysis is the impact of the frequency resolution on our capability to detect and properly identify the oscillation mode frequencies. Degrading the frequency resolution on the stellar PSD has three main effects: 1) the SNR decreases as the result of the decrease of the peak heights; 2) the observed linewidth of resolved oscillation modes is significantly affected by the frequency resolution of the dataset, such that as long as the frequency resolution is smaller than the true peak linewidth, the latter one decreases as the frequency resolution degrades because the mode becomes progressively less resolved, but as soon as the frequency resolution becomes larger than the true peak linewidth (in the worst scenario), meaning that the mode is completely unresolved, then the observed peak linewidth can become larger than the true value; 3) the number of frequency-resolved oscillation modes decreases because modes that are as close in frequency as ∼3-4 times the frequency resolution itself cannot be distinguished in general, although this limiting separation is subject to vary as a function of the SNR. Therefore by degrading the frequency resolution we expect that the overall number of modes that can be distinguished, detected, and identified in the stellar PSD decreases, as well as the accuracy and precision obtained on the individual mode frequencies.

If the frequency resolution decreases the peak loses its Lorentzian-like structure due to the loss of temporal resolving power on the mode lifetimes, so it is more likely that the peak detection tests will favor the scenario of a sinc^2 profile against that of a Lorentzian profile. The most evident effect of a frequency resolution degradation can be seen on evolved stars, where the densely populated $\ell = 1$ mixed modes forests – considering stars observed by *Kepler* for more than four years as a reference – are progressively simplified in structure as the frequency resolution decreases (e.g. see the first results on red giants using CoRoT observations spanning about 150 days, De Ridder et al. 2009). In addition, those dipole mixed modes having a stronger p-mode character are more likely to remain observable thanks to their higher oscillation amplitudes as compared to those having a stronger g-mode character instead.

For testing the capabilities of FAMED in performing a peak bagging analysis with a varying frequency resolution, we consider the low-luminosity RGB star KIC 6117517, observed by *Kepler* for more than four years, and with available oscillation mode frequencies from Corsaro et al. (2015a). This star has $\Delta\nu \simeq 10\,\mu$Hz, $T_{\rm eff} = 4687$ K (Pinsonneault et al. 2018), and exhibits a large number of oscillation modes, including some $\ell = 3$. Starting from the original KADACS light curve used in Corsaro et al. (2015a), on top of the reference PSD corresponding to an observing time of $T = 1470$ days, we reproduce three additional datasets, for observing times $T = 365$ days, 90 days, and 30 days. These observing times are chosen on purpose to roughly reproduce the frequency resolution obtained from a 1-year observation with NASA TESS in the continuous viewing zones, a ∼3-months observation during a NASA K2 Campaign, and a typical ∼1-month observation with NASA TESS. The results of our test are presented in Fig. 20. For $T = 1470$ days (top panels), corresponding to a frequency resolution of $\delta\nu_{\rm res} \simeq 0.008\,\mu$Hz, we find a very good agreement between the automated frequency extraction operated by FAMED and the literature values published by Corsaro et al. (2015a), for a total of 70 oscillation frequencies extracted by our pipeline and covering eight consecutive radial orders. Here FAMED can detect and identify all the four $\ell = 3$ modes reported in the literature, as well as all the $\ell = 2, 0$ modes and nearly all of the $\ell = 1$ mixed modes. The global radial mode frequencies obtained from the GLOBAL modality are also quite accurate thanks to the high SNR and frequency resolution of the dataset, as it can be seen from the corresponding plot shown on the right panel in the same Fig. 20. When degrading the frequency resolution to about four times the nominal value for $T = 365$ days, the frequency set extracted by FAMED reduces to 58 frequencies (hence by ∼17 %), with the four $\ell = 3$ modes reported in the literature still detected. The global radial mode frequencies from the GLOBAL modality are rather accurate once again. With one year of observation the situation has thus not changed dramatically, although most of the lost frequencies are $\ell = 1$ mixed modes that have smaller oscillation amplitudes, hence generally falling towards the wings of the $\ell = 1$ mixed mode region. But with an additional degradation of the frequency resolution, this time to about 16 times the nominal value, for $T = 90$ days, the number of frequencies extracted by FAMED reduces to 24 (meaning about 66 % less than in the nominal case), with one $\ell = 3$ mode still detected and correctly identified. Now it is evident that many of the modes with low amplitudes and/or corresponding to the chunks with the lowest SNR are being lost, while at the same time the detected $\ell = 1$ mixed modes are on average even more condensed to the $\ell = 1$ p-mode position than in the previous example. The GLOBAL modality now provides less accurate positions for the radial modes, although still good enough to allow the CHUNK modality to properly locate and identify them in the PSD. Finally, we can see that the frequency position of some of the $\ell = 2, 0$ modes as obtained from the CHUNK modality starts to exhibit a lower level of accuracy with respect to the previous tests. In the last example, for $T = 30$ days, we reach the worst scenario with a frequency resolution degraded to about 50 times

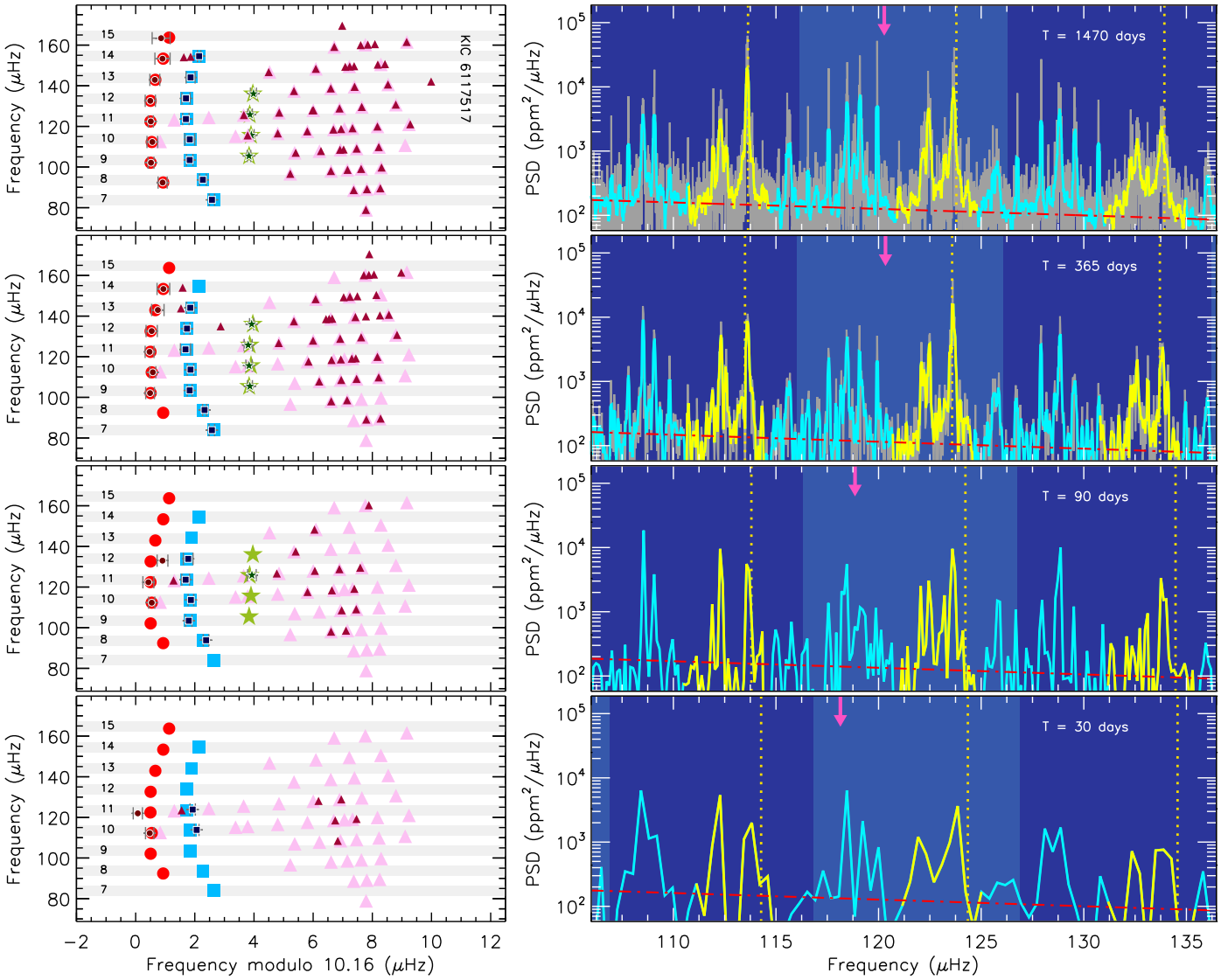

Fig. 20. The peak bagging analysis of the low-luminosity RGB star KIC 6117517 by degrading the frequency resolution of the stellar PSD. *Left panels*: the échelle diagrams obtained for four different frequency resolutions, with same description as that used in Fig. 16. The literature frequencies and the folding $\Delta\nu$ value are those provided by Corsaro et al. (2015a). *Right panels*: The three most central chunks of the stellar PSD (in gray) as seen from the GLOBAL modality for each test performed, where the $\ell = 2, 0$ regions have been highlighted in yellow (see also the description in Fig. 7). The purple arrows mark the position of $\nu_{\rm max}$ obtained from an independent background fit to each test PSD. Only global radial mode frequencies are indicated in this case (vertical dotted lines). The smoothing of the PSD is coinciding with the PSD itself for the two bottom panels because of the low frequency resolution.

the nominal value, thus corresponding to $\delta\nu_{\rm res} \simeq 0.40\,\mu$Hz, significantly larger than a typical radial mode linewidth measured in any RG star so far (e.g. Corsaro et al. 2015a; Vrard et al. 2018). Here the worsening is evident, with only 10 oscillation frequencies extracted (i.e. about 86 % reduction with respect to the first example), covering three radial orders, i.e. the ones closest to $\nu_{\rm max}$. The loss in the accuracy of the global radial mode frequencies from the GLOBAL modality is more pronounced than in the previous case, but it still suffices to allow the pipeline to properly identify the modes with the CHUNK modality. The accuracy on the final frequencies shown in the échelle is the lowest among the four examples provided, and this is now apparent on most of the $\ell = 2, 0$ modes that are extracted. Nonetheless, we stress that this loss in accuracy from the CHUNK modality is not to be attributed to the extraction process made by FAMED because the pipeline can adequately locate the position of each frequency peak in the PSD independently of the frequency resolution. This time the loss in accuracy is essentially caused by the low frequency resolution that makes individual peaks appear as broad spike-like structures, as it is also visible from the bottom panel of Fig. 20.

The value of $\Delta\nu$ estimated by the GLOBAL modality for each example ranges between 0.6 and 0.1 %, showing that the methodology presented in Sect. 4.2 is essentially independent of the frequency resolution that is adopted, and that it is very powerful in attaining a good level of accuracy even if only a few radial oscillation modes can be detected. In addition, the average ΔP_1 estimated from the extracted dipole modes is of about 58 s, 55 s, 52 s, and 49 s, from the best to the worst frequency resolution test conducted. The estimate of ΔP_1 obtained

with FAMED for these tests is therefore not changing significantly as the frequency resolution degrades. The ΔP_1 estimates derived from each test are perfectly in line with the ΔP_1 expected for a RGB star according to the literature (e.g. Bedding et al. 2011), proving that when using FAMED the evolutionary stage of a low-luminosity RGB star can be reliably inferred even with just one month of observations.

7. Conclusions & future work

In this paper we have shown that the Bayesian multi-modal approach is a very powerful technique for performing detailed asteroseismic analyses of solar-like oscillators in a robust manner. In particular, this is made possible by the rapid and relatively simple setting up of the approach, which allows us to obtain a large amount of information from an asteroseismic dataset in a relatively short amount of time, even if using a single CPU system setup. The high computational speed that characterizes the FAMED pipeline is largely supported by the adoption of DIAMONDS as a fitting code. DIAMONDS is used by FAMED to perform up to hundreds of independent fitting processes of different type within the peak bagging analysis of a single star, with most of these fits related to the fundamental peak testing phase. According to the applications presented in Sect. 6 we have seen that FAMED can be successfully exploited for a large diversity of stars of low and intermediate mass, ranging from F-type MS, characterized by large oscillation mode linewidths, hence by strong peak blending effects between adjacent oscillation modes, to SGs in different stages of evolution, and RGs from the base of the RGB up to the RGB tip and finally to the RC, including peculiar stars that show depressed dipole mode amplitudes. The extraction of oscillation modes is adequately performed even for stars that exhibit a large number of dipolar rotational multiplets, which is an indication that rotation and stellar spin inclination are accessible quantities in the automated approach presented in this work. We have seen that this is verified for stars from the MS up to even the challenging case of core-Helium-burning RGs. In all the applications discussed we have seen that the frequencies extracted with FAMED by adopting the first two modalities GLOBAL and CHUNK, are comparable in number and accuracy to those from the literature, with FAMED being often able to slightly outperform standard approaches in detecting and identifying low SNR oscillation modes (including $\ell = 3$ modes in challenging conditions), modes with strong peak blending, and modes containing a fine-structure such as that of rotation. In this regard we stress that the adoption of the data-driven approach used by FAMED for the automated extraction and identification of $\ell = 1$ mixed modes, including their rotational components when rotation is detected, yields robust results even without the use of any fitting or superposition of an asymptotic pattern for mixed modes.

We have also demonstrated that the pipeline has powerful abilities in analyzing datasets with low SNR and frequency resolution conditions, which make FAMED well suited for studies involving a large number of targets, even if relatively far way and/or observed for just a few months. This is especially relevant in view of the observations that are being carried out by NASA TESS, where already ∼1 month of data can suffice to detect individual oscillation modes (e.g. Huber et al. 2019; Campante et al. 2019; Chaplin et al. 2020), and for processing the huge amount of datasets that will be delivered by ESA PLATO in a near future. Furthermore, based on the results from our applications, we find that other outputs provided by FAMED that can be of relevance in the context of an asteroseismic characterization are: 1) a rather accurate estimate of $\Delta\nu$, often well below 1 %, with an accuracy that is essentially not sensitive to the actual SNR and frequency resolution of the dataset; 2) the ϵ term of the asymptotic relation, which provides the correct global mode identification scheme of the star analyzed; 3) a value of the observed period spacing ΔP_1 for each chunk analyzed, which can be adopted to reliably infer an evolutionary stage for RG stars (RGB versus RC); 4) the radial mode linewidths for all the radial modes identified through the stellar PSD.

As already anticipated, the extra modules ÉCHELLE and COMPLETE of the FAMED pipeline will be thoroughly presented in a forthcoming paper. These modules will provide further validation on the oscillation modes extracted with the GLOBAL and CHUNK modalities based on theoretical asymptotic relations, as well as additional parameters, mostly useful for analyzing evolved stars (see Table 1 for an overview). Future work will aim at incorporating new modules for e.g. automatically extracting the acoustic glitches based on the methodology presented by Corsaro et al. (2015b), and a global stellar spin inclination angle following the approach presented by Kuszlewicz et al. (2019).

An interesting point that arises from the methodology presented in this paper is that the multi-modal approach used by FAMED makes this pipeline suitable for applications that can differ from the peak bagging of solar-like oscillators. For example, FAMED could be extended to another class of pulsators, provided that the analysis can still be performed in the Fourier domain (e.g. for DAVs type pulsators, see Hermes et al. 2017). Future developments of this kind could be included in the pipeline by exploiting its flexibility and modular structure.

In its current state, FAMED by no means pretends to be a definitive and fully exhaustive approach to peak bagging. Our aim is, however, to provide a powerful, reliable, and at the same time easy-to-use tool to perform complicated and otherwise long-lasting analyses of stellar oscillations that can be at the disposal of the entire astrophysics community, including non-experts in the asteroseismology field. For this reason FAMED is subject to a continuous maintenance and development aimed at improving its overall functionality, reliability, and computational stability and efficiency. This will be possible by taking into account the testing and applicability verification done by the future user community of the pipeline. Additional modules to carry out specific tasks on the obtained results may be implemented according to the needs of the user community. In conclusion, we believe that FAMED already represents a promising opportunity for overcoming the long-lasting problem of automatizing the complicated analysis of stellar oscillations. FAMED, together with other possible approaches that may become available in the future, will definitely contribute to increase our capabilities to investigate large ensembles of oscillating stars in great detail.

Acknowledgements. E.C. is funded by the European Union's Horizon 2020 research and innovation program under the Marie Sklodowska-Curie grant agreement No. 664931. E.C. acknowledges participation in the PLATO PSM WP128 peak bagging exercises that helped in developing the FAMED pipeline and for its calibration in the regime of MS and SG stars. We thank R. A. García for providing KADACS datasets of the *Kepler* targets used in the applications shown in this work. We thank M. B. Nielsen and G. R. Davies for useful discussions.

References

Appourchaux, T., Antia, H. M., Benomar, O., et al. 2014, A&A, 566, A20
Appourchaux, T., Chaplin, W. J., García, R. A., et al. 2012, A&A, 543, A54
Baglin, A., Michel, E., Auvergne, M., & COROT Team. 2006, in ESA Special Publication, Vol. 624, Proceedings of SOHO 18/GONG 2006/HELAS I, Beyond the spherical Sun, 34

Ball, W. H., Chaplin, W. J., Schofield, M., et al. 2018, ApJS, 239, 34
Ballot, J., Appourchaux, T., Toutain, T., & Guittet, M. 2008, A&A, 486, 867
Beck, P. G., Montalban, J., Kallinger, T., et al. 2012, Nature, 481, 55
Bedding, T. R. & Kjeldsen, H. 2003, PASA, 20, 203
Bedding, T. R., Mosser, B., Huber, D., et al. 2011, Nature, 471, 608
Benomar, O., Appourchaux, T., & Baudin, F. 2009, A&A, 506, 15
Benomar, O., Bazot, M., Nielsen, M. B., et al. 2018, Science, 361, 1231
Benomar, O., Bedding, T. R., Mosser, B., et al. 2013, ApJ, 767, 158
Bonanno, A., Corsaro, E., Del Sordo, F., et al. 2019, A&A, 628, A106
Bonanno, A., Corsaro, E., & Karoff, C. 2014, A&A, 571, A35
Borucki, W. J., Koch, D., Basri, G., et al. 2010, Science, 327, 977
Buysschaert, B., Beck, P. G., Corsaro, E., et al. 2016, A&A, 588, A82
Campante, T. L., Corsaro, E., Lund, M. N., et al. 2019, ApJ, 885, 31
Chaplin, W. J., Serenelli, A. M., Miglio, A., et al. 2020, Nature Astronomy, 7
Christensen-Dalsgaard, J., Silva Aguirre, V., Elsworth, Y., & Hekker, S. 2014, MNRAS, 445, 3685
Corsaro, E. 2018, Asteroseismology and Exoplanets: Listening to the Stars and Searching for New Worlds, 49, 137
Corsaro, E. 2019, Frontiers in Astronomy and Space Sciences, 6, 21 (C19)
Corsaro, E. & De Ridder, J. 2014, A&A, 571, A71
Corsaro, E., De Ridder, J., & García, R. A. 2015a, A&A, 579, A83
Corsaro, E., De Ridder, J., & García, R. A. 2015b, A&A, 578, A76
Corsaro, E., De Ridder, J., & García, R. A. 2018, A&A, 612, C2
Corsaro, E., Fröhlich, H.-E., Bonanno, A., et al. 2013, MNRAS, 430, 2313
Corsaro, E., Lee, Y.-N., García, R. A., et al. 2017a, Nature Astronomy, 1, 0064
Corsaro, E., Mathur, S., García, R. A., et al. 2017b, A&A, 605, A3
Corsaro, E., Stello, D., Huber, D., et al. 2012, ApJ, 757, 190
Davies, G. R., Chaplin, W. J., Farr, W. M., et al. 2015, MNRAS, 446, 2959
Davies, G. R. & Miglio, A. 2016, Astronomische Nachrichten, 337, 774
Davies, G. R., Silva Aguirre, V., Bedding, T. R., et al. 2016, MNRAS, 456, 2183
De Ridder, J., Barban, C., Baudin, F., et al. 2009, Nature, 459, 398
Deheuvels, S., Ballot, J., Beck, P. G., et al. 2015, A&A, 580, A96
Deheuvels, S., Ouazzani, R. M., & Basu, S. 2017, A&A, 605, A75
Di Mauro, M. P., Ventura, R., Cardini, D., et al. 2016, ApJ, 817, 65
Di Mauro, M. P., Ventura, R., Corsaro, E., & Lustosa De Moura, B. 2018, ApJ, 862, 9
Fuller, J., Cantiello, M., Stello, D., Garcia, R. A., & Bildsten, L. 2015, Science, 350, 423
García, R. A., Hekker, S., Stello, D., et al. 2011, MNRAS, 414, L6
García, R. A., Mathur, S., Pires, S., et al. 2014a, A&A, 568, A10
García, R. A., Mathur, S., Salabert, D., et al. 2010, Science, 329, 1032
García, R. A., Pérez Hernández, F., Benomar, O., et al. 2014b, A&A, 563, A84
García Saravia Ortiz de Montellano, A., Hekker, S., & Themeßl, N. 2018, MNRAS, 476, 1470
Gehan, C., Mosser, B., Michel, E., Samadi, R., & Kallinger, T. 2018, A&A, 616, A24
Gizon, L. & Solanki, S. K. 2003, ApJ, 589, 1009
Grec, G., Fossat, E., & Pomerantz, M. A. 1983, Sol. Phys., 82, 55
Gruberbauer, M., Kallinger, T., Weiss, W. W., & Guenther, D. B. 2009, A&A, 506, 1043
Handberg, R., Brogaard, K., Miglio, A., et al. 2017, MNRAS, 472, 979
Handberg, R. & Campante, T. L. 2011, A&A, 527, A56
Härdle, W., Müller, M., Sperlich, S., & Werwatz, A. 2004, Nonparametric and Semiparametric Models, Springer Series in Statistics (Springer Berlin Heidelberg)
Hermes, J. J., Gänsicke, B. T., Kawaler, S. D., et al. 2017, ApJS, 232, 23
Howell, S. B., Sobeck, C., Haas, M., et al. 2014, PASP, 126, 398
Huber, D., Bedding, T. R., Stello, D., et al. 2011, ApJ, 743, 143
Huber, D., Chaplin, W. J., Chontos, A., et al. 2019, AJ, 157, 245
Jeffreys, H. 1961, Theory of Probability (3rd Ed. OUP Oxford)
Kallinger, T. 2019, arXiv e-prints, arXiv:1906.09428
Kallinger, T., De Ridder, J., Hekker, S., et al. 2014, A&A, 570, A41
Kallinger, T., Hekker, S., Mosser, B., et al. 2012, A&A, 541, A51
Kallinger, T., Mosser, B., Hekker, S., et al. 2010, A&A, 522, A1
Koch, D. G., Borucki, W. J., Basri, G., et al. 2010, ApJ, 713, L79
Kuszlewicz, J. S., Chaplin, W. J., North, T. S. H., et al. 2019, MNRAS, 488, 572
Lund, M. N., Silva Aguirre, V., Davies, G. R., et al. 2017, ApJ, 835, 172
Metcalfe, T. S., Chaplin, W. J., Appourchaux, T., et al. 2012, ApJ, 748, L10
Miglio, A., Chiappini, C., Morel, T., et al. 2013, MNRAS, 429, 423
Montalbán, J., Miglio, A., Noels, A., Scuflaire, R., & Ventura, P. 2010, ApJ, 721, L182
Mosser, B., Belkacem, K., Goupil, M. J., et al. 2011, A&A, 525, L9
Mosser, B., Belkacem, K., Pinçon, C., et al. 2017, A&A, 598, A62
Mosser, B., Goupil, M. J., Belkacem, K., et al. 2012, A&A, 540, A143
Pérez Hernández, F., García, R. A., Corsaro, E., Triana, S. A., & De Ridder, J. 2016, A&A, 591, A99
Pinsonneault, M. H., Elsworth, Y. P., Tayar, J., et al. 2018, ApJS, 239, 32
Pires, S., Mathur, S., García, R. A., et al. 2015, A&A, 574, A18
Rauer, H., Catala, C., Aerts, C., et al. 2014, Experimental Astronomy, 38, 249
Ricker, G. R., Winn, J. N., Vanderspek, R., et al. 2014, in Society of Photo-Optical Instrumentation Engineers (SPIE) Conference Series, Vol. 9143, Society of Photo-Optical Instrumentation Engineers (SPIE) Conference Series, 20
Silva Aguirre, V., Lund, M. N., Antia, H. M., et al. 2017, ApJ, 835, 173
Silva Aguirre, V., Stello, D., Stokholm, A., et al. 2020, ApJ, 889, L34
Sivia, D. & Skilling, J. 2006, Data Analysis: A Bayesian Tutorial, Oxford science publications (OUP Oxford)
Skilling, J. 2004, AIP Conference Proceedings, 735, 395
Stassun, K. G., Oelkers, R. J., Paegert, M., et al. 2019, AJ, 158, 138
Stello, D., Cantiello, M., Fuller, J., et al. 2016, Nature, 529, 364
Stello, D., Compton, D. L., Bedding, T. R., et al. 2014, ApJ, 788, L10
Stello, D., Huber, D., Bedding, T. R., et al. 2013, ApJ, 765, L41
Tange, O. 2011, ;login: The USENIX Magazine, 36, 42
Tassoul, M. 1980, ApJS, 43, 469
Trotta, R. 2008, Contemporary Physics, 49, 71
Ulrich, R. K. 1986, ApJ, 306, L37
Vrard, M., Kallinger, T., Mosser, B., et al. 2018, A&A, 616, A94
White, T. R., Bedding, T. R., Stello, D., et al. 2011, ApJ, 742, L3

Appendix A: Prior hyper-parameters for peak tests

In this appendix we provide the prior hyper-parameters that are adopted in the current version of FAMED for conducting the peak testing of detection, blending, rotation, and duplicity. As explained in Sect. 5.3.1, we have opted for uniform prior distributions for all the free parameters of the fitting models. The priors currently used by FAMED have been tuned to obtain an optimal reproducibility of the results found in the literature, as shown in the applications in Sect. 6. The prior ranges are listed in Tables A.1 and A.2 as a function of the peak fitting model, the free parameter of the model, the mode angular degree, and the evolutionary stage of the star. The quantity $S_{i,\mathrm{corr}}$ appearing in the upper prior bound for oscillation amplitudes is an estimate of the true peak height. This is obtained as the maximum value of the smoothed PSD within the frequency ranges of a given peak, which we refer to as $S_{i,\mathrm{max}}$, with the smoothing calculated using a factor Γ_{chunk}, and is subsequently corrected by first subtracting the local level of the background and by then dividing by the response function of the sampling cadence such that the height estimate takes into account any degradation of the signal as we approach to the limiting Nyquist frequency.

In most cases, the prior ranges can be tuned from the input configuring parameter file of the pipeline through a specific parameter, whose value is also listed in Tables A.1 and A.2. In particular, the user has the possibility to modify the lower bound of the prior on the linewidths, as well as any of the multiplication coefficients that appear for the upper bounds of the priors on linewidths and amplitudes. In the case of the amplitudes of model $\mathcal{M}_{\mathrm{B}}$ for less evolved stars, $\Delta\nu \geq \Delta\nu_{\mathrm{thresh}}$, the upper bound is selected as the maximum $S_{i,\mathrm{corr}}$ between that of the chunk radial mode and that of the chunk quadrupole mode (see Sect. 5.2 for a description on how the chunk radial and quadrupole modes are identified). Following the results on standard peak bagging analysis of RGB stars by Corsaro et al. (2015a), we find that in evolved stars the upper prior bound on the linewidth is larger for $\ell = 2$ modes than for $\ell = 0$ ones to account for the presence of quadrupole mixed modes. Again for the case of evolved stars, the upper prior bound on the linewidth of $\ell = 1$ modes is instead smaller than for $\ell = 0$ modes because here the dipole modes are mixed modes, hence having a longer lifetime. For model $\mathcal{M}_{\mathrm{D}}$ the prior ranges with subscripts indicating the angular degrees 0,2 imply that they are evaluated specifically for the chunk radial and quadrupole modes in relation to the free parameter they are associated with (e.g. $\ell = 0$ for $\nu_{i,0}^{\ell=0}$ and so on). Finally, all

the priors on linewidth and amplitudes incorporate the FWHM of the chunk radial mode, Γ_0, which is measured as explained in Sect. 5.3.1.

Table A.1. The prior hyper-parameters adopted for the peak testing performed in the CHUNK modality of FAMED. Each prior can be identified with its corresponding free parameter and fitting model, and may change as a function of the angular degree ℓ of the mode being tested and on the general evolutionary stage classification of the star (reported in terms of $\Delta\nu$ and $T_{\rm eff}$ thresholds), as presented in Sects. 5.3. The values of the configuring parameters used to set up each prior, if any, are listed in the last column. Some of the free parameters are the same for different models.

Model	Free parameter (units)	ℓ	Evolutionary stage	Uniform Prior range	Configuring parameter value
$\mathcal{M}_{\rm A}$, $\mathcal{M}_{\rm B}$	$\sigma_{\rm noise}$	0,1,2,3	Any	$[a_1, a_2]$	$a_1 = 0.95$, $a_2 = 1.05$
$\mathcal{M}_{\rm B}$	$\nu_{i,0}$ (μHz)	0,2	$\Delta\nu \geq \Delta\nu_{\rm thresh}$	$[r_a(\ell=2), r_b(\ell=0)]$	–
			$\Delta\nu < \Delta\nu_{\rm thresh}$	$\left[\nu_{f,i} - \sigma_{f,i}, \nu_{f,i} + \sigma_{f,i}\right]$	–
		1,3	Any	$\left[\nu_{f,i} - \sigma_{f,i}, \nu_{f,i} + \sigma_{f,i}\right]$	–
	A_i (ppm)	0	$\Delta\nu \geq \Delta\nu_{\rm thresh}$	$\left[0, \max_{\ell=0,2}\left(\sqrt{\eta\Gamma_0\pi S_{i,\rm corr}}\right)\right]$	$\eta = 3$
			$\Delta\nu < \Delta\nu_{\rm thresh}$	$\left[0, \sqrt{\eta\Gamma_0\pi S_{i,\rm corr}}\right]$	$\eta = 3$
		1	$\Delta\nu \leq \Delta\nu_{\rm SG}$ and $T_{\rm eff} \geq T_{\rm eff,SG}$, or $\Delta\nu \geq \Delta\nu_{\rm SG}$	$\left[0, \sqrt{\eta\Gamma_0\pi S_{i,\rm corr}}\right]$	$\eta = 6$
			$\Delta\nu < \Delta\nu_{\rm SG}$ and $T_{\rm eff} < T_{\rm eff,SG}$	$\left[0, \sqrt{\eta\Gamma_0\pi S_{i,\rm corr}}\right]$	$\eta = 1.5$
		2	$\Delta\nu \geq \Delta\nu_{\rm thresh}$	$\left[0, \max_{\ell=0,2}\left(\sqrt{\eta\Gamma_0\pi S_{i,\rm corr}}\right)\right]$	$\eta = 3$
			$\Delta\nu < \Delta\nu_{\rm thresh}$	$\left[0, \sqrt{\eta\Gamma_0\pi S_{i,\rm corr}}\right]$	$\eta = 8$
		3	Any	$\left[0, \sqrt{\eta\Gamma_0\pi S_{i,\rm corr}}\right]$	$\eta = 3$
	Γ_i (μHz)	0	Any	$[\Gamma_{\rm min}, \eta\Gamma_0]$	$\Gamma_{\rm min} = 10^{-4}$, $\eta = 3$
		1	$\Delta\nu \leq \Delta\nu_{\rm SG}$ and $T_{\rm eff} \geq T_{\rm eff,SG}$, or $\Delta\nu \geq \Delta\nu_{\rm SG}$	$[\Gamma_{\rm min}, \eta\Gamma_0]$	$\Gamma_{\rm min} = 10^{-4}$, $\eta = 6$
			$\Delta\nu < \Delta\nu_{\rm SG}$ and $T_{\rm eff} < T_{\rm eff,SG}$	$[\Gamma_{\rm min}, \eta\Gamma_0]$	$\Gamma_{\rm min} = 10^{-4}$, $\eta = 1.5$
		2	$\Delta\nu \geq \Delta\nu_{\rm thresh}$	$[\Gamma_{\rm min}, \eta\Gamma_0]$	$\Gamma_{\rm min} = 10^{-4}$, $\eta = 3$
			$\Delta\nu < \Delta\nu_{\rm thresh}$	$[\Gamma_{\rm min}, \eta\Gamma_0]$	$\Gamma_{\rm min} = 10^{-4}$, $\eta = 8$
		3	Any	$[\Gamma_{\rm min}, \eta\Gamma_0]$	$\Gamma_{\rm min} = 10^{-4}$, $\eta = 3$
$\mathcal{M}_{\rm C}$	$\sigma_{\rm noise}$	1	$\Delta\nu < \Delta\nu_{\rm RG}$	$[a_1, a_2]$	$a_1 = 0.95$, $a_2 = 1.05$
	$\nu_{i,0}$ (μHz)	1	$\Delta\nu < \Delta\nu_{\rm RG}$	$\left[\nu_{f,i} - \sigma_{f,i}, \nu_{f,i} + \sigma_{f,i}\right]$	–
	H_i (ppm^2/μHz)	1	$\Delta\nu < \Delta\nu_{\rm RG}$	$[0, 1.5 S_{i,\rm max}]$	–
$\mathcal{M}_{\rm D}$	$\sigma_{\rm noise}$	0,2	$\Delta\nu \geq \Delta\nu_{\rm thresh}$	$[a_1, a_2]$	$a_1 = 0.95$, $a_2 = 1.05$
	$\nu_{i,0}^{\ell=0}, \nu_{i,0}^{\ell=2}$ (μHz)	0,2	$\Delta\nu \geq \Delta\nu_{\rm thresh}$	$\left[\nu_{f,i} - \sigma_{f,i}, \nu_{f,i} + \sigma_{f,i}\right]_{\ell=0,\ell=2}$	–
	$A_i^{\ell=0}, A_i^{\ell=2}$ (ppm)	0,2	$\Delta\nu \geq \Delta\nu_{\rm thresh}$	$\left[0, \sqrt{\eta\Gamma_0\pi S_{i,\rm corr}}\right]_{\ell=0,\ell=2}$	$\eta = 3$
	$\Gamma_i^{\ell=0}, \Gamma_i^{\ell=2}$ (μHz)	0,2	$\Delta\nu \geq \Delta\nu_{\rm thresh}$	$[\Gamma_{\rm min}, \eta\Gamma_0]$	$\Gamma_{\rm min} = 10^{-4}$, $\eta = 3$

Table A.2. The prior hyper-parameters adopted for the peak rotation and duplicity testing performed in the CHUNK modality of FAMED. Similar description as for Table A.1, following what presented in Sect. 5.4. The $\ell = 3$ cases refer to those peaks flagged as candidate octupole modes according to Sect. 5.5, i.e. located inside the octupole mode search range, hence are not intended as yet confirmed $\ell = 3$ mode of the analysis.

Model	Free parameter (units)	ℓ	Evolutionary stage	Uniform Prior range	Configuring parameter value
$\mathcal{M}_{\rm E}$, $\mathcal{M}_{\rm F}$	$\nu_{i,0}$ (μHz)	1,3	$\Delta\nu \leq \Delta\nu_{\rm SG}$ and $T_{\rm eff} \geq T_{\rm eff,SG}$, or $\Delta\nu \geq \Delta\nu_{\rm SG}$	$\left[\nu_{f,i} - \sigma_{f,i}, \nu_{f,i} + \sigma_{f,i}\right]$	–
			$\Delta\nu < \Delta\nu_{\rm SG}$ and $T_{\rm eff} < T_{\rm eff,SG}$	$[r_a, r_b]_i$	–
	A_i (ppm)	1	$\Delta\nu \leq \Delta\nu_{\rm SG}$ and $T_{\rm eff} \geq T_{\rm eff,SG}$, or $\Delta\nu \geq \Delta\nu_{\rm SG}$	$\left[0, \sqrt{\eta\Gamma_0\pi S_{i,\rm corr}}\right]$	$\eta = 3$
			$\Delta\nu_{\rm thresh} \leq \Delta\nu < \Delta\nu_{\rm SG}$ and $T_{\rm eff} < T_{\rm eff,SG}$	$\left[0, \sqrt{\eta\Gamma_0\pi S_{i,\rm corr}}\right]$	$\eta = 1.5$
			$\Delta\nu < \Delta\nu_{\rm thresh}$	$\left[0, \sqrt{\eta\Gamma_0\pi S_{i,\rm corr}}\right]$	$\eta = 1$
		3	Any	$\left[0, \sqrt{\eta\Gamma_0\pi S_{i,\rm corr}}\right]$	$\eta = 3$
	Γ_i (μHz)	1	$\Delta\nu \leq \Delta\nu_{\rm SG}$ and $T_{\rm eff} \geq T_{\rm eff,SG}$, or $\Delta\nu \geq \Delta\nu_{\rm SG}$	$[\Gamma_{\rm min}, \eta\Gamma_0]$	$\Gamma_{\rm min} = 10^{-4}$, $\eta = 3$
			$\Delta\nu_{\rm thresh} \leq \Delta\nu < \Delta\nu_{\rm SG}$ and $T_{\rm eff} < T_{\rm eff,SG}$	$[\Gamma_{\rm min}, \eta\Gamma_0]$	$\Gamma_{\rm min} = 10^{-4}$, $\eta = 1.5$
			$\Delta\nu < \Delta\nu_{\rm thresh}$	$[\Gamma_{\rm min}, \eta\Gamma_0]$	$\Gamma_{\rm min} = 10^{-4}$, $\eta = 1$
		3	Any	$[\Gamma_{\rm min}, \eta\Gamma_0]$	$\Gamma_{\rm min} = 10^{-4}$, $\eta = 3$
$\mathcal{M}_{\rm F}$	$\delta\nu_{\rm rot}$ (μHz)	1,3	$\Delta\nu \leq \Delta\nu_{\rm SG}$ and $T_{\rm eff} \geq T_{\rm eff,SG}$, or $\Delta\nu \geq \Delta\nu_{\rm SG}$	$\left[2\delta\nu_{\rm res}, \frac{2}{\theta}\sigma_{f,i}\right]$	$\theta = 2.8$
			$\Delta\nu < \Delta\nu_{\rm SG}$ and $T_{\rm eff} < T_{\rm eff,SG}$	$\left[2\delta\nu_{\rm res}, \frac{1}{\theta}(r_b - r_a)\right]_i$	$\theta = 2.8$
	$\cos i$	1,3	Any	$[0, 1]$	–
$\mathcal{M}_{\rm G}$	$\nu^1_{i,0}$ (μHz)	1,3	$\Delta\nu < \Delta\nu_{\rm RG}$	$[r_a, r_b]_i$	–
	$\delta\nu_{\rm split}$ (μHz)	1,3	$\Delta\nu < \Delta\nu_{\rm RG}$	$[2\delta\nu_{\rm res}, r_b - r_a]_i$	–
	A^1_i, A^2_i (ppm)	1,3	$\Delta\nu < \Delta\nu_{\rm RG}$	$\left[0, \sqrt{\eta\Gamma_0\pi S_{i,\rm corr}}\right]$	$\eta = 1$
	Γ^1_i, Γ^2_i (μHz)	1,3	$\Delta\nu < \Delta\nu_{\rm RG}$	$[\Gamma_{\rm min}, \eta\Gamma_0]_i$	$\Gamma_{\rm min} = 10^{-4}$, $\eta = 1$